Published in final edited form as:
J Hazard Mater. 2017 January 15; 322(Pt A): 48–84. doi:10.1016/j.jhazmat.2016.06.060.

Environmental implications and applications of engineered nanoscale magnetite and its hybrid nanocomposites: A review of recent literature

Chunming Su
Ground Water and Ecosystems Restoration Division, National Risk Management Research Laboratory, Office of Research and Development, United States Environmental Protection Agency, 919 Kerr Research Drive, Ada, OK 74820, USA

Abstract

This review focuses on environmental implications and applications of engineered magnetite (Fe_3O_4) nanoparticles (MNPs) as a single phase or a component of a hybrid nanocomposite that exhibits superparamagnetism and high surface area. MNPs are synthesized via co-precipitation, thermal decomposition and combustion, hydrothermal process, emulsion, microbial process, and green approaches. Aggregation/sedimentation and transport of MNPs depend on surface charge of MNPs and geochemical parameters such as pH, ionic strength, and organic matter. MNPs generally have low toxicity to humans and ecosystem. MNPs are used for constructing chemical/biosensors and for catalyzing a variety of chemical reactions. MNPs are used for air cleanup and carbon sequestration. MNP nanocomposites are designed as antimicrobial agents for water disinfection and flocculants for water treatment. Conjugated MNPs are widely used for adsorptive/separative removal of organics, dyes, oil, arsenic, phosphate, molybdate, fluoride, selenium, Cr(VI), heavy metal cations, radionuclides, and rare earth elements. MNPs can degrade organic/inorganic contaminants via chemical reduction or catalyze chemical oxidation in water, sediment, and soil. Future studies should further explore mechanisms of MNP interactions with other nanomaterials and contaminants, economic and green approaches of MNP synthesis, and field scale demonstration of MNP utilization.

Keywords

Fe_3O_4; Hybrid nanocomposites; Superparamagnetic; Catalyst; Remediation

1. Introduction

Over the past few years, the scientific community has witnessed a dramatic increase in the number of papers published on implications and applications of magnetite (Fe_3O_4) nanoparticles (MNPs). Magnetite is a common iron oxide that exhibits outstanding physico-chemical properties due to the presence of both Fe(II) and Fe(III) in its structure. It behaves as superparamagnetic as the particle size is reduced to a few nanometers. MNPs have been used for biomedical applications such as biosensing, cell tracking, tissue engineering, magnetic resonance imaging (MRI)/optical multimodal imaging, targeted drug delivery, and hyperthermia therapeutic cancer treatment [1], [2], [3], [4], [5], [6], [7], [8]. Whereas review

articles have addressed biomedical applications of MNPs [1], [2], [3], [4], [5], [6], [7], there has been limited efforts on the literature review of environmental aspects of MNPs [9], [10]. A thorough synthesis of recent literature is needed with regard to environmental implications and applications of MNPs in order to understand the current status of research and to explore future opportunities. This review tries to meet that need.

2. Synthesis of nanoscale magnetite and its hybrid nanocomposites

Several previous review articles have covered the synthesis, protection, functionalization, and application of MNPs, as well as the magnetic properties of nanostructured systems [11], [12], [13]. Substantial progress in the size and shape control of MNPs has been made by developing methods such as co-precipitation, thermal decomposition and/or reduction, micelle synthesis, and hydrothermal synthesis. Corrosion protection strategies have been developed using surfactant/polymer coating, silica coating and carbon coating of MNPs or embedding them in a matrix/support [12]. Unique shape MNPs such as those of high aspect ratio can be achieved in two main synthetic routes: (i) direct synthesis (in which the anisotropic growth is directed by tuning the reaction conditions or by using templates) and (ii) assembly methods (in which the high aspect ratio is achieved by assembly from individual building blocks) [14]. Table 1 lists examples of reported methods for synthesis of MNPs and their hybrid composites.

2.1. Co-precipitation

Co-precipitation is a simple way to synthesize MNPs by titrating aqueous Fe^{2+}/Fe^{3+} salt solutions with a base under inert atmosphere at room temperature or at an elevated temperature. The size, shape, and composition of the magnetic NPs depend on the type of salts used (*e.g.*, chlorides, sulfates, nitrates), the Fe^{2+}/Fe^{3+} ratio, the reaction temperature, the pH value and ionic strength of the media [15], [16]. The use of organic additives as stabilization and/or reducing agents such as polyvinlyalcohol (PVA) facilitates preparation of monodisperse MNPs (4–10 nm) [15]. While elevated temperature is often used in the synthesis, room-temperature air-atmosphere co-precipitation method can also be used to tune the magnetic properties of iron oxide NPs with the compositional control between magnetite and maghemite (γ-Fe_2O_3) [17].

Organic ligands influence co-precipitation products. Citrate helps produce smaller MNPs (8 nm) compared to without citrate (14–28 nm) and better dispersion and strong magnetic performance [18]. Citrate also prevents oxidation of magnetite to produce hematite. In another study, the primary particle size of magnetite is tuned from 5 nm to 15 nm by varying the citrate/iron precursor ratio during the normal phase hydrolysis reaction, while the second iteration of citrate stabilizes the nanoclusters [19]. Inorganic ligands are also used to modify the products. Water dispersible MNPs with a phosphate monolayer capping has been synthesized by a single-step coprecipitation method using Fe^{2+}/Fe^{3+} salt solutions, ammonia and H_3PO_4. The phosphate capped MNPs show excellent long term stability (>2 years of shelf life) [20].

Substituted MNPs can be synthesized via co-precipitation. For example, cubic cobalt-substituted magnetite $Co_xFe_{3-x}O_4$ nanocubes (35–110 nm) with uniform composition

distributions of Co, Fe and O, have been obtained via solution synthesis [21]. NPs of the ferrite system $CoFe_{2-x}Al_xO_4$ (x = 0.0, 0.3, 0.7 and 1.0) have been synthesized through the co-precipitation technique to form a nano-size (20–63 nm) single spinel phase [22]. Magnetic properties such as coercivity and saturation magnetization can be controlled by changing the non-magnetic Al^{3+} ions content. In another study, mixed-ferrites produced from electroplating wastewater for metal recovery is used as the magnetic agents. With the addition of lanthanides and F^- ions, a novel magnetite near infrared photocatalyst of $Er^{3+}/Tm^{3+}/Yb^{3+}$-($CaF_2/ZnFe_2O_4/ZnO$) (ETY-FCZ) is further synthesized, which results in higher removal rates of methyl orange and salicylic acid compared to those of Ca-Zn magnetite precursor [23]. Hybrid Fe_3O_4-graphite composites [24] and hollow Fe_3O_4–Fe NPs with graphene sheets [25] have been prepared by in-situ chemical precipitation as high-performance electromagnetic wave absorbing materials. A recent study has explored low energy and chemically-mild process of co-nanoprecipitation using superparamagnetic iron oxide nanoparticles (SPIONs) and homopolymers or amphiphilic block copolymers, of varying architecture and hydrophilic/hydrophobic balance, which efficiently generates near monodisperse SPION-containing polymer NPs with complete retention of magnetism, and highly reversible aggregation and re-dispersion behavior [26]. One advantage of this method is that the quality of MNPs is reproducible. The drawback is that the size distribution of MNPs prepared by co-precipitation tend to be rather polydisperse.

2.2. Thermal decomposition and combustion

Thermal decomposition of organometallic compounds in high-boiling organic solvents containing stabilizing surfactants have been used to prepare monodisperse magnetic nanocrystals with smaller size [27], [28], [29]. Water soluble MNPs have been prepared using $FeCl_3 \cdot 6H_2O$ and 2-pyrrolidone as coordinating solvent under reflux at 245 °C [30]. The mean particle size is 4, 12, and 60 nm, respectively, when the reflux time is 1, 10, and 24 h. The shapes of the particles change from spherical at early stage to cubic morphologies with increasing reflux time. The same group has also developed a one-pot synthesis of water-soluble MNPs prepared under similar reaction conditions by the addition of α,ω-dicarboxyl-terminated poly(ethylene glycol) as a surface capping agent [31]. Most applications require a stable presentation of a defined surface chemistry; therefore, the native shell has to be completely exchanged for dispersants with irreversible affinity to the NP surface. A multiple exchange scheme has been developed to completely and irreversibly replace ligand on monodisperse MNPs synthesized with a strongly bound ligand shell of oleic acid [32]. Ligand exchange employing either citric acid or *meso*-2,3-dimercaptosuccinic acid (DMSA) ligand has been used to change monodisperse hydrophobic MNPs to hydrophilic MNPs produced by thermal decomposition of $Fe(acac)_3$ in benzyl ether [33]. Novel-morphological Fe_3O_4 nanosheets with magnetochromatic property has been prepared by a modified solvothermal method. Such nanosheets could form one-dimension photonic crystal under an external magnetic field. The Fe_3O_4 nanosheets suspension could strongly diffract visible light and display varied colors with changing the intensity of the magnetic field [34]. Monodisperse superparamagnetic MNPs coated with oleic acid have been prepared by thermal decomposition of Fe(III) glucuronate. To make the MNPs dispersible in water, the particle surface is modified with α-carboxyl-ω-bis(ethane-2,1-diyl)phosphonic acid-terminated poly(3-*O*-methacryloyl-α-d-glucopyranose)

(PMG–P). The PMG–P&Fe_3O_4 NPs have the potential to be used as contrast agents for MRI [35]. Monodisperse 8 nm MNPs have been synthesized by the thermal decomposition of iron(III) acetylacetonate in oleylamine and then are deposited onto n-type silicon wafer having the Al ohmic contact. The Au/Fe_3O_4 NPs/*n*-Si/Al heterojunction device shows unique electrical properties [36].

A facile one-pot synthesis method has been developed using combustion waves that simultaneously achieves fast reduction and direct formation of carbon coating layers on iron oxide nanostructures [37]. Hybrid composites of Fe_2O_3 NPs and nitrocellulose are fabricated by a wet impregnation process. Self-propagating combustion waves along interfacial boundaries between the surface of the metal oxide and the chemical fuels enable the release of oxygen from Fe_2O_3. This accelerated reaction directly transforms Fe_2O_3 into Fe_3O_4 nanostructures with a carbon coating layers of 5–20 nm thickness. The use of combustion waves may permit the precise manipulation of the chemical compositions of nanostructures, as well as the formation of organic/inorganic hybrid nanostructures.

2.3. Hydrothermal synthesis

A liquid–solid–solution reaction has been used under hydrothermal conditions to synthesize a broad range of nanostructured materials including magnetite. The system consists of metal linoleate (solid), an ethanol–linoleic acid liquid phase, and a water–ethanol solution at different reaction temperatures under hydrothermal conditions. Nanocrystals of Fe_3O_4 and $CoFe_2O_4$ can be prepared in very uniform sizes of about 9 and 12 nm, respectively [38]. In another study, Fe_3O_4-implanted ZnO and pristine ZnO nanosheets are synthesized hydrothermally. The composite nanosheets are photostable, reusable, and magnetically recoverable, revealing potential application in mineralization of organic pollutants [39]. A one-step hydrothermal process with silk fibroin (SF) nanofibers as the template and coating has been developed to synthesize core–shell magnetite/SF NPs with limited controllable sizes [40]. Monodispersed Fe_3O_4 vesicular nanospheres (160 nm) have been fabricated solvothermally in the mixed solution of ethylene glycol (EG) and ethylenediamine (EN) with the surfactant polyvinyl pyrrolidone (PVP) [41]. A Fe_3O_4–graphite composite has been synthesized using a one-step solvothermal method in which graphite powder in EG is mixed with $FeCl_3$ dissolved in EG and NaOAc followed by heating at 200 °C for 10 h under autogenous pressure. The Fe_3O_4–graphite composite is used as a heterogeneous Fenton-like catalyst for the degradation of antibiotic levofloxacin (LEV) in an aqueous solution [42].

An easy mixed solvent solvothermal/hydrothermal method has been developed for the one-step synthesis of monodisperse Fe_3O_4 and α-Fe_2O_3 NPs. The morphologies can be varied from spherical, to octahedral, to rice like, and even to fusiform; the size can be continuously tuned to a range within 30–290 nm. The morphology-, dimension-, and phase-controlled growth of Fe_xO_y nanocrystals can be achieved by tuning kinetic factors, such as the H_2O volume fraction, Fe^{3+} concentration, reaction temperature, and the ratio of alkali/Fe^{3+} [43]. In a separate study, a generalized hydrothermal method has been developed for the synthesis of single-crystalline magnetic spinel ferrite NPs (MFe_2O_4, M = Mg, Fe, Co, Ni, Cu, and Zn) to the smallest size (*i.e.*, 3 nm) [44]. A facile hydrothermal method has been developed to control the thickness of the carbon coating formation on the surface of magnetic NPs from

sucrose by using CH_3COONH_4 as a structure guiding agent and by adjusting the reaction time [45].

2.4. Emulsion synthesis

A combination strategy of the inverse emulsion crosslinking approach and the colloidal assembly technique has been tested to synthesize Fe_3O_4/histidine composite nanoclusters as new-type magnetic porous nanomaterials (NMs). The nanoclusters possess uniform morphology, high magnetic content and excellent protein adsorption capacity, exhibiting their great potential for bio-separation [46].

2.5. Microbial synthesis

Microbial synthesis of MNPs and Zn-substituted MNPs has been achieved by iron-reducing bacteria (*Clostridium* sp.) using akaganeite (β-FeOOH) or Zn-substituted akaganeite (β-$Zn_xFe_{1-x}OOH$) during glucose fermentation [47]. In another study, framboidal magnetite is formed as a major product in the presence of an electron shuttle [9,10-anthraquinone-2,6-disulfonate (AQDS)] via akaganeite (β-FeOOH) bioreduction by the iron(III)-reducing bacterium (IRB) *Shewanella putrefaciens* CN32 [48]. Microbial synthesis has been tested for preparing magnetically recoverable noble metal NP catalysts. Pd/Fe_3O_4, Au/Fe_3O_4, and PdAu/Fe_3O_4 nanocomposites are biosynthesized by *Shewanella oneidensis* MR-1. Microbial cells firstly transform akaganeite into magnetite, which then serves as support for the further synthesis of Pd, Au and PdAu NPs from respective precursor salts [49]. Compared with engineered MNPs synthesized by chemical approaches, bacterial MMPs have the properties of large production, monodispersity, high crystallinity, and close-to-bulk magnetization, which enable them to be the highly promising MNPs for use in nanobiotechnology [50]. A drawback of microbial synthesis is that the MNPs are likely coated with biomolecules produced by microbial activities that may not be desirable for certain applications. Removal or exchange of such coatings may be necessary.

2.6. Hybrid magnetite nanocomposites

Increasing efforts have been focused on the synthesis and applications of hybrid MNPs by taking advantages of individual NPs and their positive interactions. For example, a combination of superstructure-forming amphiphilic block copolymers and SPION produces new nano/microcomposites with unique size-dependent properties (Fig. 1) [51]. Graphene has been used to form nanocomposites with MNPs to make tunable ferromagnet [52]. A one-pot synthesis of reduced graphene oxide (RGO)/Fe_3O_4 composites has been reported. By the electrostatic interaction of exfoliated GO and Fe^{3+} ions, GO/Fe^{3+} ions are prepared in a diethylene glycol. *In situ* formation of Fe_3O_4 NPs on GO sheets and reduction of GO are then achieved simultaneously by the thermal decomposition reaction of $Fe(acac)_3$ at high temperature [53]. The growth mechanism of magnetic NPs in the presence of graphite oxide (GO) has been investigated by varying the iron precursor dosage and reaction time. The synthesized magnetic NPs are anchored on the GO sheets due to the abundant oxygen-containing functionalities on the GO sheets such as carboxyl, hydroxyl and epoxy functional groups [54]. Superparamagnetic monodisperse Fe_3O_4/GO nanocomposite has been synthesized by a facile one-pot solvothermal synthesis using $FeCl_3{\cdot}6H_2O$ as the iron resource, EG as the reaction solvent, $NaHCO_3$ as the precipitant and adding a GO

suspension to EG solvent [55]. Nanocomposites with ultra-small magnetite (Fe_3O_4) NPs (~3 nm) uniformly anchored on RGO nanosheets have been successfully synthesized for anodes in sodium-ion batteries by a novel single-step high-temperature coprecipitation approach [56]. An *in situ* synthesis of very small MNPs (<12 nm) on the surface of graphene sheets has been achieved through the direct, liquid-phase exfoliation of crystalline graphite and the subsequent chemical functionalization of the graphene sheets *via* the well-established 1,3-dipolar cycloaddition reaction [57]. A magnetic composite of multi-walled carbon nanotubes (MWCNTs) and iron oxide NPs (10–30 nm) has been prepared by chemical precipitation. Transmission electron microscopy (TEM) observation indicates that the iron oxide NPs are highly dispersed on the outer walls of the MWCNTs [58].

The combination of Fe_3O_4 with RGO generates a new hybrid substrate for the dispersion of noble metal NPs. For example, well-dispersed silver (Ag) NPs loaded on the surface of Fe_3O_4 modified RGO have been evaluated with the reduction of 4-nitrophenol (4-NP) into 4-aminophenol with excellent catalytic stability and much higher catalytic activity than the corresponding RGO/Ag catalyst [59]. A novel ternary ZnO/AgI/Fe_3O_4 nanocomposite show superior photocatalytic activity in degradation of rhodamine B (RhB), methylene blue (MB) and methyl orange than that of the ZnO/Fe_3O_4 nanocomposite due to more visible-light absorption ability and efficiently separation of the charge carriers [60].

A simple protocol for covalent immobilization of biotin onto the surface of MNPs for improving the biocompatibility of original MNPs has been realized. MNPs are first prepared by co-precipitation method which is subsequently anchored with functionalized biotin [61]. Nobel metals have been incorporated into MNPs to increase their reactivity. A simple single-step thermal decomposition of Fe(III) acetylacetonate complex, with the presence of silver seeds formed in the same reaction mixture, gives rise to novel compact heterostructures: brick-like Ag@Fe_3O_4 core–shell NPs (Fig. 2) [62]. Magnetic NPs have been synthesized and coated with tetraethyl orthosilicate and aminosilane to create functional amino groups before moxifloxacin is conjugated to the modified MNPs using glutaraldehyde as crosslinker [63].

Starch-coated MNPs have been synthesized by the precipitation–oxidation of ferrous hydroxide method. The size of the as-prepared MNPs is tuned from 15 to 100 nm by changing the time of addition of a starch solution on the reaction system. Also, the starch-coating over MNPs assures good water-dispersibility, stability, and possible biocompatibility (Fig. 3) [64]. A spherical core–shell magnetic agarose nanocomposite has been prepared using a mixture of Fe(II) and Fe(III) salts solution, Span 85 as surfactant and cyclohexane as organic solvent [65]. Coatings have been also applied to microsized magnetite, for example, polypyrrole (PPy)–coated Fe_3O_4 hybrid particles have been synthesized under sonication [66].

Uniquely shaped MNP composites have been synthesized. A hairy core–shell structure is synthesized by combining distillation–precipitation polymerization with subsequent surface-initiated atom transfer radical polymerization [67]. A facile synthesis of rose-like Au/Pd–Fe_3O_4 nanocomposites has been reported *via* controlled thermal decomposition of $Fe(CO)_5$ and reduction of $Pd(OAc)_2$, followed by the immobilization of Au NPs onto the Pd–Fe_3O_4

supports [68]. Magnetic iron oxide@SiO_2–Au@C particles with different shapes, such as pseduocube, ellipsoid, and peanut, have been synthesized using hematite as templates and precursors of magnetic iron oxide (Fig. 4) [69]. The as-obtained magnetic particles demonstrate uniform sizes, shapes, and well-designed core–shell nanostructures. Catalytic performance of the peanut-like particles keeps almost unchanged without a noticeable decrease in the reduction of 4-nitrophenol (4-NP) in 8 min even after 7 cycles, indicating excellent reusability of the particles [69].

Composite thermoplastic elastomers (CTPEs) of copolymer-grafted MNPs have been synthesized and characterized to generate magnetic CTPEs, which combines the magnetic property of MNPs and the thermoplastic elasticity of the grafted amorphous polymer matrix [70]. Calcination of hydrated iron salts in the pores of both spherical and rod-shaped mesoporous silica NPs changes the internal structure from an ordered 2D hexagonal structure into a smaller number of large voids in the particles with sizes ranging from large hollow cores down to ten nanometer voids. The phase of the iron oxide NPs is α-Fe_2O_3 when annealed at 500 °C, and Fe_3O_4 when annealed at lower temperatures [71]. Fe_3O_4/SiO_2 porous nanorods with one-dimensional core/shell structure and high aspect ratio have been synthesized by a wet chemical method. Based on the nanorods, flexible Fe_3O_4/SiO_2/PVDF nanocomposites have been first prepared by embedding the Fe_3O_4/SiO_2 nanorods in a polyvinylidene fluoride (PVDF) matrix. The Fe_3O_4/SiO_2/PVDF nanocomposite shows excellent microwave absorption performance [72]. In another study, the pre-shell-post-core route has been used to synthesize the $Fe_3O_4@SiO_2$ rattle-type nanocomposite [73].

One-dimensional Ag–Fe_3O_4 core–shell heteronanowires have been synthesized by a facile and effective coprecipitation method, in which silver nanowires (AgNWs) are used as the nucleation site for growth of Fe_3O_4 in aqueous solution [74]. In a separate study, a layer of MNPs (50 nm) are synthesized and simultaneously coated on the surface of the polyethylene terephthalate (PET) fabric using $FeSO_4$ as the precursor, NaOH as the precipitant, and sodium dodecyl benzene sulfonate as the dispersant at controlled pH during hydrothermal treatment. The magnetite-coated PET fabric is then modified with silane coupling agent A-151. The capabilities of magnetic response remain unchanged indicating durable washing [75]. Superparamagnetic poly(urea-urethane), PUU, nanocomposites have been obtained by interfacial miniemulsion polymerization with high encapsulation efficiency [76]. Magnetic PVA@Fe_3O_4/CA/AS nanocomposite films (PVA = poly(vinyl alcohol), CA = citric acid, AS = ascorbic acid) containing 4, 8, and 12 wt% of the modified NPs have been successfully manufactured under ultrasonic irradiation [77]. In a separate study, the detailed characterization of core/shell iron-oxide/silica NPs reveals how the superparamagnetic systems are actually composed of a Fe_3O_4 inner core, γ-Fe_2O_3 outer core, iron orthosilicate interphase layer, and exterior silica shell [78]. Chain-like core–shell structure $Fe_3O_4@SiO_2$@chitosan composite NPs have been synthesized by a two-step coating and following crosslinking glutaraldehyde on chitosan shell. The composite particles (105 nm) are nearly monodisperse with a core diameter of 80 nm and chitosan shell thickness of 12 nm (Fig. 5). The composite nanoparticles show a decreasing adsorption in the order, Hg^{2+} > Pb^{2+} > Cu^{2+} in water [79].

Flexible polydopamine (PDA)–$Co_{0.3}Ni_{0.7}Fe_2O_4$@SiO_2 nanofibrous membranes (NFMs) with a hierarchical structure and strong magnetism have been prepared by gelation, calcination and dopamine self-polymerization on electrospun SiO_2 NFMs [80]. Magnetic Fe_3O_4–PDA hybrid hollow microspheres, in which MNPs are firmly incorporated in the cross-linked PDA shell, have been prepared through the formation of core/shell polystyrene spheres/Fe_3O_4–PDA composites based on template-induced covalent assembly method, followed by core removal in a tetrahydrofuran solution. The Fe_3O_4–PDA hybrid hollow microspheres exhibit intrinsic peroxidase-like activity, as they could quickly catalyze the oxidation of typical substrates 3,3′,5,5′-tetramethylbenzidine (TMB) in the presence of H_2O_2 [81]. MNPs have been incorporated into Mg–Al–CO_3 layered double hydroxide (LDH) to remove Cd^{2+} from water by magnetic separation of the immobilized Cd^{2+} via $CdCO_3$ precipitation, surface adsorption and surface complexation [82].

New strategies for the controllable synthesis of complex hollow structures and their application in environmental remediation have been developed. Chinese researchers have reported a facile *in situ* growth process of SiO_2@Fe_3O_4@MnO_2, followed by an etching method to synthesize a hierarchical hollow structure, namely Fe_3O_4@MnO_2 ball-in-ball hollow spheres (Fe_3O_4@MnO_2 BBHs) for degradation of MB by catalytic generation of active radicals from peroxymonosulfate (PMS) [83]. A recent study reports fabrication of rationally-designed multicomponent nanocomposites comprising a magnetite core and an outer silver-decorated anatase shell and their application for visible-light hotodegradation of organic compounds [84]. As research continues, more high performance MNP hybrids are expected to be developed that might open up new application fields in biodetection, biocatalysis, and environmental monitoring.

2.7. Green synthesis

Green chemistry aims at minimizing environmental impact of production and utilization of chemicals including NMs. Eco-friendly green synthesis of NMs involves the use of alternate energy inputs (such as microwave irradiation) and benign reaction media (such as plant extracts and polyphenolic antioxidants) for sustainable applications and environmental remediation [85], [86]. MNPs can be used as a versatile support for functionalization of metals, organocatalysts, N-heterocyclic carbenes, and chiral catalysts. It is used as a support for important homogeneous catalytically active metals such as Pd, Pt, Cu, Ni, Co, Ir, *etc.* to obtain stable and magnetically recyclable heterogeneous catalysts [85]. Research led by Dr. Rajender S. Varma of the United States Environmental Protection Agency (U.S. EPA) has led to the utilization of natural biorenewable resources in nanoparticle synthesis, such as plant extracts and polyphenolic antioxidants from various sources, biodegradable polymers, such as cellulose, reducing sugars, and agricultural residues (beet juice), waste material (red grape pomace) from winery waste, and glycerol (biodiesel byproduct) [87]. His work avoids the use of toxic agents, such as borohydrides, hydrazines, or PVP, producing them in the matrix in which they are to be used thus reducing the risk of exposure or eliminating the use and generation of hazardous substances normally used. His group has developed NPs with a magnetic core, a property that renders them recoverable for reuse [88]. Other groups of researchers have also explored the benefits of green synthesis. For instance, a RGO/Fe_3O_4 based nanocomposite with Pd NPs has been synthesized via a green route by *Withania*

coagulans leaf extract as a reducing and stabilizing agent and its catalytic activity has been tested for the reduction of 4-NP in water with good results. The hydroxyl groups of phenolics in *W. coagulans* leaf extract is directly responsible for the reduction of Pd^{2+}, Fe^{3+} ions and GO [89]. A green synthesis of the Cu/Fe_3O_4 NPs using *Silybum marianum* L. seeds extract and their application as magnetically separable nanocatalyst for the reduction of nitroarenes have been reported [90]. In general, green synthesis is clean, nontoxic, and environment friendly. The synthesized nanocatalyst is recoverable by magnetic decantation and could be reused several times without significant loss in catalytic activity.

3. Fate, transport, and toxicity in the environment

3.1. Dispersion stability

Unlike ferrihydrite NPs that can be dispersed in water to form stable suspension due to their small size [91], suspensions of MNPs are usually unstable in the absence of a stabilizer, although one study claims a stable MNP hydrosol with no added dispersants [92]. The colloidal stability of MNPs is determined by electrostatic or steric repulsion, depending on the stabilizers. Dispersion with tertramethylammonium hydroxide (TMAH) results in a slower settling of the MNPs; however it is not recommended due to its toxicity [93]. Perfluorinated ligand-passivated MNPs have been prepared through a biphasic ligand exchange method. Reducing the O_2 content of the fluorous phase by N_2 bubbling results in a highly stable dispersion of MNPs with a single-particle size distribution maintained due to elimination of O_2 competition for adsorption against carboxylate moieties of ligands during exchange [94].

MNPs are prone to oxidation by oxygen, or corrosion by acid or base. Protection strategies have been developed with a core–shell structure, that is, the naked MNPs as a core is coated by a shell, isolating the core against the environment. Coating materials can be organic compounds such as surfactant and polymers or inorganic substances such as silica, carbon, precious metals or oxides [11]. A technique to solubilize fine magnetic inorganic particles in general organic solvents has been proposed via surfaces modification by long-chain carboxylic acids [95]. A versatile mussel-inspired multidentate block copolymer with pendant multiple catechol groups is an excellent stabilizer of colloidal ultrasmall superparamagnetic MNPs as promising MRI contrast agents [96]. Other polymeric dispersants (PAA: polyacrylic acid, PMA: polymethacrylic acid, PAAMA: polymaleic acid-co-acrylic acid) on the dispersion stability of MNPs have been investigated by the settling test, the transmittance, zeta-potential, and particle size measurements. It is observed that the critical concentration for maximizing the dispersion stability of MNPs is in the range of concentration ratio (dispersant/MNPs) of 0.1–0.01 and the dispersion-stability of MNPs is not improved when the dispersant concentration is above this critical value [97].

3.2. Fate and transport of engineered magnetite nanoparticles

Upon release of engineered NPs into the aqueous environment, their fate and transport and hence their potential environmental and public health impacts will largely depend on how stable these NPs are as suspended particles. Factors such as humic acid (HA) affect surface charge status and aggregation potential of MNPs. At low loadings, the presence of HA can

induce a shift in the point of zero charge (PZC) of MNPs from pH 7.1 to lower values due to partial neutralization of the positive charges on MNPs. At high loadings, however, HA is capable of completely cover magnetite particles giving rise to a suspension Zeta potential similar to its own [98]. Laboratory-scale SPION transport experiments have been conducted using quartz sand columns to study the influence of primary particle size (20 nm and 80 nm) and surface functionalization (plain, –COOH and $–NH_2$ groups) on particle mobility. Particle surface properties (surface functionalization and resulting zeta potential) have a major influence while their primary particle size turns out to be less relevant. In particular, the mobility of SPION is significantly increased in the presence of natural organic matter (NOM) due to the sorption of NOM onto the particle surface resulting in a more negative zeta potential [99]. Compared to nonmagnetic NPs, stability and transport of magnetic NPs are influenced also by the magnetically induced aggregation and retention in that magnetically induced aggregation and subsequent straining results in greater retention [100].

The impact of aggregation state on transport and deposition of MNPs is not fully understood. Instruments such as small-angle X-ray scattering (SAXS) and cryogenic transmission electron microscopy (cryo-TEM) can be used to directly observe the aggregate structure of iron oxides such as ferrihydrite NPs and show how the aggregate structure responds to changing ionic strength [101]. The same approaches can be applied to MNPs. Column tests on ferrihydrite indicate that, for usual ionic strength in European aquifers (2–5 mM), under natural flow condition ferrihydrite NPs are likely to be transported for 5–30 m. For higher ionic strength, corresponding to contaminated aquifers, (*e.g.*, 10 mM) the travel distance decreases to a few meters [91]. MNPs are expected to travel less than ferrihydrite NPs in the same aquifers although such tests are yet to be undertaken. For future applications to aquifer remediation using iron-based NPs, ionic strength and injection rate may be used as tuning parameters to control their mobility in the subsurface and therefore the radius of influence during field injections.

A comparison between laboratory- and field-based investigations into the size-dependent reactivity of MNP has been conducted. Synthetic MNPs (~6 nm, ~44 nm, and ~90 nm) are emplaced in the subsurface of a landfill. Laboratory analog dissolution experiments are conducted using synthetic groundwater. Field results indicate that an organic coating develops on the particle surfaces largely inhibiting reactivity. Limited dissolution of MNPs occur, with the amount of dissolution decrease as particle size decrease. Conversely, the laboratory analogs without organics reveal greater dissolution of the smaller particles. These results show that the presence of dissolved organics leads to a nearly complete reversal in the size-dependent reactivity trends displayed between the field and laboratory experiments indicating that size-dependent trends observed in laboratory investigations may not be relevant in organic-rich natural systems [102]. Sedimentation dynamics and aggregate formation of MNPs for different water flow velocities and starting particle concentrations have been studied recently. Dependence of the sedimentation time on the particle concentration does not follow the trend predicted by theory, the disagreement might be caused by the formation of fractal-like structures [103]. Reactions of goethite and magnetite with sulfide solutions under CH_4 and/or CO_2 atmospheres are monitored *in situ* with Raman spectroscopy. The iron (oxyhydr)oxide minerals are inert to sulfide solution under CH_4 atmosphere, and that the addition of CO_2 to this system triggers the sulfidization reactions

and produces iron monosulfide, mackinawite and pyrrhotite [104]. More such detailed studies are needed to shed more light on the fate and transformation of engineered MNPs in the field and their roles in coupled contaminant degradation in the environment.

3.3. Fate and transport of naturally occurring magnetite nanoparticles

Redox-induced cycling of iron is primarily controlled by microorganisms in the environment. Bacteria grow using both Fe(II) and Fe(III) bound in solid-phase iron minerals, and changing environmental conditions enable the sharing of electrons in mixed-valent iron oxides between bacteria with different metabolisms. This is shown through magnetic and spectroscopic measurements that the phototrophic Fe(II)-oxidizing bacterium *Rhodopseudomonas palustris* TIE-1 oxidizes MNPs using light energy. This process is reversible in co-cultures by the anaerobic Fe(III)-reducing bacterium *Geobacter sulfurreducens* [105]. The activity of microorganisms is a key component of the biogeochemical cycle of iron in natural systems, where MNPs and green rusts are often observed as products of microbially driven redox processes [48]. Transport of naturally occurring MNPs has been rarely studied. More investigation is needed to understand fully how they move, relative to their synthetic counterparts, through geomedia in aquatic environments.

3.4. Toxicity assessment

A few studies have addressed the effects of MNPs on plants. Pumpkin plants (*Cucurbita maxima*), grown in an aqueous medium containing MNPs (20 nm), can absorb, translocate, and accumulate the particles in the plant tissues [106]. The uptake of NPs also depends on plant species as no uptake of MNPs is found to occur by treated lima bean plants (*Phaseolus limensis*). On the other hand, a separate study [107] did not notice any uptake of 25 nm MNPs by the pumpkin plants although MNPs induced more oxidative stress than Fe_3O_4 bulk particles in the ryegrass and pumpkin roots and shoots as indicated by significantly increased: (i) superoxide dismutase and catalase enzyme activities, and (ii) lipid peroxidation. It has been hypothesized that large size NPs cannot penetrate through the cell wall and transportation across the plasma membranes is also limited. The cell wall pore sizes vary from 2 to 20 nm, while the size of ions and water molecules are about 0.28 nm [108].

The genotoxicity of MNP with different particle sizes (10, 30 nm) and surface coatings (PEG or polyethylene glycol, PEI or polyethylenimine) have been assessed using three standard genotoxicity assays, the *Salmonella* typhimurium reverse mutation assay (Ames test), the *in vitro* mammalian chromosome aberration test, and the *in vivo* micronucleus assay. The mutagenicity of MNPs depend on their particle size and surface coating. MNPs with PEG coating exhibit mutagenic activity without chromosomal and clastogenic abnormalities, and smaller MNPs (10 nm) have stronger mutagenic potential than larger ones (30 nm); whereas, MNPs with PEI coating are not genotoxic in all three standard genotoxicity assays [109]. In another study, SPIONs are found not toxic to cells in cell viability assays [110]. No human epithelial cell deaths occur in the presence of SPIONs coated with positively ($–NH_3^+$) and negatively ($–COO^–$) charged shells, but cell proliferation is influenced by surface chemistry. Proliferation reduction is dose dependent and highest for bare SPIONs. Negatively charged SPIONs are the most biocompatible [111].

Administration of Fe_3O_4-ZnO core–shell NPs does not cause significant changes to mice with respect to mortality, clinical observations, body weight, food intake, water consumption, urinalysis, haematology, serum biochemistry, and organ weights [112]. A 52-day continuous semi-static waterborne exposure (test media renewed daily) regimen was employed to investigate the accumulation and elimination profiles of two iron oxide NMs (nano-Fe_2O_3 and nano-Fe_3O_4) in zebrafish (*Danio rerio*). The experiment reveal that: (1) high accumulation of nano-Fe_2O_3 and nano-Fe_3O_4 are found in zebrafish; (2) accumulated NPs in zebrafish can be eliminated efficiently when fish are moved to NP-free water; and (3) iron oxide NPs may be adsorbed via the gastrointestinal tract, and store for more than 12 days [113]. The Fe_3O_4 hexagons coated with a dopamine-based ligand to increase dispersibility in aqueous buffers are only minimally toxic to RAW264.7 cells [114]. Toxicity of sulfhydryl-modified Fe_3O_4@SiO_2 core/shell NPs in mouse fibroblast (L-929) cell lines is low, and the material lacks hemolytic activity, indicating good biocompatibility of this Fe_3O_4@SiO_2@DMSA nanocomposite [115].

The safety of MNPs to human health is still an important topic of debate. A recent study has detected the toxicity and biological behavior of bare MNPs on human umbilical vascular endothelial cells (HUVECs), and demonstrated that bare MNPs disturb the process of autophagy in HUVECs, and eventually lead to endothelial dysfunction and inflammation [116]. A recent literature review [117] suggests that local myocardial delivery of SPION-mediated therapeutic agents might produce myocardial iron overload, resulting in deterioration of myocardial injury and exacerbating cardiac function via oxidative stress mediated iron toxicity, and undermining therapeutic effects. Protective measures should be taken into consideration before developing clinical applications. Given that SPION toxicity mainly stems from oxidative stress, surface modification with an antioxidant (such as N-Acetylcysteine or Trolox) may be a new method to suppress oxidative damage and injury. The thiolated SPIONs with mercaptosuccinic acid (MSA) and cysteine (Cys) have no toxic effects for stem cells [118]. Long-term *in vivo* studies in murine models have shown that dimercaptosuccinic acid (DMSA)-coated MNPs accumulate in spleen, liver and lung tissues during extended periods of time (at least up to 3 months) without any significant signs of toxicity detected [119]. On the other hand, polyethylene glycol (NP-PEG-$(NH_2)_2$)-coated MNPs show a delay in the arrival of the particles to the liver tissue. Superparamagnetic Fe_3O_4 supraparticles@MIL-100(Fe) (MIL: Materials of Institut Lavoisier) core–shell nanostructure microspheres show a good biocompatibility in the *in vitro* cytotoxicity test [120]. More research is needed to fully understand the degree of toxicity of MNPs to humans and organisms.

4. Environmental analytical chemistry and catalysis

4.1. Sensors and measurements

A previous review has summarized and discussed various sensing applications of iron oxide NPs in biomedical fields (Fig. 6) [121]. Nanocomposites such as Fe_3O_4@Au hybrids offer novel opportunities for designing new electrochemical aptasensors with unique versatility for binding diverse targets, including proteins and peptides. MNP based immunosensors are used for the detection of biological and chemical pathogens, contaminants, and other

important analytes [121]. A sensitive H_2O_2 biosensor for evaluation of oxidative stress has been fabricated on the basis of the RGO nanocomposites decorated with Au, Fe_3O_4, and Pt NPs (RGO/AuFe_3O_4/Pt) modified glassy carbon electrode (GCE) and used to detect the released H_2O_2 from cancer cells and assess the oxidative stress elicited from H_2O_2 in living cells [122]. A biosensor for glucose detection has been developed using water-dispersible and biocompatible chitosan-functionalized graphene (CG) and MNPs with a detection limit of 16 μM, and a linear detection range up to 26 mM glucose. This may allow for applications in more clinical areas such as *in vivo* biosensors and MRI agents [123]. A microscale well-plate colorimetric assay for the multiplexed detection of glucose and cholesterol in clinical human blood samples has been developed utilizing one-pot nanocomposite entrapping MNPs as peroxidase mimetics and glucose oxidase (GOx)/ cholesterol oxidase (ChOx) in mesoporous silica [124]. A magnetic core-plasmonic shell nanoparticle attached to hybrid GO based multifunctional nanoplatform has the capability for highly selective separation of Alzheimer's disease biomarkers from whole blood sample, followed by label-free surface enhanced Raman spectroscopy (SERS) identification in femto gram level [125]. MNPs have been used as a component to fabricate a bimodal nanohybrid for the luminescent ON/OFF detection of glutathione [126]. An electrochemical immunosensor based on MNPs has been developed to determine microcystin-(leucine-arginine) in river water [127]. Vanillin molecularly imprinted stir bar has been constructed based on Fe_3O_4@Polyaniline NPs with magnetic field-induced self-assembly process. The molecular imprinting stir bar shows superior selectivity and fast binding kinetics for vanillin, and is used for the enrichment of vanilla-flavor enhancers (vanillin, ethyl maltol and methyl vanillin) in infant milk powders before measurement by high performance liquid chromatography (HPLC)-UV [128]. A sensing methodology that combines magnetic separation (MS) and magnetic relaxation switching (MS-MRS) for one-step detection of bacteria and viruses has been reported. Compared with a traditional MRS sensor, an MS-MRS sensor shows enhanced sensitivity, better reproducibility, and convenient operation, thus providing a promising platform for point-of-care testing [129]. A protease-activated ratiometric fluorescent probe based on fluorescence resonance energy transfer between a pH-sensitive fluorescent dye and biocompatible MNPs has been constructed to image the pH of subcutaneous tumor xenografts [130].

A multifunctional probe consists of a ternary nanocomposite of magnetite/ceria-codecorated titanoniobate nanosheet (MC-TiNbNS) is utilized for the enrichment and dephosphorylation of phosphopeptides [131]. A new type of magnetic halloysite nanotubes molecularly imprinted polymer (MHNTs@MIP) based on halloysite nanotubes (HNTs) with embedded MNPs has been prepared through surface imprinting technology, using 2,4-dichlorophenoxyacetic acid (2,4-D) as a template, 4-vinylpyridine as the monomer, divinylbenzene as cross-linking agents, and 2,2-azodiisobutyronitrile as initiator (Fig. 7) [132]. Magnetic cyclodextrin nanocomposites (β-CD-Fe_3O_4) could detect and remove β-naphthol from wastewater as a spectral probe [133].

Selective and magnetic separation of various biological molecules can be accomplished by engineering the surface of MNPs. For example, MNPs with high magnetization and an amino-functionalized surface have been used to magnetically separate prevalent urinary crystals in the patient's urine [134]. A MNP-based assay has been developed for the

detection of bacteria (*Escherichia* coli, *Proteus* mirabilis and *Pseudomonas* aeruginosa) causing urinary tract infections in patient samples with a much improved efficiency [135]. MNPs are used to separate amyloid beta (Aβ) protein aggregates, which include fibrils and oligomers that are neurotoxic and are considered to cause Alzheimer's disease from biological samples [136].

MNPs are also used in inorganic analytical chemistry. A new magnetic adsorbent, 3-mercaptopropionic acid coated 3-aminopropyl triethoxysilane modified MNPs, is used for the extraction and preconcentration of arsenic ions in aqueous solutions followed by determination using electrothermal atomic absorption spectrometry (AAS). Under the optimum conditions, wide linear range of 30–25,000 ng L^{-1} and low detection limit of 10 ng L^{-1} are obtained [137]. An coupled Au/Fe_3O_4/GO hybrid material improves the catalytic activity, stability, and separation capability of AuNPs and Hg^{2+} [138]. Multiwalled carbon nanotubes (MWCNTs) have been modified by MNPs with application for the preconcentration of cadmium [139], [140] and lead [139] prior to analysis by AAS. Hydrophobic ionic liquid as a green coating agent is deposited on the surface of synthesized MNPs to improve their extraction capability toward Pd(II) ions as diethyldithiocarbamate (DDTC) complex [141]. Magnetic core–shell silica NPs modified by 3-[2-(2-aminoethylamino) ethylamino]propyl-trimethoxysilane are used as a new adsorbent for simultaneous extraction and preconcentration of bismuth and lead ions through magnetic solid-phase extraction (MSPE) method. After adsorption, these ions are desorbed with nitric acid followed by determination with electrothermal AAS [142]. Novel dipyridile-modified MNPs have been used for the extraction and determination of low levels of Pb^{2+} ions in various samples of rice, baking powder, wheat, and other foodstuffs [143]. MNPs coated with either dopamine or glutathione have been developed as a new, simple and reliable method for the separation/pre-concentration of trace amounts of AgNPs followed by their quantification using inductively coupled plasma mass spectrometry (ICP-MS). The MNPs selectively captures AgNPs in a mixture containing both nano-particulate and ionic silver, which addresses the challenges of separation and quantification of AgNPs in addition to the total silver in environmental samples [144]. Chinese scientists have reported novel phosphatidylserine-functionalized Fe_3O_4@SiO_2 NPs and enzyme-encapsulated liposomes for the visual detection of Cu^{2+} by employing phosphatidylserine for Cu^{2+} recognition and the enzymatic catalysis/oxidation of 3,3′,5,5′-tetramethylbenzidine sulfate (TMB) as a signal generator. It can be used to detect as little as 0.1–0.5 μM of Cu^{2+} in river water using naked-eye observation and 0.05 μM of Cu^{2+} in river water using UV–vis spectrophotometry. These detection limits are much lower than the maximum allowable level of Cu^{2+} (~20 μM) in drinking water defined by the USEPA [145].

MNPs have been used to construct a novel nitrite sensor by electropolymerization of alizarin red on the surface of glassy carbon electrode modified with Fe_3O_4-MWCNT composite nanofilm [146]. In another study, an electrochemical sensor has been developed based on the functionalized graphene anchored with MNPs and loaded on a glassy carbon electrode (GCE) for the detection of nitrite in tap, river and rain water samples [147]. Fluorescent chemosensors containing MNPs have been developed for detecting anions such as ClO^- and SCN^- [148]. A robust reusable fluoride sensor comprised of a receptor in charge of the chemical recognition and a fluorophore responsible for signal recognition has been

designed. Highly fluorescent carbon quantum dot (CD) and magnetically separable nickel ethylenediaminetetraacetic acid (EDTA) complex bound-silica coated MNPs (Fe_3O_4@SiO_2–EDTA–Ni) are used as fluorophore and fluoride ion receptor, respectively [149]. A highly efficient MRS system based on poly(vinyl alcohol) functionalized nanomagnetic iron oxide (PVA@NMIO) particles detects boric acid or borate ester (BA/BE) [150].

MNPs have been used as a component in the substrate for surface-enhanced Raman scattering (SERS) techniques. For example, Fe_3O_4@Au NPs are assembled into arrayed microstructures on a wafer scale with enhancement factors > 10^6 [151]. Ag-coated magnetic core–shell microspheres (Fe_3O_4@PEI@Ag) has been developed using polyethyleneimine (PEI) as an interlayer to construct a versatile SERS substrate, which is verified by the detection of adsorbed *p*-aminothiophenol molecules and human IgG with a detection limit as low as 10^{-11} M and 10^{-14} g mL^{-1}, respectively (Fig. 8) [152]. Ag–Fe_3O_4 nanocomposites are assembled into an orderly arrayed SERS substrate holding clean and reproducible properties with an applied external magnetic field for detection of 4-mercaptobenzoic acid. The enhancement factors (EF) on the SERS substrate are up to 5.2×10^6 and the detection limit is down to ~10^{-10} M [153]. Rapid and sensitive SERS identification and quantification of arsenic species in multiple matrices have been realized using a Fe_3O_4@Ag magnetic substrate with a portable SERS sensor for onsite monitoring of arsenic speciation determination of As(III) and As(V). The entire process can be completed within 2 min. Moreover, the active SERS substrate can be used for As sensing in complex media such as juice, wine, and soils [154]. Quick and reliable measurements of contaminants in environmental media are in great need for monitoring and remediation decision-making. More fruitful discoveries can be made to take advantages of MNPs in sample pre-concentration and detection of a wider range of target compounds.

4.2. Enzyme carrying and recycling

MNPs and their hybrids are known to adsorb proteins including enzymes. For example, uniform superparamagnetic Fe_3O_4/carboxymethyl chitosan composite nanospheres [155] and the core–shell structure Fe_3O_4/SiO_2 magnetic icrospheres/nanospheres [156] show fast and efficient lysozyme adsorption. It is still a great challenge to deliver proteins and peptides with excellent bioactivity and controlled release. In a recent study, a pH-responsive delivery system has been obtained by anchoring 8-nm MNPs onto mesoporous support (SBA-15) (0.6–1 μm with a pore size of 6.2 nm). The pH-stimulative response is based on the interaction between the tris(aminomethyl)ethane (TAE) groups anchored onto the pore outlet of mesoporous silica scaffolds and the carboxybenzaldehyde (CBA) groups coated on the MNPs, which can lead to a rapid release under the acid condition (pH = 5) and a zero release with the increase of pH value (pH = 7.4) [157]. Enhancement of enzyme activity and enzyme recycling has been achieved by magnetic spherical polyelectrolyte brushes (MSPB) [158]. A magnetic enzyme nanosystem has been constructed with defined core–shell structure for rapid, efficient, and reusable tryptic digestion of proteins [159]. Magnetic chitosan/Fe_3O_4 NPs modified by 3-aminopropyltriethoxysilane have been used as carriers for the immobilization of pullulanase (a debranching enzyme) with high stability and activity. Immobilized pullulanase exhibits good resistance to metal ions and detergents [160]. Magnetic Fe_3O_4@SiO_2 NPs have been prepared with molecular imprinting method

using cellulase as the template. And the surface of the NPs is chemically modified with arginine. The prepared NPs are used as support for specific immobilization of cellulase. The half-life of the immobilized cellulase is 2-fold higher than that of the free enzyme at 50 °C [161]. These studies suggest that the prepared imprinted NPs have the potential industrial applications for the purification or immobilization of enzymes.

4.3. Recyclable magnetite catalysts and magnetite-supported catalysts

MNPs are popular materials used in the field of catalysis as they combine interesting reactivity with an easy, economical and environmentally benign mode of recovery. A recent review has summarized the recent progress made in the assembly of magnetic NPs and their direct application in catalysis with examples of such bare NPs including iron oxide (Fe_2O_3 and Fe_3O_4), metal ferrites (MFe_2O_4, M = Cu, Co and Ni), Fe^0, Co^0, Ni^0, and multi-component NPs [162]. Another recent review has focused on the magnetic NP surface functionalization by different species such as inorganic, organic, silane reagents and biomolecules, biomolecules immobilization methods and their potential applications in catalysis [163]. Photocatalytic degradation of toxic organic pollutants in the magnetic iron oxide–semiconductor composite photocatalytic system can effectively break through the bottleneck of single-component semiconductor oxides with low activity under visible light and the challenging recycling of the photocatalyst from the final products [164]. There are crucial steps in precious- and nonprecious-metal-catalyzed CC and CX coupling reactions by using magnetically separable catalysts [165].

Halogenated organic compounds can be selectively removed from wastewater by using PdNPs on magnetite catalyst (Pd/Fe_3O_4), which is very active and magnetically extractable. This technique is sensitive to the presence of heavy metals and sulphides, which is a drawback. These components require removal before catalysis by Pd for dehalogenation [166]. A novel core–shell structural Fe_3O_4@MgAl-LDH@Au nanocatalyst exhibits excellent activity for the oxidation of 1-phenylethanol [167]. MNPs are effectively employed as heterogeneous catalyst for hydrogenation of ketone moiety to alcohol moiety by $NaBH_4$ under the microwave radiation process [168]. An efficient and benign protocol has been reported for the synthesis of medicinally important pyrazole derivatives, 4-methoxyaniline, and Ullmann-type condensation reaction using MNPs (20–30 nm)-supported CuO NPs and the catalysts are recycled six times without loss in catalytic activity [169].

Water dispersible Fe_3O_4@carbon quantum dots (CQDs) hybrid nanoflowers show highly efficient photocatalytic activities because of their strong absorption in the visible light range and upconversion photoluminescence. The MNPs not only allow efficient magnetic separation and recycling of the photocatalyst, but also promote the photocatalytic activities of the CQDs [170]. MNPs coated with amino functional groups allow for amide bond formation with the carboxylic acid groups on zinc tetra- or octa-carboxyphthalocyanine (ZnTCPc or ZnOCPc respectively) [171]. Alumina-supported MNPs are used in hydrazine-mediated heterogeneously catalyzed reductions of nitroarenes to anilines [172]. Magnetically recoverable catalysts have been prepared by thermal decomposition of palladium acetylacetonate in the presence of MNPs. These NP mixtures are able to perform selective hydrogenation of 2-methyl-3-butyn-2-ol to 2-methyl-3-buten-2-ol, demonstrating

clear differences in catalytic behavior depending on the catalyst structure (Fig. 9) [173]. Monodisperse magnetic sandwiched Fe_3O_4@Au//poly(ethyleneglycol methacrylate) (Fe_3O_4@Au/PEGDMA) core–shell microspheres show effective catalytic reduction of 4-NP to 4-aminophenol (4-AnP) [174].

Nanometer-sized magnetic stirring bars containing PdNPs (denoted as Fe_3O_4-NC-PZS-Pd) for heterogeneous catalysis in microscopic system have been developed for the hydrogenation of styrene and Fe_3O_4-NC-PZS-Pd show an activity similar to that of the commercial Pd/C catalyst, but much better stability. And the stirring bars display far better catalytic activity than the commercial Pd/C for the hydrogenation of MB [175]. The magnetically separable Pd nanocatalyst prepared by reacting palladium acetate with acetylacetonate-functionalized doubly silica-coated magnetic NPs is active for Suzuki cross-coupling reaction of acyl halides with boronic acids [176]. Surface modification of MNPs with triethoxyethylcyanide groups has been used for the immobilization of PdNPs to produce Fe_3O_4/Ethyl-CN/Pd for catalyzing the Suzuki cross-coupling reaction of various aryl halides (ArI, ArBr, ArCl) with phenylboronic acid in aqueous phase [177]. In another study, Pd-Fe_3O_4 composite NPs supported on graphene (Pd/Fe_3O_4/G) are used for Suzuki and Heck carbon–carbon coupling reactions [178]. A novel strategy to construct magnetic recyclable hollow capsules with Pd and MNPs embedded in polypyrrole (PPy) shell has been reported for the reduction of 4-NP by $NaBH_4$. Compared with bare Pd and Fe_3O_4 NPs, the stability of both Pd and Fe_3O_4 NPs in hollow capsules is largely improved owing to the protection of PPy shell [179].

A novel nanomagnetic basic catalyst of Cs_2CO_3 supported on hydroxyapatite-coated $Ni_{0.5}Zn_{0.5}Fe_2O_4$ magnetic NPs ($Ni_{0.5}Zn_{0.5}Fe_2O_4$@HAP-Cs_2CO_3) has been used for the preparation of pyrazolo[1,2-*b*]phthalazine-5,10-diones [180]. A magnetic Fe_3O_4/BiOCl nanocomposite is prepared by a facile deposition–precipitation process that displays excellent catalytic activity for the photodegradation of RhB under simulated solar light irradiation [181]. Magnetically separable ternary g-C_3N_4/Fe_3O_4/BiOI nanocomposites show novel visible-light-driven photocatalysis in degradation of RhB, MB, and methyl orange under the visible-light irradiation. The excellent activity of the magnetic nanocomposite is attributed to more harvesting of the visible-light irradiation and efficiently separation of the electron–hole pairs [182]. Nanomagnetic Fe_3O_4-Cu(II)-Schiff base is a highly active and selective catalyst for the oxidation of sulfides and thiols by H_2O_2 [183].

A facile Cu_2O@Fe_3O_4-catalyzed cyclization of ene-yne-ketone for the formation of CO and CC double bonds to prepare furans has been reported [184]. A series of magnetically separable catalysts based on Co–Rh bimetallic compounds supported on MNPs have been tested for dicyclopentadiene (DCPD) hydroformylation reactions, achieving excellent selectivity and conversion [185]. The hydrogenation of nitrobenzene is catalyzed over magnetically recoverable Pt deposited on MWCNTs with high yield of aniline [186]. A new family of Zn-containing magnetic oxides of different structures has been developed for syngas conversion to methanol [187]. A magnetic GO-loaded Ce-doped titania (MGO–Ce–TiO_2) hybridized composite exhibits good adsorption capacity, high visible-light photoactive and magnetic separability as a novel photocatalyst in the degradation of antibiotic tetracyclines (TC) [188]. Maghemite/magnetite NPs functionalized with TiO_2 show up to

89% of phenol photodegradation under UV irradiation [189]. So far most studies have been conducted in simple synthetic aqueous solutions. Information is lacking about the performance of the MNP based catalysts in real environmental media. Future investigations should focus on the improvement of the longevity of the catalysts in real world applications.

4.4. Activation of oxidants for organic contaminants degradation

MNPs have been studied for the activation of PMS to generate active radicals for degradation of pharmaceutical acetaminophen (APAP) in water. The MNPs effectively catalyze PMS for removal of APAP, and the reactions well follow a pseudo-first-order kinetics pattern. Higher MNP dose, lower initial APAP concentration, neutral pH, and higher reaction temperature favor the APAP degradation [190]. MNP-activated persulfate oxidation for trichloroethene (TCE) shows a great potential for the practical application of this technique in *in situ* TCE-contaminated groundwater remediation [191]. Dinitrotoluene is effectively degraded by H_2O_2 with MNPs at pH 1–9 with the optimal pH 3 [192]. Magnetic CuO-Fe_3O_4 composite is used as a heterogeneous catalyst for phenol degradation by persulfate [193]. A polyhydroquinone (PHQ)-coated Fe_3O_4/MWCNTs/PHQ catalyst has been used to degrade antibiotic flumequine (FLU) by persulfate oxidation from which two possible pathways are proposed involving hydroxylation, decarbonylation, and ring opening (Fig. 10) [194].

Magnetic core/shell nanospheres (MCS, Fe_3O_4/carbon) have been synthesized by a hydrothermal method and their supported manganese oxide NPs (Mn/MCS) have been obtained by redox reactions between MCS and $KMnO_4$. The Mn/MCS catalysts are able to effectively activate $KHSO_5$ for phenol degradation in aqueous solutions. Sulfate radicals are suggested to be the primary reactive species generated from PMS for phenol catalytic oxidation (Fig. 11) [195]. 3D flower-like microspheres constructed by 2D Bi_2WO_6 nanosheets loaded with spherical MNPs have been used as a photocatalyst to degrade RhB under visible light irradiation assisted with H_2O_2 [196]. The heterogeneous UV/Fenton degradation of tetrabromobisphenol A (TBBPA) is catalyzed by nanocrystalline Fe_3O_4 and $Fe_{2.04}Cr_{0.96}O_4$. The substitution of chromium greatly increases the BET specific surface area and surface hydroxyl amount, which improves the heterogeneous UV/Fenton catalytic activity of magnetite [197]. MNPs (~12 nm) show good oxidative capacity to promote heterogeneous Fenton-like reactions for the removal of nalidixic acid (NAL), a recalcitrant quinolone antibacterial agent. It is suggested that oxidative degradation of adsorbed NAL is by reactive oxygen species (ROS) produced via oxidation of both dissolved and structural Fe^{2+} ions [198]. Functionalized MNPs in alginate beads is used in the advanced Fenton oxidation of a malodorous compound (3 methyl-indole: 3-MI) without significant leaching of iron [199]. A magnetic photocatalytic $CoFe_2O_4$/g-C_3N_4 composite degrades MB in aqueous medium under visible light irradiation [200]. Novel $CuFe_2O_4$@C_3N_4 core–shell photocatalysts show photo Fenton-like discoloration of Orange II dye using H_2O_2 as an oxidant under visible-light irradiation [201]. MNPs prepared by steel pickling waste liquor to reduce the cost of preparation are comparable to those obtained by the common co-precipitation method for the heterogeneous Fenton-like catalytic degradation of bisphenol A (BPA) [202]. Oxidative removal of BPA involving PMS activated by $CuFe_2O_4$ magnetic NPs

is through surface-bound, rather than free radicals generated by a surface catalyzed-redox cycle involving both Fe(III) and Cu(II) [203].

MNPs synthesized in diethylene glycol in the presence of carboxylic acids can be easily dispersed in aqueous media and other polar solvents due to being coated by a layer of hydrophilic polyol and carboxylic acid ligands *in situ*. They are an active, recyclable, and highly selective catalyst for the epoxidation of cyclic olefins with H_2O_2 [204]. Magnetic microspheres (Fe_3O_4/Cu) reduce and degrade RhB and MB in the presence of $NaBH_4$ [205]. Fe_3O_4@SiO_2@HPW (12-tungstophosphoric acid) NPs show excellent photocatalytic efficiency for the degradation of RhB under UV light irradiation [206]. Reusable TiO_2/graphene nanocomposites responsive to external optical and magnetic fields are used to degrade MB in simulated solar light resulting in excellent photocatalytic performance [207]. Ferrite NPs similar to MNPs, such as $CoFe_2O_4$ catalyze the oxidation of benzyl alcohol (BzOH) to benzaldehyde (BzH) with H_2O_2 under solvent-free conditions [208]. In another study, with titanate nanotubes (TNTs) as catalyst support, a novel $CoFe_2O_4$/TNTs hybrid has been constructed for decomposition of RhB by PMS. Compared to the pure $CoFe_2O_4$, the as-prepared $CoFe_2O_4$/TNTs not only exhibits better performance, but also realizes higher total organic carbon removal and less cobalt leaching, which is attributed to the enhanced catalytic ability from smaller $CoFe_2O_4$ NPs and the unique ion-exchange ability from TNTs support [209]. The performance of MNP based catalysts for *in situ* oxidation of contaminants in soil and groundwater has not been fully evaluated. Laboratory tests give detailed information about possible mechanisms, yet field tests are required to validate the potential for practical applications.

4.5. Polymerization of organic compounds

The spontaneous surface induced polymerization of dissolved organic matter on environmental mineral particles has been demonstrated with carboxylated core–shell MNPs by using a ubiquitous polyphenolic precursor. Through the adsorption and *in situ* surface polymerization of gallic acid (GA), a polygallate (PGA) coating is formed on the MNPs (PGA@MNP) with possible antioxidant capacity. Observed also is the formation of ester and ether linkages between gallate monomers both in solution and in the adsorbed state. Higher polymers are formed in the course of several weeks both on the surface of MNPs and in the dispersion medium. The ratio of the absorbances of PGA supernatants at 400 and 600 nm (*i.e.*, the E4/E6 ratio commonly used to characterize the degree of polymerization of humic materials) is determined to be 4.3, similar to that of HA [210]. The implications that the MNPs may be involved in the formation of humic substances in nature merits further investigation.

5. Air cleanup

Table 2 lists examples of MNP based NMs for environmental applications including air cleanup. MNPs have been used as an adsorption interface for the concurrent removal of gaseous benzene, toluene, ethylbenzene and m-xylene (BTEX), and SO_2 [211]. Pt decorated octahedral Fe_3O_4 catalyst prepared by addition of a Pt^{4+} and Fe^{2+} mixture into a KOH solution leads to the simultaneous formation of an octahedral Fe_3O_4 and *in situ* reduction of

Pt^{4+}, which exhibits excellent catalytic activity for CO oxidation under moisture conditions [212]. In another study, Pd NP catalysts supported on Fe_3O_4, Co_3O_4, and $Ni(OH)_2$ nanoplates are used in the low temperature oxidation of CO and the Pd/Co_3O_4 catalyst has particularly high activity for CO oxidation as a result of the strong interaction between the Pd NPs and the Co_3O_4 nanoplates [213]. PtNPs (1.2 ± 0.1 nm) synthesized *in situ* on MNPs (32 nm) previously deposited on alumina supports, is highly active towards the preferential oxidation of CO in a H_2-rich reformate stream and gives 100% CO conversion at 25 °C. Although the preferential oxidation of CO in H_2-rich stream is used in the production of clean H_2 for H_2-based fuel cells, this catalyst can be used for CO removal from contaminated air [214]. Composites of magnetite and two-line ferrihydrite with GO have been tested as H_2S adsorbents (Fig. 12) [215]. The addition of GO increases the surface area of the composites due to the formation of new micropores, leading to an increase in the H_2S adsorption capacity; the opposite effect is recorded for the ferrihydrite composites [215]. Magnetic $TiO_2@SiO_2@Fe_3O_4$ and $Cu/TiO_2@SiO_2@Fe_3O_4$ photocatalysts show good catalytic activity in the CO_2 reduction reaction to produce methanol and the addition of Cu improves the productivity [216].

6. Wastewater and surface water treatment

6.1. Magnetic antimicrobial agents for water disinfection

Efficient disinfection and microbial control without harmful disinfection byproducts can be achieved with the use of MNPs based antibacterial material that can be recovered readily from matrix solution for reuse with an external magnetic field, avoiding waste of the disinfectant and possible contamination of the residual disinfectant to environment. Magnetic graphene–carbon nanotube iron nanocomposites inactivate Gram-positive (*e.g.*, *Staphylococcus* aureus) and Gram-negative (*e.g.*, *E. coli*) bacterial species [217]. Highly efficient recyclable antibacterial MNPs, consisting of a Fe_3O_4 core with an antibacterial poly quaternary ammonium (PQA) coating, show 100% biocidal against *E. coli* [218]. Magnetic GO (MGO) with MNPs well dispersed on GO nanosheets exert excellent antibacterial activity against *E. coli*. The inactivation mechanism of *E. coli* by M-GO includes both the membrane stress and oxidation stress during the incubation period [219]. PEG-coated MNPs functionalized with H-RWRWRW-NH_2 ((RW)3), an antimicrobial peptide, is used as a novel magnetic-responsive support against *E. coli* and *Bacillus* subtilis 168 [220]. MNPs pre-coated with oleic acid and bearing novel antimicrobial N-heterocyclic choline analogues, namely *O*-, *N*- and *O*,*N*-bis-undecyl-substituted *N*-(2-hydroxyethyl)-1,2,3,4-tetrahydroisoquinolinium derivatives, are effective antimicrobial therapy for Gram-positive (*S. aureus*, *Bacillus cereus*) and Gram-negative (*E. coli*, *P. aeruginosa*, *P. mirabili*) bacterial strains and fungi (*Candida albicans*, *Aspergillus* niger) [221].

Conjugation with silver gives MNPs wider applications. MNPs are coated with a PDA layer through the autopolymerization of dopamine and subsequently, Ag^+ ions are directly reduced into AgNPs by the PDA coating and the AgNPs (15 nm) are inlaid homogeneously and tightly onto the Fe_3O_4@PDA NPs to form Fe_3O_4@PDA@Ag magnetic composite. The obtained material has enhanced antibacterial ability due to the plenty of AgNPs immobilized on the PDA coating against *E. coli* and *S. aureus* [222]. The antibacterial film prepared from

$Ag_3PO_4/TiO_2/Fe_3O_4$ nanocomposite presents excellent bactericidal activity and recyclability toward *E. coli* cells under visible-light irradiation. In addition to the intrinsic cytotoxicity of silver ions, the elevated bactericidal efficiency of $Ag_3PO_4/TiO_2/Fe_3O_4$ is largely attributed to its highly enhanced photocatalytic activity. The photogenerated hydroxyl radicals and superoxide ions on the formed $Ag/Ag_3PO_4/TiO_2$ interfaces cause considerable morphological changes in the microorganism's cells and lead to the death of the bacteria [223]. AgNPs deposited onto mesoporous composite particles of carbon inlaid with MNPs (Ag–Fe_3O_4@carbon) with a novel bowl structure show efficient antibacterial activities to *E. coli* and *S. aureus*, as well as high catalytic activity to the reduction of 4-NP by $NaBH_4$ [224]. AgNP-decorated magnetic GO (MGO-Ag) exhibits excellent antibacterial activity against *E. coli* and *S. aureus* [225]. Ag-$CoFe_2O_4$-GO exhibits excellent antibacterial activity against *E. coli* and *S. aureus* compared with $CoFe_2O_4$, Ag-$CoFe_2O_4$, and $CoFe_2O_4$-GO composite. This superior disinfecting effect is possibly attributed to the combination of GO nanosheets and AgNPs [226]. Cu_2O NPs functionalized with $NiFe_2O_4$ induce magnetomechanical stress and alteration of cellular membrane integrity and programmed cell death signaling in the yeast, *Saccharomyces* cerevisiae [227]. Chitosan is a naturally occurring biopolymer that is biocompatible, antifungal and antibacterial with wound healing ability, anticancerous property, anticholesteremic properties, and immunoenhancing effect. MNP doped chitosan beads are reusable agents against *E. coli* and *S. aureus* [228]. Algicidal bacteria offer a promising option for killing cyanobacteria. In a recent study, a newly isolated strain of *Bacillus methylotrophicus*, ZJU, has been used to control *Microcystis* aeruginosa. The strain ZJU as an algicidal agent is embedded in MNPs and wheat bran in the process of immobilization. The magnetization enables efficient re-collection of the immobilized bacteria by magnetic means [229].

6.2. Modification of nanocomposite membrane and flocculation of wastewater

MNP doped nanocomposite membrane has been made by synthesizing MNPs through co-precipitation, blending with polysulfone/*N*-methylpyrrolidone solution, and finally, dispersing in membrane structure after coagulation of casted polymeric solution. An increase in MNP concentration in membrane matrix causes permission flux to rise. On the other side, any increases in MNP content improves dyes dispersion and polyethylene glycol rejection as organic contaminant [230]. Economic and rapid removing of turbidity and reduction of sludge water content in sewage wastewater could be achieved with MNPs [231].

6.3. Adsorptive and separative removal of organic contaminants

Separation of ionic dye pollutants from aqueous solutions is often necessary in environmental cleanup. MNPs show MB dye adsorption [232]. Amine functionalized magnetic CNTs effectively remove cationic dyes from binary systems [233]. HA coated MNPs remove MB from aqueous solution [234]. Mesoporous-silica-capped Fe_3O_4 mesoporous clusters exhibit excellent adsorption of MB from aqueous solution and is easily regenerated by the photo-Fenton degradation reaction as a result of its high specific surface area, accessible pore channels, and good magnetic separation properties [235]. Fe_3O_4/GO nanocomposites effectively remove Congo red as an anionic dye and MB as a cationic dye in aqueous solutions [236]. A C18-functionalized core–shell magnetic mesoporous silica composite ($Fe_3O_4/mSiO_2$-C18) has excellent adsorption ability toward MB dye due to the

large surface area and the abundant hydrophobic C18 groups [237]. Reversible pH-responsive behavior and controlled adsorption/desorption of MB have been demonstrated on hybrid materials consisting of polyacid brushes using poly(itaconic acid) (PIA) and poly(acrylic acid) (PAA) at the amine functional groups of chitosan and MNPs [238].

Magnetic Fe_3O_4 chitosan NPs (m-Fe_3O_4-CNs) adsorb bromothymol blue (BB) from aqueous solutions [239]. Sunset yellow anionic dye is removed by aminopropyltriethoxysilane modified MNPs [240]. A Fe_3O_4/metal-organic frameworks (MOFs) composite adsorbs MB and methyl violet from an aqueous solution and the used Fe_3O_4/MOFs could be regenerated by acetonitrile [241]. Magnetic modified corncobs show good adsorption performances for Congo red [242]. MWCNTs decorated with MNPs are modified by polyaniline to remove methyl orange and Congo red [243]. Magnetically responsive RGO is used to prepare Pickering emulsions especially for water-in-oil emulsions that is used to remove Nile red dye from dodecane [244]. Fe_3O_4@3-aminophenol-formaldehyde (Fe_3O_4@APF) core–shell resin polymer magnetic nanocomposites are excellent adsorbent for the removal of methyl blue [245]. Fe_3O_4/chitosan/TiO_2 nanocomposites show good adsorptive, photocatalytic, regenerated, and magnetic properties for degradation of MB in wastewater [246].

A novel multifunctional microsphere with an iron oxide-improved mesoporous silica shell and a Fe_3O_4@SiO_2 core (Fe_3O_4@nSiO_2@mSiO_2-Fe core–shell) are utilized as a catalyst for the removal of 1,1,1-trichloro-2,2-bis(4-chlorophenyl) ethane (DDT) and its derivatives, *i.e.*, 1,1-dichloro-2,2-bis(4-chlorophenyl) ethane (DDD) and 1,1-dichloro-2,2-bis(4-chlorophenyl) ethylene (DDE) [247]. Magnetic MWCNTs nanocomposite has been used for removal of four nitrofurans, namely, furazolidone (FZD), nitrofurazone (NFZ), nitrofurantoin (NFT), and furaltadone (FTD) from aqueous solution [248]. Magnetic core–shell Fe_3O_4@layered double oxide (Fe_3O_4@LDO) microspheres remove more 2,5-dihydroxybenzoic acid (2,5-DHBA) from aqueous samples compared with Fe_3O_4@LDH (Fig. 13) [249]. Novel mesoporous cetyltrimethylammonium bromide (CTAB)-functionalized magnetic microspheres with a core/shell structure (mesoporous Fe_3O_4@SiO_2@CTAB-SiO_2) effectively remove perfluorooctane sulfonates (PFOS) from water at acidic conditions (pH = 3) [250].

Pharmaceuticals such as antibiotics in aquatic environments poses potential risks to the ecology and human health even at trace levels. A novel adsorbent, Fe_3O_4 incorporated polyacrylonitrile nanofiber mat (Fe-NFM) is able to remove tetracycline (TC), a typical class of antibiotics, from aqueous solution. Compared to conventional NP adsorbents which have difficulties in downstream separation, the novel nanofiber mat can be simply installed as a modular compartment and easily separated from the aqueous medium, promising its potential in drinking and wastewater treatment for micro-pollutant removal [251], [252]. Four types of organic acid-functionalized (oleic, undecenoic, caprylic or hexanoic acid) MNPs have been tested to remove TC from aqueous solution. The undecenoic acid-coated MNPs (UA-MNPs) exhibit the highest adsorption efficiency. Moreover, the UA-MNPs possess excellent ability to adsorb the other three major types of TC antibiotics, including chlortetracycline, oxytetracycline and doxycycline [253]. Removal of sulfonamide antibiotics is performed using oriented immobilized laccase from *Echinodontium taxodii*

onconcanavalin A-activated Fe_3O_4 NPs. These NPs show higher enzyme loading and activity recovery compared with conventional covalent binding [254]. The removal of three widely detected and abundant pharmaceuticals, namely, ibuprofen, diclofenac, and sulfadiazine, by two Fe_3O_4-exchange resins show potential application for water purification [255]. Carbamazepine (CBZ) and diatrizoate (DTZ) are from the group of pharmaceutical and personal care products known to be persistent and non-biodegradable in wastewater treatment. Adsorptive removal of CBZ and DTZ using MNPs (10 nm), along with those coated with either methacrylic acid (MAA), $Al(OH)_3$, or SiO_2 have been evaluated. Results show that maximum DTZ adsorption capacities of MAA-, $Al(OH)_3$-, and SiO_2-coated MNPs are much higher than that of the uncoated MNPs [256].

Polychlorinated biphenyls (PCBs) present challenging issues due to human health concerns. MNPs are covered by a silica layer bonded β-cyclodextrin (β-CD) to construct core–shell Fe_3O_4@β-CD composites for removing PCB28 and PCB52 in aqueous solutions with promising results [257]. The removal of BPA is inhibited in the presence of NOM. The fabrication of powdered activated carbons impregnated with iron oxide NPs (IONPACs) allows for the simultaneous removal of BPA and NOM. The adsorption capacities of BPA and NOM are in the following sequence: bare PAC < hematite/PAC < magnetite/PAC < ferrihydrite/PAC [258]. Aqueous HA is removed with aminopropyl functionalized silica coated MNPs that show excellent desorption and regeneration properties. Zeta potential and XPS analysis reveal that electrostatic interaction and surface complexation between protonated amino groups and the disassociated HA molecules are the main adsorption mechanism [259]. Double functionalized magnetic NPs (DFMNPs) have been developed for extraction of BPA in an aqueous phase. In the preparation of DFMNPs, amide and pyridine groups are simultaneously introduced into the surface of magnetic NPs [260].

A magnetic adsorbent has been synthesized by encapsulation of magnetic functionalized NPs using alginate as a green biopolymer matrix to remove *p*-nitrophenol. A cationic surfactant, cetylpyridinium chloride (CPyCl), is used to confer a hydrophobic character to the magnetic beads and thus to promote their adsorption efficiency [261]. Magnetic porous silica–GO hybrid composites (Fe_3O_4@mSiO_2/GO) show good performance in removing *p*-nitrophenol from aqueous solution [262]. Eendocrine-disrupting chemicals 4-*n*-nonylphenol (4-*n*-NP) and BPA are adsorbed by M-GO with excellent results [263]. Four novel amino functionalized core–shell molecularly imprinted magnetic polymers (*n*Fe_3O_4@NH_2MIP) have been synthesized using different amines, *i.e.,* ethylenediamine (EDA), diethylenetriamine (DETA), triethylentetramine (TETA) and tetraethylenepentamine (TEPA), for adsorption of 2,4,6-TCP [264]. An herbicide diquat is removed by GO nanocomposite (GO-Fe_3O_4) [265]. Compared to conventional drinking water treatment (CT), a nano-treatment (NT) with quaternized magnetic microspheres reduces the concentrations of dissolved organic carbon, organic halogens (AOX), bromide and disinfection by-products more effectively. The NT completely eliminates the cytotoxicity, and greatly reduce the genotoxicity and oxidative stress of all raw water. In contrast, the CT increases the cytotoxicity of Taihu Lake and the Zhongshan River water, genotoxicity of Taihu Lake and the Mangshe River water, as well as the levels of superoxide dismutase and malondialdehyde of the Mangshe River water because CT increases disinfection by-products such as trihalomethane (THMs) and haloacetic acids as compared to raw river waters [266].

Adsorption does not destroy organic contaminants, rather it transfers contaminants from one media to the other. If complete destruction is required, alternative treatment such as chemical oxidation or reduction can be used.

6.4. Separative removal of algae from surface water

Magnetophoretic separation of algal biomass from water takes advantage of colloidal interactions between functionalized MNPs and algal cells. MNPs coated with PEI significantly reduce the energy barrier between MNPs and algae and thereby increased their heteroaggregation and algal harvesting efficiency in the separation of *Scenedesmus* dimorphus as well as in the recovery efficiency of MNPs from algal biomass through a chemical-free ultrasonic method [267]. A steric acid-coated Fe_3O_4–ZnO nanocomposite shifts hydrophobicity under UV_{365} irradiation to make magnetic nanocomposites detach from the concentrated algal biomass. The detachment is partially induced by the oxidation of steric acid coating layers due to the generation of radicals (*e.g.*, OH) by ZnO under UV_{365} illumination. Consequently, the nanocomposite surface shifted from hydrophobic to hydrophilic, which significantly reduced the adhesion between magnetic particles and algae as predicted by the extended Derjaguin and Landau, Verwey, and Overbeek (EDLVO) theory. Such unique hydrophobicity shift may also find many other potential applications that require recovery, recycle, and reuse of valuable NMs to increase sustainability and economically viability (Fig. 14) [268].

6.5. Reusable sorbents for oil spill cleanup

MNPs conjugated with carbonaceous NMs (RGO film and graphene foam) offer a facile approach for the cleanup of pollution by crude oil, petroleum products, and toxic organic solvents (Fig. 15) [269]. The magnetic polymer-based graphene foam (MPG) for oil–water separation has been fabricated by the synergistic effects of the deposition of Fe_3O_4 on graphene sheets and the self-assembly of graphene on polyurethane (PU) sponge. The resulting MPG exhibits superhydrophobicity and superoleophilicity with the water contact angle (CA) of 158 ± 1° and the oil CA of 0°. A broad variety of oils and organic solvents can be removed from oil–water mixtures under manipulation by a magnet bar with high absorption capacity and selectivity. Significantly, the MPG can remain high absorption capacity for oil-water separation after several absorption/desorption cycles, demonstrating its good reusability [270]. MNP functionalized MWCNTS display excellent adsorption for toluene, ethylbenzene, and xylene [271]. Hybrid inorganic/organic composite materials synthesized from the coupling of amine-functionalized MNPs and pre-established shell cross-linked knedel-like polymer nanoconstructs show good capability to capture crude oil. These materials could be used in the cleaning of water contaminated during the process of drilling, extraction, and transport of crude oil [272]. MNPs prepared by micro-emulsion method and functionalized by organic species are effective for oil spill removal from the water surface. This is due to the fact that the small nano size, low density, hydrophobic character and high surface area of Fe_3O_4 facilitate the penetration process of NPs inside the oil. The contents of oil spill are simultaneously aggregated and easily removed by an external magnetic field [273]. PVP-coated MNPs separate a reference MC252 oil from oil–water mixture under environmentally relevant conditions with a high removal efficiency [274].

A recent study reports on fabrication of superhydrophobic and superoleophilic microparticles with magnetic property by combining the oxidation and self-polymerization of dopamine and formation of MNPs on the surface of the PDA particles, followed by modification with low surface energy material. The modified PDA/Fe_3O_4 particles show high water repellency with CA measured at 153.7 ± 1.6° and high oil affinity. Superhydrophobic sponge is prepared by modifying with the achieved microparticles. The sponge exhibits high absorption capability of oil, with weight gains ranging from 1348% to 7268% [275]. Researchers have explored utilization of low-cost clay minerals conjugated with MNPs for oil removal. For example, three organic–inorganic hybrid materials (vinyl benzene linear polymer modified SBA-15, attapulgite and halloysite nanotubes) in the shape of powder and the corresponding magnetic polysulfone microcapsules have been developed for removal of oil and dyes from environmental aqueous samples, respectively. The developed magnetic polysulfone microcapsules exhibit high adsorption capacity of 13.8–17.3 g g^{-1} for oil [276]. High performance and low-cost MNP based NMs for oil removal merits further investigation.

6.6. Separative removal of inorganics, radionuclides, and rare earth elements

6.6.1. Common inorganics—MNPs and their hybrids are very attractive candidates for low-cost adsorbents for the effective co-removal of heavy metals/metalloids from contaminated water due to their reusability, ease of magnetic separation, high removal efficiency, high surface area, and fast kinetics (Table 2). Examples of studies showing the adsorption capacities for select metalloids and metal ions are listed in Table 3. Notably, Chinese scientists have developed low-priced HA-coated MNP sorbent material for removing heavy metals from water with greatly enhanced stability of the material and increased removal efficiency with negligible leaching of NPs [277]. Compared to cationic pollutants, the removal of anionic pollutants by adsorption is more difficult because most adsorbents carry predominantly negative charges in neutral and alkaline environments.

6.6.1.1. Arsenic, phosphate, molybdate, fluoride, selenium: Arsenic is a known carcinogenic element and its removal from water supplies is needed to reduce its exposure through drinking water and food consumption. Magnetite is known to be an As adsorbent [278]. MNPs are more promising adsorbents for As removal because of their great adsorption capacity and easy separation. For example, using the high specific surface area of MNPs (12 nm), it is able to reduce the mass of waste associated with As(V) and As(III) removal from water by orders of magnitude [279]. Arsenic adsorption increases with decreasing MNP particle size [280] and phosphate competes against As for adsorption [281]. CTAB modified MNPs adsorb more As(V) than MNPs alone [282]. Fe_3O_4–graphene–LDH removes almost twice as much As(V) as LDH alone [283]. Fe_3O_4–GO adsorbs more As than Fe_3O_4–RGO because more functional groups exist on the Fe_3O_4–GO. As(III) is more favorably adsorbed than As(V) onto both adsorbents. This is advantageous, in terms of the process energy consumption, because energy saving could be achieved via omitting the reduction process to fabricate Fe_3O_4–RGO from Fe_3O_4–GO and the pre-oxidation process to convert As(III) to As(V) [284]. Functionalized MNPs show improved performance. For example, starch-bridged MNPs at an Fe-to-As molar ratio of 7.6 remove 100% As(V) from an initial 300 mg L^{-1} As(V) spent ion exchange brine (6% W/W NaCl), compared to only

20% removal when bare MNPs are used [285]. The starch acts as a stabilizer to prevent the NPs from agglomerating and as a bridging agent allowing the NPs to flocculate and precipitate while maintaining their high As sorption capacity. An earlier study has shown that starch-stabilized MNPs offer a much faster sorption rate and greater capacity than carboxymethyl cellulose (CMC)-stabilized magnetite [286]. MNPs (20 nm) show fast As(V) removal (reaching equilibrium within 2 h) that is not significantly influenced by pH (pH 7.7–8.3), ionic strength (0–0.1 M KNO_3) and temperature (20–30 °C) [287]. Smaller MNPs (5.8 ± 0.9 nm) exhibits excellent distribution coefficient K_d (5800 mL g^{-1}) for As and are also effective sorbents for toxic soft metals such as Hg, Ag, Pb, Cd, and Tl [288]. MNPs coated sand shows efficient As(V) removal from drinking water [289].

A recent study shows As adsorption by MNPs increases with increasing temperatures. As(V) predominantly forms bidentate binuclear corner-sharing complexes (^{2}C), and As(III) forms tridentate hexanuclear corner-sharing (^{3}C) complexes on MNP surfaces. More intriguingly, XANES and XPS results reveal complex redox transformation of the adsorbed As on MNPs exposed to air: Concomitant with the oxidation of MNPs, the oxidation of As(III) and MNPs is expected, but the observed As(V) reduction is surprising because of the role played by the reactive Fe(II) [290]. A pilot column test of a commercially available, food-grade magnetite (98 nm) has demonstrated removal of As(V) from Guanajuato, Mexico groundwater [291]. A magnetically separable nanomaterial Fe_3O_4–TiO_2 eliminates the disadvantages of MNP agglomeration and iron leaching and takes advantage of the fact that TiO_2 NPs are also effective As(V) and As(III) adsorbent [292]. A granular AC/$MnFe_2O_4$ composite with a mass ratio of 2:1 shows maximum Langmuir adsorption capacities of 1253 mg g^{-1} for As(III) and 1314 mg g^{-1} for As(V) at 30 °C and 70 min contact time. These adsorption capacities are among the highest (Table 3). The results show that As(III) and As(V) removal is strongly pH-dependent with an optimum pH value of 7.0 and 4.0, respectively [293]. Multiwalled boron nitride nanotubes (BNNTs) functionalized with MNPs are used for As(V) removal [294]. MNPs surface-coated with 3-mercaptopropanoic acid (3-MPA) show twice the As(V) adsorption capacity as compared to MNPs alone, which is attributed to the increase of active adsorption sites [295]. Other promising adsorbents include CNTs functionalized with MNPs for As(V) and As(III) [296] and chitosan-coated MNPs for As(III) [297].

GO modified with Fe_3O_4 and MnO_2 NPs provides more adsorption sites for removing As(III) and As(V) by reducing the aggregation of Fe_3O_4 and MnO_2 NPs. In addition, the MnO_2 NPs promote the oxidation of As(III) to As(V) and simultaneously participate in the adsorption of arsenic with Fe_3O_4. Furthermore, arsenic adsorption remain stable in a wide pH range of 2–10, which is a limitation in most adsorbents [298]. Magnetic porous Fe–Mn binary oxide nanowires have been fabricated to remove As(III) with the adsorption capacity increasing with increasing manganese oxide in the composite, and with an initial Fe:Mn molar ratio of 1:3 exhibiting the highest adsorption capacity [299]. A novel composite adsorbent (HBC–Fe_3O_4–MnO_2) has been synthesized by combining honeycomb briquette cinders (HBC) with Fe_3O_4 and MnO_2 through a co-precipitation process for enhanced As(III) and As(V) removal. More As(III) is removed than As(V). Co-ions HCO_3^- and PO_4^{3-} inhibit As removal; whereas, Cl^-, NO_3^-, and SO_4^{2-} have no influence [300]. The hybrids of single-layer GO with $MnFe_2O_4$ NPs show excellent adsorption properties for efficient

removal of Pb(II), As(III), and As(V) from contaminated water [301]. Dihalogen crosslinked Fe_3O_4 core–shell NPs synthesized by crosslinking amine functionalized $Fe_3O_4@SiO_2$ core–shell NPs with 1,2-bromochloroethane are loaded on to the RGO to obtain nanocomposites for removing As(V), As(III) and Hg(II) [302]. Magnetite occurs naturally as NPs. Four natural magnetite samples from an iron ore deposit and two synthetic commercial reference samples, show a widely variable As(V) adsorption behavior with no clear predictable pattern among samples [303].

Phosphate removal via adsorption is an effective means for controlling eutrophication in water bodies. A magnetic adsorbent, amine-functionalized silica magnetite (NH_2–Al/SiO_2/Fe_3O_4) behaves as a cationic adsorbent by adjusting the pH value of the aqueous solution to make amino groups protonated. The NH_2–Al/SiO_2/Fe_3O_4 adsorbs dissolved phosphate with the maximum adsorption at pH 3.0. Desorption of phosphate occurs in 0.05 M NaOH [304]. A magnetic core–shell composite with a Fe_3O_4 core and a carbon shell (denoted as MFC) is further functionalized by ZrO_2 (denoted as MFC@ZrO_2) for phosphate adsorption. Negligible phosphate adsorption is observed on MFC, while ZrO_2 functionalization leads to markedly enhanced phosphate adsorption [305]. $Fe_3O_4@SiO_2$ core/shell magnetic NPs coated with hydrous lanthanum oxide have been tested for separation of phosphate from water with a removal efficiency of higher than 95% attained for real effluent of a wastewater treatment plant. The adsorbed phosphate could be nearly completely desorbed with NaOH solution for further use [306]. Magnetic core–shell Fe_3O_4@LDHs composites show good phosphate adsorption efficiency with the maximum adsorption capacity following the order: Fe_3O_4@Zn–Al–LDH > Fe_3O_4@Mg–Al–LDH > Fe_3O_4@Ni–Al–LDH [307]. A $MnFe_2O_4$ (5.1 nm) exhibits good phosphate removal. Adsorbed phosphate is desorbed using 15 w/v% NaOH solution and recovered via hydroxyapatite crystallization in the desorption solution [308]. A novel combination of magnetic adsorptive and coagulative strategy has been used to remove molybdate from surface water. The ferromagnetic nanoclusters and ferromagnetic nanoclusters-ferric flocs composite coagulant show decreasing removal rate: ferromagnetic nanoclusters-$FeCl_3$ > $FeCl_3$ > $AlCl_3$ > $TiCl_4$ [309]. In another study, $ZnFe_2O_4$ NPs are used for removing and recovering molybdate from water [310].

A novel adsorbent of γ-AlOOH@CS (pseudoboehmite and chitosan shell) magnetic NPs shows good performance at pH 4–10 to remove fluoride from drinking water [311]. A series of doped and un-doped magnetic adsorbents $CuCe_xFe_{2-x}O_4$(x = 0.0–0.5) prepared with the micro-emulsion method have been compared for fluoride removal from water. Doped ferrites (x = 0.1–0.5) are superior to un-doped ferrites (x = 0) regarding the active sites, functional groups and fluoride adsorption [312]. Compared with either natural magnetite (<5 μm) or nanaosized zerovalent iron (NZVI) (~10 nm), MNP (10–20 nm) is a better adsorbent for selenite, while NZVI shows better adsorption performance for selenate [313]. Competition of anions for adsorption on MNPs and their hybrids needs to be more fully evaluated for practical applications. What works well in the laboratory setting may not work well in the field. More field-scale research is required.

6.6.1.2. Cr(VI) and Cr(III): A novel β-cyclodextrin (β-CD) polymer adsorbent named β-cyclodextrin/ethylenediamine/M-GO (CD-E-MGO) removes Cr(VI) from water with good

results [314]. Easily separable HA coated magnetite (HA-Fe_3O_4) NPs effectively adsorbs and reduces Cr(VI) to nontoxic Cr(III) (Fig. 16) [315]. No detectable transformation of the Fe_3O_4 core occurs during Cr(VI) adsorption and reduction, suggesting HA on the surface of HA-Fe_3O_4 is responsible for the reduction of Cr (VI) to Cr(III). The functional groups associated with HA act as ligands leading to the Cr(III) complex via a coupled reduction–complexation mechanism [315]. Magnetic carbon–iron nanoadsorbents fabricated by carbonizing cellulose and reducing MNPs or $Fe(NO_3)_3$ (the products are denoted as MC–O and MC–N, respectively) have demonstrated great Cr(VI) removal via Cr(VI) reduction and precipitation of Cr(III) [316]. A cross-linked chitosan derivative with quaternary ammonium and magnetic properties (QM-chitosan) removes both Cr (VI) and phosphate from aqueous environments [317]. Magnetite nanospheres with hollow interiors [318] and MNPs synthesized by chemical co-precipitation [319] both successfully remove Cr(VI) and Pb^{2+} from water [320]. Magnetic iron oxide/mesoporous silica nanocomposites consisting of iron oxide NPs embedded within mesoporous silica (MCM-41) and modified with aminopropyl functional groups exhibit a superior equilibrium Cr(III) adsorption than that for unmodified mesoporous silica [321]. Single ion kinetic studies have revealed Cr(VI) to be better adsorbed than Cd^{2+} onto citrate-coated MNPs. Otherwise Cd^{2+} adsorption ratio is improved with Cr(VI) in the binary mixture [322]. In a recent work, a novel “dumbbell-like” magnetic Fe_3O_4/halloysite nanohybrid (Fe_3O_4/HNTs@C) with oxygen-containing organic group grafting on the surface of natural halloysite nanotubes (HNTs) and homogeneous Fe_3O_4 nanospheres selectively aggregating at the tips of modified halloysite nanotubes has been successfully synthesized. The Fe_3O_4/halloysite nanohybrid Exhibits 100 times higher adsorption ability than that of unmodified halloysite nanotubes. More importantly, with the reduction of Fe_3O_4 and electron–donor effect of oxygen-containing organic groups, Cr(VI) ions are easily reduced into low toxicity Cr(III) and then adsorbed onto the surface of halloysite nanohybrid [323]. Compared to other reductants for Cr(VI) reduction to Cr(III) such as NZVI, MNPs have the advantage of remaining to be magnetic for easy separation; whereas, NZVI corrodes rapidly in oxic environments to form non-magnetic iron oxides.

6.6.1.3. Cationic heavy metal ions Hg^{2+}, Pb^{2+}, Cd^{2+}, Cu^{2+}, Zn^{2+}, Co^{2+}, Ni^{2+}: Cationic heavy metal ions are persistent pollutants in wastewater and their removal is required to meet regulatory standards. MNPs and their hybrids are effective sorbents for their removal with high adsorption capacities (Table 3). For example, bare MNPs and γ-Fe_2O_3 NPs are able to remove Hg^{2+}effiently [324]. Fe_3O_4@SiO_2 magnetic NPs modified by grafting poly(1-vinylimidazole) oligomer (FSPV) show excellent removal of Hg^{2+} at pH 4–10 even at the presence of HA. Common ions including Na^+, K^+, Ca^{2+}, Mg^{2+}, Cl^-, NO_3^-, and SO_4^{2-} (up to 100 mM ionic strength) slightly increase the adsorption of Hg^{2+} by FSPV [325]. Mercapto modified MNPs show excellent Hg^{2+} removal [326]. Imine functionalized MNPs show selective removal of Pb^{2+} or Zn^{2+} by varying the concentrations of EDTA [327], and multi-amine grafted mesoporous silica embedded with nano-magnetite removes Pb^{2+} and Cu^{2+} [328]. A novel magnetic nano-sorbent has been synthesized by Schiff’s base formation via covalent bonding of gelatin to the surface of nano-magnetite-immobilized-3-aminopropyltrimethoxysilane (Nano-Fe_3O_4-Si-N = Gelatin) and it has the maximum capacity of Cd^{2+} and Pb^{2+} as 49.5 and 82.9 mg g^{-1}, respectively [329]. Dithiocarbamate functionalized silica coated MNPs display great affinity for Hg^{2+}, but they are not effective

at removing As and Cd from seawater [330]. MNPs with a surface functionalization of dimercaptosuccinic acid (DMSA) are an effective sorbent material for Hg^{2+}, Ag^{+}, Pb^{2+}, Cd^{2+}, and Tl^{+}, which effectively bind to the DMSA ligands and for As, which binds to the iron oxide lattices. DMSA-Fe_3O_4 has a capacity of 227 mg of Hg g^{-1}, a 30-fold larger value than conventional resin based sorbents (GT-73) [288]. A novel adsorbent, 2-mercaptobenzamide modified itaconic acid-grafted-magnetite nanocellulose composite [P(MB-IA)-g-MNCC] selectively removes Hg^{2+} at the optimum pH of 8.0 [331]. Resin loaded magnetic β-cyclodextrin bead and GO sheet (MCD-GO-R) is an excellent adsorbent for Hg^{2+} removal at pH 4–10 [332]. A novel 3-aminopropyltriethoxysilane modified graphite nanosheets (GNS) decorated with Fe_3O_4 NPs (Fe_3O_4-GNS-NH_2 hybrids) has been developed for adsorption of Hg^{2+}. The main adsorption mechanism for Hg^{2+} is the formation of N-metal ions chemical complex, and the solution pH value has a major impact on Hg^{2+} adsorption with optimal removal at pH 4–6 [333]. Another method has been developed for removing Hg^{2+} from a high-salt matrix using Tween-20-stabilized gold NP (Tween 20-Au NPs) as Hg^{2+} adsorbents and composites of RGO and MNPs as NP collectors. Citrate ions adsorbed on the surface of the Tween 20-Au NPs reduce Hg^{2+} to Hg^{0}, resulting in the deposition of Hg^{0} on the surface of the NPs. Compared with the reported NP-based methods for removing Hg^{2+}, Tween 20-Au NPs offer the rapid (within 30 min), efficient (>99% elimination efficiency), durable (>10 cycles), and selective removal of Hg^{2+}, CH_3Hg^{+}, and $C_2H_5Hg^{+}$ in a high-salt matrix without the interference of other metal ions [334]. A novel magnetic composite microsphere (MCM) based on polyacrylamide (PAM)-grafted chitosan and silica-coated MNPs (CS-PAM-MCM) has been applied as an efficient adsorbent for the removal of Hg^{2+}, Pb^{2+}, and Cu^{2+} in respective single, binary, and ternary metal systems. Compared with chitosan magnetic composite microsphere (CS-MCM) without modification, CS-PAM-MCM show improved adsorption capacity for each metal ion and highly selective adsorption for Hg^{2+} from Pb^{2+} and Cu^{2+} [335]. Magnetic hydroxypropyl chitosan/oxidized MCNTs (MHC/OMCNTs) composites remove Pb^{2+}, exhibiting an optimal pH 5.0 [336]. A ternary nanocomposite hydrogel consisting of magnetic attapulgite/fly ash/poly(acrylic acid) (ATP/FA/PAA) exhibits good adsorption selectivity toward Pb^{2+}, and the adsorbed ion could be completely desorbed with HCl aqueous solution [337]. Nanoporous adsorbents of ZnO/$ZnFe_2O_4$/C show high Pb^{2+} adsorption performance. XRD and XPS data suggest that Zn^{2+} is substituted by a portion of Pb^{2+} on the surface of ZnO nanocrystals. This adsorbent may have limited applications if Zn^{2+} is also present in the wastewater [338].

Core–shell magnetic Fe_3O_4@C NPs functionalized with sulfonic and carboxylic acid groups remove Pb^{2+}, Hg^{2+}, and Cd^{2+} ions quickly to reach equilibrium within 5 min, with the maximum adsorption capacities $Pb^{2+} > Hg^{2+} > Cd^{2+}$ [339]. Chain-like core–shell structure Fe_3O_4@SiO_2@chitosan composite shows a decreasing adsorption in the order, $Hg^{2+} > Pb^{2+} > Cu^{2+}$ [340]. Hybrid MNP sorbents synthesized through surface encapsulation of MNPs by o-phenylenediamine via cross-linking using formaldehyde and glutaraldhyde show superior selectivity for Pb^{2+} removal and good adsorption of Cd^{2+} [341]. A recent study has demonstrated a one-pot solvothermal synthetic method for fabricating MFe_2O_4 (M = Mn, Co)–MoS_2–carbon dot (CD) nanohybrid composites (MnFMC, CoFMC) with excellent Pb^{2+} removal ability. The as-prepared composites exhibit high adsorption performance and show

preferential Pb^{2+} sorption behavior with a high level concentration of competing cations (Ca^{2+}/Mg^{2+}) [342]. In another study, Fe_3O_4@$Zr(OH)_x$ yolk–shell nanospheres (YSNs) and another adsorbent without hollow cavities, *i.e.*, Fe_3O_4@SiO_2@$Zr(OH)_x$ core–shell nanospheres (CSNs), have been used for the removal of Pb^{2+}. The Fe_3O_4@$Zr(OH)_x$ YSNs exhibits higher Pb^{2+} adsorption capacity as compared to that of Fe_3O_4@SiO_2@$Zr(OH)_x$ CSNs due to the existence of cavities between Fe_3O_4 cores and $Zr(OH)_x$ shells [343]. Poly(1-vinylimidazole)-grafted Fe_3O_4@SiO_2 magnetic NPs remove both free Cd^{2+} and nitrilotriacetic acid (NTA) complexed Cd^{2+} at pH 5–11, and the adsorbent could be regenerated with 10 mM HCl in 10 min, and the removal of both types of Cd^{2+} maintains above 95% in five consecutive adsorption/regeneration cycles [344]. Sodium dodecyl sulfate-modified MNPs also show good Cd^{2+} removal [345].

Amino-functionalized Fe_3O_4@SiO_2 magnetic nano-adsorbent shows highly selective removal of Zn^{2+} from hot-dip galvanizing pickling waste that mainly contains $ZnCl_2$ and $FeCl_2$ in aqueous HCl media. The maximum adsorption occurs at pH 5 and Fe^{2+} does not interfere [346]. Sodium alginate-MNP nanocomposite beads adsorbs Cu^{2+} from aqueous solutions [347]. SPIONs coated with poly(methylmethacrylate) (PMMA) by emulsion polymerization process show some selectivity for Cu^{2+}, Mn^{2+}, and Zn^{2+} with the removal efficiency decreasing in the order $Cu^{2+} > Mn^{2+} > Zn^{2+} > Cd^{2+} > Pb^{2+} > Co^{2+} > Ni^{2+}$ [348]. Potassium ferrate(VI) (K_2FeO_4, Fe(VI)) removes Co^{2+}, Ni^{2+}, and Cu^{2+} by the formation of MFe_2O_4 spinel phase and partially through their structural incorporation into octahedral positions of γ-Fe_2O_3 (maghemite) NP. In contrast, Cd^{2+} ions either do not form the spinel ferrite structure or are not incorporated into the lattic of iron(III) oxide phase due to the distinct electronic structure and ionic radius (Fig. 17) [349]. A novel magnetic hydroxamic acid modified polyacrylamide/Fe_3O_4 adsorbent (M-PAM-HA) have been prepared with acrylamide by microemulsion polymerization and then nucleophilic substitution of hydroxamic acid for the removal of Cd^{2+}, Pb^{2+}, Co^{2+} and Ni^{2+} [350]. EDTA functionalized MGO (EDTA-MGO) is a good adsorbent for Pb^{2+}, Hg^{2+} and Cu^{2+} in that metal chelation and electrostatic attraction improve the adsorption capacity [351]. The presence of anions show positive effect on Cu^{2+} removal by aminated Fe_3O_4/GO (AMGO). In the single-ion systems, Cl^-, ClO_4^-, and NO_3^- slightly increase the Cu^{2+} adsorption onto AMGO at low pH, while the Cu^{2+} adsorption is largely enhanced by the presence of SO_4^{2-}, CO_3^{2-}, and HPO_4^{2-}. The enhancing effects is in the following sequence: $HPO_4^{2-} > CO_3^{2-} > Cl^- > SO_4^{2-} > NO_3^- = ClO_4^-$ [352]. Adsorbents that can remove multiple heavy metal ions simultaneously are perhaps more useful for practical applications since the metals are usually co-contaminants in wastewater. Selective removal of a particular metal ion is sometimes required for recovery. Thus different types of adsorbents using MNP as a major component may be further developed for a specific purpose.

6.6.2. Radionuclides—Uranium (VI) adsorption by oxine functionalized MNPs is strongly dependent on pH and independent of ionic strength, indicating that the sorption is mainly dominated by inner-sphere surface complexation [353]. Fe_3O_4@TiO_2 nanocomposites remove U(VI) endothermically and spontaneously [354]. Amino functionalized magnetic GO composite displays a high efficiency for the removal of U(VI) [355]. The bio-nanocomposites of fungus-Fe_3O_4 adsorbs Sr(II), Th(IV), and U(VI), which is

independent of ionic strength, indicating that inner-sphere surface complexation with oxygen-containing functional groups dominates their sorption. The maximum sorption capacities of fungus-Fe_3O_4 are for Sr(II) and U(VI) at pH 5.0, and Th(IV) at pH 3.0 [356]. Four new MNP containing different chelating groups as ester, amide, and azacrown moieties at the lower rim of calix[4]arenes have been prepared by the reaction of formylated calix[4]arenes and amino propyl modified MNPs (APTMS-MNP). MNPs containing picolinamide units exhibit superior and more efficient extraction percentage for uranium ions at lower pH values [357]. Uranium incorporation into magnetite and its behaviour during subsequent oxidation has been investigated at high pH to determine the uranium retention mechanism(s) on formation and oxidative perturbation of magnetite in systems relevant to radioactive waste disposal. Ferrihydrite is exposed to $U(VI)_{aq}$ containing cement leachates (pH 10.5–13.1) and crystallization of magnetite is induced via addition of $Fe(II)_{aq}$. A combination of XRD, chemical extraction and XAS techniques provide direct evidence that U(VI) is reduced and incorporated into the magnetite structure, possibly as U(V), with a significant fraction recalcitrant to oxidative remobilization. Immobilization of U(VI) by reduction and incorporation into magnetite at high pH, and with significant stability upon reoxidation, has clear and important implications for limiting uranium migration in geological disposal of radioactive wastes [358]. No information about the size of magnetite was given in this study, but it may be relevant to MNPs as well. Copper ferrocyanide-functionalized MNPs show the effectiveness of the nano-adsorbents toward the removal of Cs [359]. Neptunium-237 is a radionuclide of great interest owing to its long half-life (2.14×10^6 years) and relative mobility as the neptunyl ion (NpO_2^+) under many surface and groundwater conditions. Reduction to Np(IV) is beneficial due to its low solubility. Natural magnetites often contain titanium impurities which have been shown to enhance radionuclide sorption via titanium's influence on the Fe^{2+}/Fe^{3+} ratio in the absence of oxidation. New evidence shows that Ti-substituted MNPs reduce NpO_2^+ to Np(IV) under reducing conditions. No evidence of NpO_2 NP precipitation is obtained. Instead XAS confirms the nearly exclusive presence of Np(IV) on the titanomagnetite surface and provides supporting data indicating preferential binding of Np to terminal Ti–O sites as opposed to Fe–O sites [360]. Radioactive Tc(IV) has been shown experimentally and computationally to be able to favorably incorporate into magnetite but not trevorite ($NiFe_2O_4$) structure [361]. It remains to be seen if such substituted magnetite is stable over long periods of time for immobilization of radioactive elements at contaminated sites.

6.6.3. Rare earth elements—Nanocomposite of GO and silane modified magnetic NPs (silane@Fe_3O_4) have been synthesized in a form of dendritic structure that is used as a monomer for synthesis of europium ion imprinted polymer. The imprinted polymer modified silica fiber is first validated in the aqueous and blood samples for successful extraction and detection of europium. The imprinted polymer modified silica fiber is also used for preconcentration and separation of europium metal ion from various soil samples of coal mine areas. However, the same silica fiber is also used for wastewater treatment and shows 100% performance for europium removal. The findings suggest that dendritic nanocomposite could be potentially used as a highly effective material for the enrichment and preconcentration of europium or other trivalent lanthanides/actinides in nuclear waste management [362]. An adsorbent prepared based on the attachment of organophosphorus

acid extractants to the surface of MNPs has been coated with oleic acid for adsorption of lanthanum, cerium, praseodymium, and neodymium [363].

6.7. Simultaneous separative removal of organic and inorganic contaminants

Mixed organic/inorganic contaminants often occur in aquatic environments. For example, potentially toxic metals and dyes commonly coexist in industrial wastewaters, posing a serious threat to public health and the environment and making the treatment more challenging. Magnetic composites consisting of Fe_3O_4, GO, and Mg_3Al–OH LDH, denoted as MGL composites, are able to remove the heavy-metal Pb^{2+} and the hydrophobic organic pesticide 2,4-dichlorophenoxyacetic acid (2,4-D) from aqueous solutions [364]. Magnetic activated carbons and biochars produced by wet impregnation with iron oxides show strong sorption of the hydrophobic phenanthrene and copper, zinc, and lead [365]. Fe_3O_4/GO nanocomposites synthesized using a novel solvothermal method remove 17β-estradiol (E_2) and Pb^{2+} synergistically [366]. Porous magnetic CoFe oxide nanosheets ($Co_{2.698}Fe_{0.302}O_4$) show fast removal ability and good adsorption capacity for both organic waste Congo red and Cr(VI) [367]. Xanthate functionalized MGO is an ideal adsorbent for Hg^{2+} and MB removal with a higher adsorption capacity [368]. A magnetic MWCNTs nanocomposite shows high efficiency for simultaneous removal of furazolidone (FZD) and Cu^{2+} from aqueous solutions. The Cu^{2+} suppresses FZD binding in the simultaneous adsorption and FZD preloading experiment; whereas, the impact of FZD on Cu^{2+} desorption is almost negligible [369]. A new versatile MNP conjugated with quaternary ammonium compounds (QACs) (M-QAC) has been developed by the Chinese researchers that exhibits excellent disinfection and adsorption performance at the same time. The M-QAC is constructed by a Fe_3O_4 core surrounded by a polyethylenimine-derived corona. When dispersed in water, the M-QAC particles are able to interact simultaneously with multiple contaminants, including pathogens and heavy metallic cations and anions, in minutes. Subsequently, the M-QACs along with those contaminants can be easily removed and recollected by using a magnet [370]. Scientists from China have also developed a novel magnetic PDA–LDH (MPL) bifunctional material, which is fabricated by an easy and green approach for the simultaneous removal of Cu^{2+} and anionic dyes, methyl orange and Congo red [371]. Such a green and facile synthesis method, efficient removal performance and superior reusability suggest that the MPL assemblies have practical application potential for integrative and efficient treatment of coexisting toxic pollutants. More research should be conducted to develop more versatile adsorbents that can remove multiple organic and inorganic co-contaminants for greater technical merits and economic efficiency.

6.8. Chemical reductive removal of contaminants

The decomposition efficiency of polychlorinated biphenyls (PCBs) has been compared using Fe^0 and three iron (hydr)oxides, *i.e.*, α-Fe_2O_3, Fe_3O_4, and α-FeOOH, as catalysts under an inert, oxidizing or reducing atmosphere composed of N_2, $N_2 + O_2$, or $N_2 + H_2$. N_2 is the optimum atmosphere for PCB decomposition using iron or iron compounds. No matter which PCB congener is tested, Fe_3O_4 shows the highest activity. Reactive characteristics of Cl atoms on benzene rings followed para > meta > ortho [372]. Nano-sized hybrid Fe^0 and Fe_3O_4 efficiently degrade 3,3′,4,4′-tetrachlorobiphenyl (PCB77). The degradation of PCB77 by Fe^0/Fe_3O_4 NPs is a dechlorination process. Fe_3O_4 provides Fe^{2+} and Fe^{3+} for

enhancing the PCB77 degradation by NZVI, suggesting a synergy between Fe^0 and Fe_3O_4 [373]. A triple-functional nanocomposite has been prepared by integrating superparamagnetic Fe_3O_4 and Pd NPs onto mesoporous Fe_3O_4@*n*SiO_2@*m*SiO_2 nanospheres to degrade 1,1,1-trichloro-2,2-bis(4-chlorophenyl) ethane (DDT), a highly persistent organochlorine pollutant in environment. These magnetic mesoporous materials display excellent capabilities of capturing and catalytically degrading DDT in water at temperatures as low as 150 °C. The nanocomposites can be magnetically separated from the dispersion after adsorption, and then be easily regenerated which is accompanied by catalytic reaction. The whole treatment process is convenient, energy-saving, and just requires ambient pressure and mild reaction conditions [247]. The same Fe_3O_4@*n*SiO_2@*m*SiO_2 catalyst without Pd NPs doping requires a higher temperature (350 °C) to completely degrade DDT [374]. Ag/halloysite nanotubes/Fe_3O_4 (Ag/HNTs/Fe_3O_4) nanocatalyst has been synthesized in which Fe_3O_4 NPs (5–8 nm) are loaded in the internal hollow lumen of HNTs and Ag NP (20 nm) are randomly deposited on the external surface of HNTs/Fe_3O_4. The resultant Ag/HNTs/Fe_3O_4 exhibits excellent catalytic activity (with conversion of 100% in 38 min) to the reduction of 4-NP with $NaBH_4$ [375]. MWCNTs-Fe_3O_4–Pd/Fe nanohybrids provide rapid adsorption, gradual dechlorination of 2,4-dichlorophenol, and final desorption of phenol. MWCNTs-Fe_3O_4–Pd/Fe nanohybrids outperform unsupported Pd/Fe NPs, which are difficult to retrieve, and are easily passivated and aggregated [376]. Ball milling has been used to prepare two ultrafine magnetic biochar/Fe_3O_4 and activated carbon (AC)/Fe_3O_4 hybrid materials targeted for use in pharmaceutical removal by adsorption and mechanochemical degradation of pharmaceutical compounds of CBZ and TC [377].

Redox sensitive contaminants such as Cr(VI) can be remedied using magnetite via chemical reduction to the very insoluble Cr(III) species. An recent study has investigated the Cr(VI) reduction performance of synthetic and natural magnetites of different particle size and found that only the finest magnetite show considerable Cr(VI) reduction yields. Mechanochemical mixing of the finer magnetites with 5% micron-sized Fe^0 increases dramatically their reductive reactivity despite the fact that the same quantity of Fe^0 added by itself reduces negligible amounts of Cr(VI) [378]. Biogenic MNPs synthesized by the Fe(III)-reducing bacterium *Geobacter sulfurreducens*, has been tested for the potential to remediate alkaline Cr(VI) contaminated waters associated with chromite ore processing residue (COPR). The performance of this biomaterial is compared to NZVI. Both NPs exhibit a considerable capacity for the remediation of COPR related Cr(VI) contamination, with the NZVI demonstrating greater reactivity than the biogenic MNPs. However, the biosynthesized MNP is also capable of significant Cr(VI) reduction and demonstrates a greater efficiency for the coupling of its electrons towards Cr(VI) reduction than the NZVI [379]. Magnetic Fe_3O_4@poly(m-phenylenediamine) particles (Fe_3O_4@PmPDs) with well-defined core–shell structure show high Cr(VI) removal that is attributed to the adsorption of Cr(VI) on protonated imino groups and the efficient reduction of Cr(VI) to Cr(III) by amine, followed by Cr(III) chelated on imino groups [380]. MNPs have been used as an additive material in a ZVI reaction to reduce nitrate in groundwater resulting in markedly increased nitrate reduction, with the rate proportionally increasing with MNP loading. MNPs act as a corrosion promoter for Fe^0 corrosion as well as an electron mediator that facilitated electron

transport from Fe^0 to adsorbed nitrate [381]. The performance of MNPs for chemical reduction of these and other redox sensitive contaminants merits further investigation.

7. Sewage sludge stabilization, soil improvement, soil, sediment, and groundwater remediation

Anaerobic digestion (AD) is a widely used process to stabilize waste sewage sludge and produce biogas renewable energy. A recent study has tested NZVI and MNPs used in the mesophilic AD processes (37 ± 1 °C) to improve biogas production and heavy metal (Cd, Co, Cu, Zn, Ni and Cr) immobilization. Compared with AD without iron NPs, the application of iron NPs at dose of 0.5% shows positive impact not only on biogas production, but also on improvement of metals stabilization in the digestate. Metals are found concentrated in Fe–Mn bound and residual fractions and little is accumulated in the liquid digestate and most mobile fractions of solid digestate (water soluble, exchangeable, and carbonates bound). In addition, iron nanoparticles could promote the immobilization of phosphorus within the sludge during AD [382]. A biochar-mineral complexes (BMCs) containing Fe_3O_4 has been developed as a soil improvement material. It has a higher mineral content, surface functionality, exchangeable cations, high MNP, and higher water-extractable organic compounds. Two biochars produced under different pyrolysis conditions are activated with a phosphoric acid treatment. A mixture of clay, chicken litter, and minerals are added to the biochar, and then this composite is torrefied at either 180 or 220 °C. The BMCs improve mycorrhizal colonisation, wheat growth and nutrient uptake, and soil quality [383].

Degradation of polycyclic aromatic hydrocarbons (PAHs) in contaminated soils through Fenton-like oxidation catalyzed by magnetite has been reported [398]. PAHs degradation is improved in soils pre-treated with availability-enhancement agents such as ethanol or cyclodextrin. This study shows the promising efficiency of magnetite for PAHs oxidation at circumneutral pH over soluble Fe^{2+} in contaminated soils. Furthermore, MNPs are magnetic sorbents so that the adsorbed pollutants can be recovered. A coal-based magnetic activated carbon (MAC) is identified as the strongest of four AC and BC derived magnetic sorbents for PAHs remediation. An 8.1% MAC amendment (w/w, equal to 5% AC content) is found to be as effective as 5% (w/w) pristine AC in reducing aqueous PAHs within three months by 98% [384]. A recent study has investigated effectiveness of starch-stabilized MNPs for *in situ* enhanced sorption and immobilization of As(V) in a model sandy loam soil. Batch tests show that the NPs offer an As(V) distribution coefficient of 10,000 L g^{-1}, which is >3 orders of magnitude greater than that of the soil. Batch and column experimental results reveal that the NP treatment greatly reduce water-leachable As(V) and the leachability of As(V) remaining in the soil per TCLP (Toxicity Characteristic Leaching Procedure) analysis. While the NPs are deliverable in the soil, the effective travel distance of the NPs can be manipulated by controlling the injection flow rate. Under natural groundwater flow conditions (velocity $\leq 2.4 \times 10^{-4}$ cm s^{-1}), the delivered MNPs are confined within a limited distance (<6.1 cm) [385]. Magnetite strongly retains As, and is relatively stable under Fe(III)-reducing conditions common in aquifers that release As. A laboratory microcosm experiment has investigated a potential As remediation method involving magnetite

formation, using groundwater and sediments from the Vineland Superfund site. The microcosms are amended with various combinations of nitrate, $FeSO_4$, and lactate, and are incubated for more than 5 weeks. In the microcosms enriched with 10 mM nitrate and 5 mM $Fe(II)_{aq}$, black MNPs are produced, and As removal from solution is observed even under sustained Fe(III) reduction stimulated by the addition of 10 mM lactate. The enhanced As retention is mainly attributed to co-precipitation within magnetite and adsorption on a mixture of magnetite and ferrihydrite. Sequential chemical extraction, XAS and magnetic susceptibility measurements show that these minerals form at pH 6–7 following nitrate-Fe(II) addition, and As-bearing magnetite is stable under reducing conditions. SEM and XRD indicate that MNPs are produced as coatings on fine sediments, and no aging effect is detected on morphology over the course of incubation. These results suggest that a magnetite based strategy may be a long-term remedial option for As-contaminated aquifers [386].

Microsized magnetic particles (97.5% Fe, mostly ZVI) have been tested as P adsorbents in a microcosm experiment in a context of lake restoration. MPs are added to sediment cores from a hypertrophic lake, at $Fe:P_{Mobile}$ molar ratio of 285:1 and 560:1 under both, oxic and anoxic conditions. It has been found that, under anoxic conditions (anoxic), magnetic particls are able to reduce P release rate from the sediment to the overlying water and to reduce sedimentary P_{Mobile} concentration (a 22–25% reduction within 0–4 cm depth compared to controls). Under oxic conditions, the addition of MPs do not affect P fluxes across the sediment and water interface since the lake sediment is naturally rich in iron oxides. However a measured reduction in sedimentary P_{Mobile} concentration (12–16% reduction in 0–10 cm depth) contributes to a potential reduction in long-term P efflux [387]. Because magnetite is a major corrosion product of ZVI, part of the P removing capacity could be derived from magnetite, either microscale or nanoscale. Polyferric sulphate has been widely used for emergent control on incidental release of heavy metals such as Cd^{2+} to surface water, causing precipitation of Cd-loaded polyferric flocs to the sediment. To date, little is known about whether the dissolution of the flocs in the presence of dissimilatory iron reducing bacteria (DIRB) can occur and how the dissolution influences the fate of Fe and Cd in the sediment. A recent study has demonstrated that *Shewanella oneidensis* MR-1, as representative DIRB, has the ability to reduce the flocs, resulting in the release of Fe^{2+} and Cd^{2+} to the solution and subsequent formation of iron minerals such as goethite and magnetite as a consequence of microbial Fe(III) reduction. The newly formed goethite and magnetite can re-immobilize Cd (Fig. 18) [388]. Studies like this provide solid evidence for natural attenuation of metals in the sediment.

Chlorinated solvents are common groundwater contaminants due to their wide use in industry and commerce. Magnetite is known to be able to degrade certain chlorinated solvents under laboratory conditions [389], [390], [391], [392], [393], [394]. A study also shows that 0.3% magnetite in aquifer sediment was responsible for the natural attenuation of *cis*-dichloroethene (*cis*-DCE) in a groundwater plume [395]. A recent study has reported CCl_4 degradation by different minerals with the normalized rate constant in the order of Fe^0 > GR > Fe(II) sorbed goethite > magnetite [396]. Another study found the rate constants for *cis*-DCE degradation in the order of GR > $Fe(OH)_2$ > mackinawite = magnetite [397]. More recently, a general trend of mineral reactivity toward chlorinated solvent degradation has

been approximated as follows: disordered FeS > FeS > Fe^0 > FeS_2 > sorbed Fe^{2+} > GR = magnetite > biotite = vermiculite [398]. Compared to Fe^0, iron sulfides, and GR, magnetite is less reactive in dechlorination; however, magnetite is more resistant to oxidation than the other minerals and its role in dechloration can be significant if magnetite is present in large quantities in aquifers.

8. Discussion

The potential number of hybrid nanocomposites that may conjugate MNPs with other NMs could be astronomical and it may be impractical to try out every possible combinations. Thus it is imperative that optimal experimental design is conceived to be scientifically feasible and economically cost-effective. Scale-up of synthesis methods may be challenging for making large quantities of MNP hybrid catalysts and reactants for environmental applications. The development of a low-cost, fast, and large-scale process for the synthesis and manipulation of MNPs is essential for incorporating materials with diverse practical applications. Green synthesis is an area in need of further investigation. More economical raw materials may be exploited for synthesizing MNPs. For example, a recent study has attempted to make MNPs using ferric iron recovered from waste iron ore tailing and reagent grade $FeCl_2$ by coprecipitation, for the decolourisation of RhB under visible light (VL)/ sunlight [399]. Euphorbia stracheyi Boiss plant root extract has been used as a natural source of reducing and stabilizing agent for supporting Pd NPs on MNPs. The Pd/Fe_3O_4 NPs can efficiently catalyze the reductive amination of aldehydes at room temperature [400]. Clay minerals are cheap and abundant. Eco-friendly pillared montmorillonites, in which the pillars consist of a magnetic iron oxide (γ-Fe_2O_3) have been synthesized using mild reaction conditions and benign products. The composite shows catalytic degradation of dichlorophenol (DCP) in the presence of PMS or H_2O_2 and peracetic acid [401]. A method has been reported to synthesize magnetic expanded perlite composite through a co-precipitation method using single iron source and yellow pea as a reducing agent. The suggested method is environment friendly, easy, and biogenic. The combination of MNPs with expanded perlite and its modification with ibuprofen results in a new, cost-effective, and eco-friendly magnetic adsorbent for dye (Direct Red-81) removal from contaminated streams [402].

Because magnetite is a major component of the passivation layer of granular ZVI, and because magnetite (both nanosized and microsized) is also a Fe^0 corrosion product when NZVI is used for source zone treatment of chlorinated solvents [403], [404], magnetite is an important link with respect to contaminant degradation and removal. Researchers have explored means of depassivation of aged ZVI by divalent cations. For example, a recent study has evaluated dechlorination of trichloroethylene (TCE) by aged Fe^0 in the presence of a series of divalent cations with the result that while no significant degradation of TCE is observed in Milli-Q water or in solutions of Ba^{2+}, Sr^{2+}, or Ca^{2+}, very effective TCE removal is observed in solutions containing Mg^{2+}, Mn^{2+}, Co^{2+}, Fe^{2+}, Ni^{2+}, Zn^{2+}, Cu^{2+}, or Pb^{2+}. The depassivation process is proposed to involve (i) surface complexation of cations on surface coatings of aged Fe^0, (ii) dissolution of the hydrated surface as a consequence of magnetite exposure, and (iii) transport of electrons from underlying Fe^0 via magnetite to TCE, resulting in TCE dechlorination and, for some cations (Co^{2+}, Ni^{2+}, Cu^{2+}, and Pb^{2+}),

reduction to their zero or +1 valence state (with potential for these reduced metals to enhance TCE degradation) [405]. Surfactants have been used to increase reactivity of NZVI-based materials. In a recent study, pentachlorophenol (PCP) is treated with Ni/Fe NPs. An increase in the Ni/Fe dosage enhances the removal of PCP. The most effective nickel percentage is 0.5%. Among the selected surfactants including carboxymethyl cellulose, Triton X-100, and CTAB, CTAB markedly enhances the removal of PCP by Ni/Fe [406]. Short-chain organic acids such as oxalic acid have been used as a complexation agent for ferrous iron to depassivate the iron oxide layer to generate fresh NZVI surfaces for PCP degradation by NZVI [407]. Oxalic acid is a greener treatment agent than doping metal on NZVI.

More research should be conducted on the field-scale impact of magnetite on groundwater contaminant degradation. NZVI corrodes away within a few months in groundwater but magnetite can be persistent [404]. More work is needed to characterize the formation and transformation of magnetite in groundwater systems where active remediation takes place. More laboratory and field tests could be performed to evaluate MNPs for soil treatment. Other NPs have been investigated, for example, a new class of stabilized Fe–Mn binary oxide nanoparticles is prepared with a water-soluble starch or CMC as a stabilizer [408]. The NPs are characterized and tested with respect to sorption of As(III) and As(V) from water and for immobilization of As(III) in soil. While arsenic sorption capacities are comparable for bare, or stabilized Fe–Mn nanoparticles, particle stabilization enables the NPs to be delivered into soil for *in situ* immobilization of As(III). High As(III) sorption capacity is observed at pH 5–9. Column breakthrough tests demonstrate soil mobility of CMC-stabilized NPs. Once delivered, the NPs remain virtually immobile in soil under typical groundwater conditions, serving as a fixed sink for arsenic [408].

More attention should be paid to evaluation of the role magnetite plays in the natural attenuation of contaminants in soil and groundwater. Microorganisms (*e.g.*, *G. metallireducens*) can reduce hydrous ferric oxide to magnetite and/or to Fe(II) surface species bound to the magnetite surface under Fe(III)-reducing conditions. These biogenic magnetite and sorbed Fe(II) surface species could be regenerated by Fe(II) produced by microorganisms after their oxidation by chlorinated solvents. Thus, abiotic degradation by biogenic minerals may be long lasting if reducing conditions are maintained. This relationship can be used to design “in situ permeable reactive barriers” systems [398].

Magnetite had been considered as a stable end product of the bioreduction of Fe(III) minerals (*e.g.*, ferrihydrite, lepidocrocite, hematite) or of the biological oxidation of Fe(II) compounds (*e.g.*, siderite), with GR as a mixed Fe(II)–Fe(III) hydroxide intermediate. Biotic transformation of magnetite to GR had not been demonstrated until now. A recent study has investigated the capability of an iron-educing bacterium, *Shewanella putrefaciens*, to reduce magnetite at circumneutral pH in the presence of dihydrogen as sole inorganic electron donor. During incubation, GR and/or siderite ($Fe(II)CO_3$) formation occurs as secondary iron minerals, resulting from the precipitation of Fe(II) species produced via the bacterial reduction of Fe(III) species present in magnetite. Taking into account the exact nature of the secondary iron minerals and the electron donor source is necessary to understand the exergonic character of the biotic transformation of magnetite to GR, which had been

considered to date as thermodynamically unfavorable at circumneutral pH. This finding reinforces the hypothesis that GR would be the cornerstone of the microbial transformations of iron-bearing minerals in the anoxic biogeochemical cycle of iron and opens up new possibilities for the interpretation of the evolution of Earth's history and for the understanding of biocorrosion processes in the field of applied science [409]. This may also have important implications when engineered MNPs are used for environmental remediation.

9. Summary

This review covers only a selective portion of a huge and ever increasing body of recent literature on environmental implications and applications of MNPs. MNPs are attractive and promising materials for helping solve environmental contamination problems due to their paramagnetism that leads to easy separation from the environmental media and recyclability of use, as well as the large surface area for contaminant adsorption and immobilization. MNPs possess chemical reducing power that can reduce toxic chemicals to less toxic or non-toxic forms. MNPs are widely used as reusable catalysts for oxidative degradation of recalcitrant contaminants. The following are main points of this review.

- There are a variety of synthesis methods for making MNPs and their hybrids each with its own advantages and disadvantages. A suitable method has to be the one that produces the desired MNPs with specific size, shape, and shelf life.
- Fate and transport of MNPs and their hybrids depend on the surface charge properties and properties of the porous media and solution chemistry.
- MNPs have low to none toxicity to humans and ecosystems. Surface modification has to be made to make them biocompatible.
- MNPs are important advanced anode materials for lithium-ion batteries.
- MNPs are widely used in making biosensors, chemical sensors, and recyclable catalysts.
- MNPs are widely used as adsorptive and separative removal of a wide range of contaminants from wastewater.
- MNPs may be important in active remediation and natural attenuation of contaminants.
- Further studies are needed to explore ways to cost effectively synthesize MNPs and to develop practical methods for soil and groundwater remediation.

Acknowledgements

The work upon which this paper is based was supported by the U.S. Environmental Protection Agency through its Office of Research and Development. This work has not been subjected to agency review and, therefore, doesn't necessarily reflect the views of the agency and no official endorsement should be inferred. Any product or trade name mentioned here is for information purposes only and not to constitute endorsement.

Abbreviations

AC	activated carbon
AD	anaerobic digestion
AAS	atomic absorption spectrometry
APAP	Acetaminophen
AQDS	9,10-anthraquinone-2,6-disulfonate
BB	bromothymol blue
BC	bacterial cellulose
BMCs	biochar-mineral complexes
BPA	bisphenol A
BTEX	benzene, toluene, ethylbenzene and xylenes
CA	contact angle
CBZ	carbamazepine
β-CD	β-cyclodextrin
CG	chitosan-functionalized grapheme
CMC	carboxymethyl cellulose
CNF	carbon nanofiber
CNTs	carbon nanotubes
CQDs	carbon quantum dots
CSN	core–shell nanospheres
CTAB	cetyltrimethylammonium bromide
CTPEs	composite thermoplastic elastomers
2,4-D	2,4-dichlorophenoxyacetic acid
DCP	dichlorophenol
DCPD	dicyclopentadiene
DFMNPs	double functionalized magnetic nanoparticles
DIRB	dissimilatory iron reducing bacteria
DMSA	dimercaptosuccinic acid
DSPE	dispersed solid-phase extraction

EDTA-MGO	ethylenediaminetetraacetic acid-magnetic graphene oxide
EG	ethylene glycol
FLU	flumequine
GA	gallic acid
GO	graphene/graphite oxide
GR	green rust
HA	humic acid
HNTs	halloysite nanotubes
HPLC	high performance liquid chromatography
HUVEC	human umbilical vein endothelial cells
ICP-MS	inductively coupled plasma-mass spectrometry
LDH	layered double hydroxide
MAA	methacrylic acid
MB	methylene blue
MCM	magnetic composite microsphere
MCS	magnetic core/shell
MC-TiNbNS	magnetite/ceria-codecorated titanoniobate nanosheet
m-Fe_3O_4-CN	magnetic Fe_3O_4 chitosan nanoparticles
MGO	magnetic graphene oxide
MNCs	magnetic nanocomposites
MNPs	magnetite nanoparticles
M-QAC	magnetite-quaternary ammonium compounds
MWCNTs	multi-walled carbon nanotubes
MS-MRS	magnetic separation and magnetic relaxation switching
NMs	nanomaterials
NFMs	nanofibrous membranes
NOM	natural organic matter
4-NP	4-nitrophenol
4-*n*-NP	4-*n*-nonylphenol

NPs	nanoparticles
NZVI	nanosized zerovalent iron
PAHs	polycyclic aromatic hydrocarbons
PCP	pentachlorophenol
PDA	polydopamine
PET	polyethylene terephthalate
PEG	polyethylene glycol
PEI	polyethylenimine
PFOS	perfluorooctane sulfonates
PGA@MNP	polygallate coated magnetic nanoparticles
PHQ	polyhydroquinone
PMMA	poly(methylmethacrylate)
PMS	peroxymonosulfate
PPy	polypyrrole
PQA	poly quaternary ammonium
PUU	poly(urea-urethane)
PVA	polyvinlyalcohol
PVP	poly(vinylpyrrolidone)
PVDF	polyvinylidene fluoride
PZC	point of zero charge
QAC	quaternary ammonium compounds
RGO	reduced graphene oxide
RhB	rhodamine B
ROS	reactive oxygen species
SEM	scanning electron microscope
SERS	surface enhanced Raman spectroscopy
SPE	solid-phase extraction
SPION	superparamagnetic iron oxide nanoparticles
TBBPA	tetrabromobisphenol A

TC	tetracycline
TCE	trichloroethene
TCLP	toxicity characteristic leaching procedure
TEM	transmission electron microscopy
TEPA	tetraethylenepentamine
TETA	triethylentetramine
XAS	X-ray absorption spectroscopy
XANES	X-ray adsorption near edge structure
XPS	X-ray photoelectron spectroscopy
XRD	X-ray diffraction
YSN	Yolk–shell nanospheres
ZVI	Zerovalent iron

References

[1]. Wu W, Wu Z, Yu T, Jiang C, Kim W-S Recent progress on magnetic iron oxide nanoparticles: synthesis, surface functional strategies and biomedical applications Sci. Technol. Adv. Mater, 16 (2015), pp. 23501–23543

[2]. Sun S-N, Chao W, Zhu Z-Z, Hou Y-L, Venkatraman SS, Xu Z-C Magnetic iron oxide nanoparticles: synthesis and surface coating techniques for biomedical applications Chin. Phys. B, 23 (2014), p. 037503

[3]. Shi D, Sadat ME, Dunn AW, Mast DB Photo-fluorescent and magnetic properties of iron oxide nanoparticles for biomedical applications Nanoscale, 7 (2015), pp. 8209–8232 [PubMed: 25899408]

[4]. Sharifi S, Seyednejad H, Laurent S, Atyabi F, Saei AA, Mahmoudi M Superparamagnetic iron oxide nanoparticles for in vivo molecular and cellular imaging Contrast Media Mol. Imaging, 10 (2015), pp. 329–355 [PubMed: 25882768]

[5]. Revia RA, Zhang M Magnetite nanoparticles for cancer diagnosis, treatment, and treatment monitoring: recent advances Mater. Today, 19 (2016), pp. 157–168

[6]. Talelli M, Aires A, Marciello M Protein-modified magnetic nanoparticles for biomedical applications Curr. Org. Chem, 20 (2016), pp. 1252–1261

[7]. Sonmez M, Georgescu M, Alexandrescu L, Gurau D, Ficai A, Ficai D, Andronescu E Synthesis and applications of Fe3O4/SiO2 core–shell materials Curr. Pharm. Des, 21 (2015), pp. 5324–5335 [PubMed: 26377652]

[8]. Dutta S, Parida S, Maiti C, Banerjee R, Mandal M, Dhara D Polymer grafted magnetic nanoparticles for delivery of anticancer drug at lower pH and elevated temperature J. Colloid Interface Sci, 467 (2016), pp. 70–80 [PubMed: 26773613]

[9]. Horst MF, Lassalle V, Ferreira ML Nanosized magnetite in low cost materials for remediation of water polluted with toxic metals, azo- and antraquinonic dyes Front. Environ. Sci. Eng, 9 (2015), pp. 746–769

[10]. Sharma VK, McDonald TJ, Kim H, Garg VK Magnetic graphene–carbon nanotube iron nanocomposites as adsorbents and antibacterial agents for water purification Adv. Colloid Interface Sci, 225 (2015), pp. 229–240 [PubMed: 26498500]

[11]. Lu AH, Salabas EL, Schuth F Magnetic nanoparticles: synthesis protection, functionalization, and application Angew. Chem. Int. Ed, 46 (2007), pp. 1222–1244

[12]. Wu W, He Q, Jiang C Magnetic iron oxide nanoparticles: synthesis and surface functionalization strategies Nanoscale Res. Lett, 3 (2008), pp. 397–415 [PubMed: 21749733]

[13]. Unsoy G, Gunduz U, Oprea O, Ficai D, Sonmez M, Radulescu M, Alexie M, Ficai A Magnetite: from synthesis to applications Curr. Topics Med. Chem, 15 (2015), pp. 1622–1640

[14]. Fratila RM, Mitchell SG, del Pino P, Grazu V, de la Fuente JM Strategies for the biofunctionalization of gold and iron oxide nanoparticles Langmuir, 30 (2014), pp. 15057–15071 [PubMed: 24911468]

[15]. Lee J, Isobe T, Senna M Magnetic properties of ultrafine magnetite particles and their slurries prepared via in-situ precipitation Colloids Surf. A: Physicochem. Eng. Aspects, 109 (1996), pp. 121–127

[16]. Kim JH, Kim SM, Kim YI Properties of magnetic nanoparticles prepared by co-precipitation J. Nanosci. Nanotechnol, 14 (2014), pp. 8739–8744 [PubMed: 25958595]

[17]. Vikram S, Dhakshnamoorthy M, Vasanthakumari R, Rajamani AR, Rangarajan M, Tsuzuki T Tuning the magnetic properties of iron oxide nanoparticles by a room-temperature air-atmosphere (RTAA) co-precipitation method J. Nanosci. Nanotechnol, 15 (2015), pp. 3870–3878 [PubMed: 26505017]

[18]. Chen J, Yuan TJ Effects of citrate on preparation and properties of nano-Fe_3O_4 J. Mater. Eng, 43 (2015), pp. 85–89

[19]. Yoon KY, Xue Z, Fei Y, Lee JH, Cheng V, Bagaria HG, Huh C, Bryant SL, Kong SD, Ngo VW, Rahmani A-R, Ahmadian M, Ellison CJ, Johnston KP Control of magnetite primary particle size in aqueous dispersions of nanoclusters for high magnetic susceptibilities J. Colloid Interface Sci, 462 (2016), pp. 359–367

[20]. Muthukumaran T, Philip J A single pot approach for synthesis of phosphate coated iron oxide nanoparticles J. Nanosci. Nanotechnol, 15 (2015), pp. 2715–2725 [PubMed: 26353485]

[21]. Yang W, Yu Y, Wang L, Yang C, Li H Controlled synthesis and assembly into anisotropic arrays of magnetic cobalt-substituted magnetite nanocubes Nanoscale, 7 (2015), pp. 2877–2882 [PubMed: 25611252]

[22]. Zaki HM, Al-Heniti SH, Al-Hadeethi Y, Alsanoosi AM Magnetic nanoparticles: synthesis, characterization and magnetic properties of cobalt aluminum ferrite J. Nanosci. Nanotechnol, 16 (2016), pp. 4733–4741 [PubMed: 27483815]

[23]. Huang S, Wang H, Zhu N, Lou Z, Li L, Shan A, Yuan H Metal recovery based magnetite near-infrared photocatalyst with broadband spectrum utilization property Appl. Catal. B: Environ, 181 (2016), pp. 456–464

[24]. Li XA, Wang CS, Han XJ Electromagnetic wave absorbing property of composite Fe_3O_4-graphite prepared by in-situ chemical precipitation J. Mater. Eng, 43 (2015), pp. 44–49

[25]. Qu B, Zhu C, Li C, Zhang X, Chen Y Coupling hollow Fe_3O_4–Fe nanoparticles with graphene sheets for high-performance electromagnetic wave absorbing material ACS Appl. Mater. Interfaces, 8 (2016), pp. 3730–3735 [PubMed: 26829291]

[26]. Giardiello M, Hatton FL, Slater RA, Chambon P, North J, Peacock AK, He T, McDonald TO, Owen A, Rannard SP Stable, polymer-directed and SPION-nucleated magnetic amphiphilic block copolymer nanoprecipitates with readily reversible assembly in magnetic fields Nanoscale, 8 (2016), pp. 7224–7231 [PubMed: 26973155]

[27]. Park J, An K, Hwang Y, Park J-G, Noh H-J, Kim J-Y, Park J-H, Hwang N-M, Hyeon T Ultra-large-scale syntheses of monodisperse nanocrystals Nat. Mater, 3 (2004), pp. 891–895 [PubMed: 15568032]

[28]. Sun S, Zeng H, Robinson DB, Raoux S, Rice PM, Wang SX, Li G Monodisperse MFe_2O_4 (M = Fe, Co, Mn) nanoparticles J. Am. Chem. Soc, 126 (2004), pp. 273–279 [PubMed: 14709092]

[29]. Redl FX, Black CT, Papaefthymiou GC, Sandstrom RL, Yin M, Zeng H, Murray CB, O'Brien SP Magnetic, electronic, and structural characterization of nonstoichiometric iron oxides at the nanoscale J. Am. Chem. Soc, 126 (2004), pp. 14583–14599 [PubMed: 15521779]

[30]. Li Z, Sun Q, Gao M Preparation of water-soluble magnetite nanocrystals from hydrated ferric salts in 2-pyrrolidone: mechanism leading to Fe_3O_4 Angew. Chem, 117 (2005), pp. 125–128

[31]. Hu FQ, Wei L, Zhou Z, Ran YL, Li Z, Gao MY Preparation of biocompatible magnetite nanocrystals for in vivo magnetic resonance detection of cancer Adv. Mater, 18 (2006), pp. 2553–2556

[32]. Bixner O, Lassenberger A, Baurecht D, Reimhult E Complete exchange of the hydrophobic dispersant shell on monodisperse superparamagnetic iron oxide nanoparticles Langmuir, 31 (2015), pp. 9198–9204 [PubMed: 26226071]

[33]. Palma SICJ, Marciello M, Carvalho A, Veintemillas-Verdaguer S, del Puerto Morales M, Roque ACA Effects of phase transfer ligands on monodisperse iron oxide magnetic nanoparticles J. Colloid Interface Scie, 437 (2015), pp. 147–155

[34]. Zhuang L, Zhang W, Zhao Y, Shen H, Lin H, Liang J Preparation and characterization of Fe_3O_4 particles with novel nanosheets morphology and magnetochromatic property by a modified solvothermal method Sci. Rep, 5 (2015), p. 9320 [PubMed: 25799320]

[35]. Patsula V, Kosinová L, Lovrić M, Hamzić LF, Rabyk M, Konefal R, Paruzel A, Šlouf M, Herynek V, Gajović S, Horák D Superparamagnetic Fe_3O_4 nanoparticles: synthesis by thermal decomposition of iron(III) glucuronate and application in magnetic resonance imaging ACS Appl. Mater. Interfaces, 8 (2016), pp. 7238–7247 [PubMed: 26928653]

[36]. Deniz AR, Çaldıran Z, Metin Ö, Meral K, Aydoğan Ş The investigation of the electrical properties of Fe_3O_4/n-Si heterojunctions in a wide temperature range J. Colloid Interface Sci, 473 (2016), pp. 172–181 [PubMed: 27078739]

[37]. Shin J, Lee KY, Yeo T, Choi W Facile one-pot transformation of iron oxides from Fe_2O_3 nanoparticles to nanostructured Fe_3O_4@C core–shell composites via combustion waves Sci. Rep, 6 (2016), p. 21792, 10.1038/srep21792 [PubMed: 26902260]

[38]. Wang X, Zhuang J, Peng Q, Li Y A general strategy for nanocrystal synthesis Nature, 437 (2005), pp. 121–124 [PubMed: 16136139]

[39]. Karunakaran C, Vinayagamoorthy P, Jayabharathi J Nonquenching of charge carriers by Fe_3O_4 core in Fe_3O_4/ZnO nanosheet photocatalyst Langmuir, 30 (2014), pp. 15031–15039 [PubMed: 25425261]

[40]. Sheng W, Liu J, Liu S, Lu Q, Kaplan DL, Zhu H One-step synthesis of biocompatible magnetite/silk fibroin core–shell nanoparticles J. Mater. Chem. B, 2 (2014), pp. 7394–7402 [PubMed: 32261964]

[41]. Song H, Liu M, Li S, Chen L, Lin C, Zhang L Polyvinyl pyrrolidone-assisted solvothermal synthesis of Fe_3O_4 vesicular nanospheres J. Nanosci. Nanotechnol, 15 (2015), pp. 3998–4002 [PubMed: 26505038]

[42]. Wang L, Zhao Q, Hou J, Yan J, Zhang F, Zhao J, Ding H, Li Y, Ding L One-step solvothermal synthesis of magnetic Fe_3O_4–graphite composite for Fenton-like degradation of levofloxacin J. Environ. Sci. Health Part A, 51 (2016), pp. 52–62

[43]. Tong G, Liu Y, Wu T, Tong C, Du F H_2O-steered size/phase evolution and magnetic properties of large-scale, monodisperse Fe_xO_y nanomaterials J. Mater. Chem. C, 3 (2015), pp. 5506–5515

[44]. Tiano AL, Papaefthymiou GC, Lewis CS, Han J, Zhang C, Li Q, Shi C, Abeykoon AMM, Billinge SJL, Stach E, Thomas J, Guerrero K, Munayco P, Munayco J, Scorzelli RB, Burnham P, Viescas AJ, Wong SS Correlating size and composition-dependent effects with magnetic Mössbauer, and pair distribution function measurements in a family of catalytically active ferrite nanoparticles Chem. Mater, 27 (2015), pp. 3572–3592

[45]. Zhao H, Cui H-J, Fu M-L A general and facile method for improving carbon coat on magnetic nanoparticles with a thickness control J. Colloid Interface Sci, 461 (2016), pp. 20–24 [PubMed: 26397904]

[46]. Yang Q, Lan F, Yi Q, Wu Y, Gu Z A colloidal assembly approach to synthesize magnetic porous composite nanoclusters for efficient protein adsorption Nanoscale, 7 (2015), pp. 17617–17622 [PubMed: 26452125]

[47]. Kim Y, Yul Y Microbial synthesis and characterization of superparamagnetic Zn-substituted magnetite nanoparticles J. Nanosci. Nanotechnol, 15 (2015), pp. 6129–6132 [PubMed: 26369212]

[48]. O'Loughlin EJ, Gorski CA, Scherer MM Effects of phosphate on secondary mineral formation during the bioreduction of akaganeite (β-FeOOH): green rust versus framboidal magnetite Curr. Inorg. Chem, 5 (2015), pp. 214–224

[49]. Tuo Y, Liu G, Dong B, Zhou J, Wang A, Wang J Microbial synthesis of Pd/Fe_3O_4 Au/Fe_3O_4 and PdAu/Fe_3O_4 nanocomposites for catalytic reduction of nitroaromatic compounds Sci. Rep, 5 (2015), p. 13515 [PubMed: 26310728]

[50]. Chen C, Wang P, Li L Applications of bacterial magnetic nanoparticles in nanobiotechnology J. Nanosci. Nanotechnol, 16 (2016), pp. 2164–2171 [PubMed: 27455615]

[51]. Schmidtke C, Eggers R, Zierold R, Feld A, Kloust H, Wolter C, Ostermann J, Merkl J-P, Schotten T, Nielsch K, Weller H Polymer-assisted self-assembly of superparamagnetic iron oxide nanoparticles into well-defined clusters: controlling the collective magnetic properties Langmuir, 30 (2014), pp. 11190–11196 [PubMed: 25152249]

[52]. Lin AL, Rodrigues JNB, Su C, Milletari M, Loh KP, Wu T, Chen W, Castro Neto AH, Adam S, Wee ATS Tunable room-temperature ferromagnet using an iron-oxide and graphene oxide nanocomposite Sci. Rep, 5 (2015), p. 11430 [PubMed: 26100970]

[53]. Lee J, Kwon SG, Park J-G, Hyeon T Size dependence of metal-insulator transition in stoichiometric Fe_3O_4 nanocrystals Nano Lett., 15 (2015), pp. 4337–4342 [PubMed: 26079048]

[54]. Wang Y, He Q, Qu H, Zhang X, Guo J, Zhu J, Zhao G, Colorado HA, Yu J, Sun L, Bhana S, Khan MA, Huang X, Young DP, Wang H, Wang X, Wei S, Guo Z Magnetic graphene oxide nanocomposites: nanoparticles growth mechanism and property analysis J. Mater. Chem. C, 2 (2014), pp. 9478–9488

[55]. Fu M, Li J One-pot solvothermal synthesis and adsorption property of Pb(II) of superparamagnetic monodisperse Fe_3O_4/graphene oxide nanocomposite Nanosci. Nanotechnol. Lett, 6 (2014), pp. 1116–1122

[56]. Zhang S, Li W, Tan B, Chou S, Li Z, Dou S One-pot synthesis of ultra-small magnetite nanoparticles on the surface of reduced graphene oxide nanosheets as anodes for sodium-ion batteries J. Mater. Chem. A, 3 (2015), pp. 4793–4798

[57]. Tsoufis T, Syrgiannis Z, Akhtar N, Prato M, Katsaros F, Sideratou Z, Kouloumpis A, Gournis D, Rudolf P In situ growth of capping-free magnetic iron oxide nanoparticles on liquid-phase exfoliated grapheme Nanoscale, 7 (2015), pp. 8995–9003 [PubMed: 25920624]

[58]. Cao Y Preparation and magnetic properties of a multi-walled carbon nanotube-iron oxide nanoparticle composite Fullerenes Nanotubes Carbon Nanostruct., 23 (2015), pp. 623–626

[59]. Ji Z, Shen X, Yue X, Zhou H, Yang J, Wang Y, Ma L, Chen K Facile synthesis of magnetically separable reduced graphene oxide/magnetite/silver nanocomposites with enhanced catalytic activity J. Colloid Interface Sci, 459 (2015), pp. 79–85 [PubMed: 26263498]

[60]. Shekofteh-Gohari M, Habibi-Yangjeh A Ultrasonic-assisted preparation of novel ternary ZnO/AgI/Fe_3O_4 nanocomposites as magnetically separable visible-light-driven photocatalysts with excellent activity J. Colloid Interface Sci, 461 (2016), pp. 144–153 [PubMed: 26397921]

[61]. Islam MR, Bach LG, Vo TS, Lim KT Covalent immobilization of biotin on magnetic nanoparticles: synthesis, characterization, and cytotoxicity studies J. Nanosci. Nanotechnol, 15 (2015), pp. 176–180 [PubMed: 26328324]

[62]. Brollo MEF, Lopez-Ruiz R, Muraca1 D, Figueroa SJA, Pirota KR, Knobel M Compact Ag@Fe_3O_4 core–shell nanoparticles by means of single-step thermal decomposition reaction Sci. Rep, 4 (2014), p. 6839, 10.1038/srep06839 [PubMed: 25354532]

[63]. Guldu OK, Unak P, Medine EI, Barlas FB, Muftuler FZB, Timur S Radioiodinated magnetic nanoparticles conjugated with moxifloxacin: synthesis and in vitro biological affinities Int. J. Polym. Mater. Polym. Biomater, 64 (2015), pp. 253–259

[64]. Tancredi P, Botasini S, Moscoso-Londoño O, Méndez E, Socolovsky L Polymer-assisted size control of water-dispersible iron oxide nanoparticles in range between 15 and 100 nm Colloids Surf. A: Physicochem. Eng. Aspects, 464 (2015), pp. 46–51

[65]. Serenjeh FN, Hashemi P, Rasoolzadeh F A simple method for the preparation of spherical core–shell nanomagnetic agarose particles Colloids Surf. A: Physicochem. Eng. Aspects, 465 (2015), pp. 47–53

[66]. Park DE, Chae HS, Choi HJ, Maity A Magnetite–polypyrrole core–shell structured microspheres and their dual stimuli-response under electric and magnetic fields J. Mater. Chem. C, 3 (2015), pp. 3150–3158

[67]. Yan X, Kong J, Yang C, Fu G Facile synthesis of hairy core–shell structured magnetic polymer submicrospheres and their adsorption of bovine serum albumin J. Colloid Interface Sci, 445 (2015), pp. 9–15 [PubMed: 25594881]

[68]. Woo H, Park JC, Park S, Park KH Rose-like Pd–Fe_3O_4 hybrid nanocomposite-supported Au nanocatalysts for tandem synthesis of 2-phenylindoles Nanoscale, 7 (2015), pp. 8356–8360 [PubMed: 25901692]

[69]. Li M, Li X, Qi X, Luo F, He G Shape-controlled synthesis of magnetic iron oxide@SiO_2–Au@C particles with core–shell nanostructures Langmuir, 31 (2015), pp. 5190–5197 [PubMed: 25892156]

[70]. Jiang F, Zhang Y, Wang Z, Wang W, Xu Z, Wang Z Combination of magnetic and enhanced mechanical properties for copolymer-grafted magnetite composite thermoplastic elastomers ACS Appl. Mater. Interfaces, 7 (2015), pp. 10563–10575 [PubMed: 25954980]

[71]. Song HM, Zink JI, Khashab NM Engineering the internal structure of magnetic silica nanoparticles by thermal control Part. Part. Syst. Charact, 32 (2015), pp. 307–312

[72]. Liu X, Chen Y, Cui X, Zeng M, Yu R, Wang G-S Flexible nanocomposites with enhanced microwave absorption properties based on Fe_3O_4/SiO_2 nanorods and polyvinylidene fluoride J. Mater. Chem. A, 3 (2015), pp. 12197–12204

[73]. Chen X, Tan L, Meng X Synthesis of magnetic rattle-type silica with controllable magnetite and tunable size by pre-shell-post-core method J. Nanosci. Nanotechnol, 16 (2016), pp. 3003–3008 [PubMed: 27455750]

[74]. Ma J, Wang K, Zhan M Growth mechanism and electrical and magnetic properties of Ag–Fe_3O_4 core–shell nanowires ACS Appl. Mater. Interfaces, 7 (2015), pp. 16027–16039 [PubMed: 26151331]

[75]. Zhang H, Liu Y, Zhou Y Preparation of magnetic PET fabric loaded with Fe_3O_4 nanoparticles by hydrothermal method J. Text. Inst, 106 (2015), pp. 1078–1088

[76]. Chiaradia V, Valério A, Feuser PE, de Oliveira D, Araújo PHH, Sayer C Incorporation of superparamagnetic nanoparticles into poly(urea-urethane) nanoparticles by step growth interfacial polymerization in miniemulsion Colloids Surf. A: Physicochem. Eng. Aspects, 482 (2015), pp. 596–603

[77]. Mallakpour S, Javadpour M An innovative strategy for the production of novel magnetite poly(vinyl alcohol) nanocomposite films with double-capped synthesized Fe_3O_4 nanoparticles with citric acid and vitamin C Compos. Interfaces, 22 (2015), pp. 867–884

[78]. Rowe MP, Sullivan S, Desautels RD, Skoropata E, van J Lierop Rational selection of superparamagnetic iron oxide/silica nanoparticles to create nanocomposite inductors J. Mater. Chem. C, 3 (2015), pp. 9789–9793

[79]. Shi H, Yang J, Zhu L, Yang Y, Yuan H, Yang Y, Liu X Removal of Pb^{2+} Hg^{2+}, and Cu^{2+} by chain-like Fe_3O_4@SiO_2@chitosan magnetic nanoparticles J. Nanosci. Nanotechnol, 16 (2016), pp. 1871–1882 [PubMed: 27433691]

[80]. Zhu Z, Li G, Zeng G, Chen X, Hu D, Zhang Y, Sun Y Fast capture of methyl-dyes over hierarchical amino-$Co_{0.3}Ni_{0.7}Fe_2O_4$@SiO_2 nanofibrous membranes J. Mater. Chem. A, 3 (2015), pp. 22000–22004

[81]. Liu S, Fu J, Wang M, Yan Y, Xin Q, Cai L, Xu Q Magnetically separable and recyclable Fe_3O_4–polydopamine hybrid hollow microsphere for highly efficient peroxidase mimetic catalysts J. Colloid Interface Sci, 469 (2016), pp. 69–77 [PubMed: 26871276]

[82]. Shan R-R, Yan L-G, Yang K, Hao Y-F, Du B Adsorption of Cd(II) by Mg–Al–CO_3- and magnetic Fe_3O_4/Mg–Al–CO_3-layered double hydroxides: kinetic, isothermal, thermodynamic and mechanistic J. Hazard. Mater, 299 (2015), pp. 42–49 [PubMed: 26073520]

[83]. Zhang S, Fan Q, Gao H, Huang Y, Liu X, Li J, Xu X, Wang X Formation of Fe_3O_4@MnO_2 ball-in-ball hollow spheres as a high performance catalyst with enhanced catalytic performances J. Mater. Chem. A, 4 (2016), pp. 1414–1422

[84]. Wang Y, Pan F, Dong W, Xu L, Wu K, Xu G, Chen W Recyclable silver-decorated magnetic titania nanocomposite with enhanced visible-light photocatalytic activity Appl. Catal. B: Environ, 189 (2016), pp. 192–198

[85]. Gawande MB, Branco PS, Varma RS Nano-magnetite (Fe_3O_4) as support for recyclable nano-catalysts in the development of sustainable methodologies Chem. Soc. Rev, 42 (2013), pp. 3371–3393 [PubMed: 23420127]

[86]. Varma RS Journey on greener pathways: from the use of alternate energy inputs and benign reaction media to sustainable applications of nano-catalysts in synthesis and environmental remediation Green Chem., 16 (2014), pp. 2027–2041

[87]. Sharma VK Festschrift in honor of Rajender S. Varma ACS Sustain. Chem. Eng, 4 (2016), pp. 640–642

[88]. Nasir Baig RB, Varma RS Organic synthesis via magnetic attraction: benign and sustainable protocols using magnetic nanoferrites Green Chem., 15 (2013), pp. 398–417

[89]. Atarod M, Nasrollahzadeh M, Sajadi SM Green synthesis of Pd/RGO/Fe_3O_4 nanocomposite using Withania coagulans leaf extract and its application as magnetically separable and reusable catalyst for the reduction of 4-nitrophenol J. Colloid Interface Sci, 465 (2016), pp. 249–258 [PubMed: 26674242]

[90]. Sajadi SM, Nasrollahzadeh M, Maham M Aqueous extract from seeds of Silybum marianum L. as a green material for preparation of the Cu/Fe_3O_4 nanoparticles: a magnetically recoverable and reusable catalyst for the reduction of nitroarenes J. Colloid Interface Sci, 469 (2016), pp. 93–98 [PubMed: 26874271]

[91]. Tosco T, Bosch J, Meckenstock RU, Sethi R Transport of ferrihydrite nanoparticles in saturated porous media: role of ionic strength and flow rate Environ. Sci. Technol, 46 (2012), pp. 4008–4015 [PubMed: 22356610]

[92]. Drozdov AS, Ivanovski V, Avnir D, Vinogradov VV A universal magnetic ferrofluid: nanomagnetite stable hydrosol with no added dispersants and at neutral pH J. Colloid Interface Sci, 467 (2016), pp. 307–312 [PubMed: 26844393]

[93]. Peeters K, Lespes G, Zuliani T, Ščančar J, Milačič R The fate of iron nanoparticles in environmental waters treated with nanoscale zero-valent iron, FeONPs and Fe_3O_4NPs Water Res., 94 (2016), pp. 315–327 [PubMed: 26971807]

[94]. Kim Y, Lee S, Kim S Preparation of fluorous solvent-dispersed Fe_3O_4 nanocrystals: role of oxygen in ligand exchange Langmuir, 32 (2016), pp. 3348–3353 [PubMed: 27018461]

[95]. Fujimori A, Ohmura K, Honda N, Kakizaki K Creation of high-density and low-defect single-layer film of magnetic nanoparticles by the method of interfacial molecular films Langmuir, 31 (2015), pp. 3254–3261 [PubMed: 25727135]

[96]. Li P, Chevallier P, Ramrup P, Biswas D, Vuckovich D, Fortin M-A, Oh JK Mussel-inspired multidentate block copolymer to stabilize ultrasmall superparamagnetic Fe_3O_4 for magnetic resonance imaging contrast enhancement and excellent colloidal stability Chem. Mater, 27 (2015), pp. 7100–7109

[97]. Song G-D, Kim M-H, Maeng W-Y Optimization of polymeric dispersant concentration for the dispersion-stability of magnetite nanoparticles in water solution J. Nanosci. Nanotechnol, 14 (2014), pp. 9525–9533 [PubMed: 25971094]

[98]. Hu JD, Zevi Y, Kou X-M, Xiao J, Wang X-J, Jin Y Effect of dissolved organic matter on the stability of magnetite nanoparticles under different pH and ionic strength conditions Sci. Total Environ, 408 (2010), pp. 3477–3489 [PubMed: 20421125]

[99]. Cuny L, Herrling MP, Guthausen G, Horn H, Delay M Magnetic resonance imaging reveals detailed spatial and temporal distribution of iron-based nanoparticles transported through water-saturated porous media J. Contam. Hydrol, 182 (2015), pp. 51–62 [PubMed: 26335945]

[100]. Hong Y, Honda RJ, Myung NV, Walker SL Transport of iron-based nanoparticles: role of magnetic properties Environ. Sci. Technol, 43 (2009), pp. 8834–8839 [PubMed: 19943654]

[101]. Legg BA, Zhu M, Comolli LR, Gilbert B, Banfield JF Impacts of ionic strength on three-dimensional nanoparticle aggregate structure and consequences for environmental transport and deposition Environ. Sci. Technol, 48 (2014), pp. 13703–13710 [PubMed: 25380400]

[102]. Swindle AL, Madden ASE, Cozzarelli IM, Benamara M Size-dependent reactivity of magnetite nanoparticles: a field-laboratory comparison Environ. Sci. Technol, 48 (2014), pp. 11413–11420 [PubMed: 25203482]

[103]. Bakhteeva I, Medvedeva I, Byzov I, Zhakov S, Yermakov A, Uimin M, Shchegoleva N Magnetic field-enhanced sedimentation of nanopowder magnetite in water flow Environ. Technol, 36 (2015), pp. 1828–1836 [PubMed: 25650300]

[104]. Wang M, Chou I-M, Lu W, De B Vivo Effects of CH_4 and CO_2 on the sulfidization of goethite and magnetite: an in situ Raman spectroscopic study in high-pressure capillary optical cells at room temperature Eur. J. Mineral, 27 (2015), pp. 193–201

[105]. Byrne JM, Klueglein N, Pearce C, Rosso KM, Appel E, Kappler A Redox cycling of Fe(II) and Fe(III) in magnetite by Fe-metabolizing bacteria Science, 347 (2015), pp. 1473–1476 [PubMed: 25814583]

[106]. Zhu H, Han J, Xiao JQ, Jin Y Uptake, translocation, and accumulation of manufactured iron oxide nanoparticles by pumpkin plants J. Environ. Monit, 10 (2008), pp. 713–717 [PubMed: 18528537]

[107]. Wang H, Kou X, Pei Z, Xiao JQ, Shan X, Xing B Physiological effects of magnetite (Fe_3O_4) nanoparticles on perennial ryegrass (Lolium perenne L.) and pumpkin (Cucurbita mixta) plants Nanotoxicology, 5 (2011), pp. 30–42 [PubMed: 21417686]

[108]. Srivastava N Iron nanoparticles induced toxicity in Sesbania cannabina: A morphological aspect Adv. Sci. Focus, 2 (2014), pp. 135–139

[109]. Liu Y, Xia Q, Liu Y, Zhang S, Cheng F, Zhong Z, Wang L, Li H, Xiao K Genotoxicity assessment of magnetic iron oxide nanoparticles with different particle sizes and surface coatings Nanotechnology, 25 (2014), pp. 425101–425111 [PubMed: 25274166]

[110]. Mbeh DA, Javanbakht T, Tabet L, Merhi Y, Maghni K, Sacher E, L'Hocine Yahia Protein corona formation on magnetite nanoparticles: effects of culture medium composition, and its consequences on superparamagnetic nanoparticle cytotoxicity J. Biomed. Nanotechnol, 11 (2015), pp. 828–840 [PubMed: 26349395]

[111]. Mbeh DA, Mireles LK, Stanicki D, Tabet L, Maghni K, Laurent S, Sacher E, L'Hocine Yahia Human alveolar epithelial cell responses to core–shell superparamagnetic iron oxide nanoparticles (SPIONs) Langmuir, 13 (2015), pp. 3829–3839

[112]. Yun J-W, Yoon J-H, Kang B-C, Cho N-H, Seok SH, Min SK, Min JH, Che JH, Kim YK The toxicity and distribution of iron oxide–zinc oxide core–shell nanoparticles in C57BL/6 mice after repeated subcutaneous administration J. Appl. Toxicol, 35 (2015), pp. 593–602 [PubMed: 25572658]

[113]. Zhang Y, Zhu L, Zhou Y, Chen J Accumulation and elimination of iron oxide nanomaterials in zebrafish (Danio rerio) upon chronic aqueous exposure J. Environ. Sci, 30 (2015), pp. 223–230

[114]. Wang H, Shrestha TB, Basel MT, Pyle M, Toledo Y, Konecny A, Thapa P, Ikenberry M, Hohn KL, Chikan V, Troyer DL, Bossmann SH Hexagonal magnetite nanoprisms: preparation: characterization and cellular uptake J. Mater. Chem. B, 3 (2015), pp. 4647–4653 [PubMed: 32262479]

[115]. Guo X, Mao F, Wang W, Yang Y, Bai Z Sulfhydryl-modified Fe_3O_4@SiO_2 core/shell nanocomposite: synthesis and toxicity assessment in vitro ACS Appl. Mater. Interfaces, 7 (2015), pp. 14983–14991 [PubMed: 26083720]

[116]. Zhang L, Wang X, Miao Y, Chen Z, Qiang P, Cui L, Jing H, Guo Y Magnetic ferroferric oxide nanoparticles induce vascular endothelial cell dysfunction and inflammation by disturbing autophagy J. Hazard. Mater, 304 (2016), pp. 186–195 [PubMed: 26551222]

[117]. Shen Y, Huang Z, Liu X, Qian J, Xu J, Yang X, Sun A, Ge J Iron-induced myocardial injury: an alarming side effect of superparamagnetic iron oxide nanoparticles J. Cell Mol. Med, 19 (2015), pp. 2032–2035 [PubMed: 26041641]

[118]. Haddad PS, Britos TN, Li LM, Li LDS Preparation, characterization and tests of incorporation in stem cells of superparamagnetic iron oxide J. Phys. Conf. Ser, 617 (2015), pp. 12002–12010

[119]. Ruiz A, Gutiérrez L, Cáceres- Vélez PR, Santos D, Chaves SB, Fascineli ML, Garcia MP, Azevedo RB, Morales MP Biotransformation of magnetic nanoparticles as a function of coating in a rat model Nanoscale, 7 (2015), pp. 16321–16329 [PubMed: 26381991]

[120]. Yu S, Wan J, Chen K A facile synthesis of superparamagnetic Fe_3O_4 supraparticles@MIL-100(Fe) core–shell nanostructures: preparation, characterization and biocompatibility J. Colloid Interface Sci, 461 (2016), pp. 173–178 [PubMed: 26397925]

[121]. Urbanova V, Magro M, Gedanken A, Baratella D, Vianello F, Zboril R Nanocrystalline iron oxides composites, and related materials as a platform for electrochemical, magnetic, and chemical biosensors Chem. Mater, 26 (2014), pp. 6653–6673

[122]. Wang L, Zhang Y, Cheng C, Liu X, Jiang H, Wang X Highly sensitive electrochemical biosensor for evaluation of oxidative stress based on the nanointerface of graphene nanocomposites blended with gold Fe_3O_4, and platinum nanoparticles ACS Appl. Mater. Interfaces, 33 (2015), pp. 18441–18449

[123]. Zhang W, Li X, Zou R, Wu H, Shi H, Yu S, Liu Y Multifunctional glucose biosensors from Fe_3O_4 nanoparticles modified chitosan/graphene nanocomposites Sci. Rep, 5 (2015), p. 11129 [PubMed: 26052919]

[124]. Kim M.l., Cho D, Park HG Colorimetric quantification of glucose and cholesterol in human blood using a nanocomposite entrapping magnetic nanoparticles and oxidases J. Nanosci. Nanotechnol, 15 (2015), pp. 7955–7961 [PubMed: 26726446]

[125]. Demeritte T, Nellore BPV, Kanchanapally R, Sinha SS, Pramanik A, Chavva SR, Ray PC Hybrid graphene oxide based plasmonic-magnetic multifunctional nanoplatform for selective separation and label-free identification of alzheimer's disease biomarkers ACS App. Mater. Interfaces, 7 (2015), pp. 13693–13700

[126]. Nguyen P-D, Cong VT, Son SJ, Min J Fabrication of magnetic upconversion nanohybrid for luminescent resonance energy transfer-based detection of glutathione J. Nanosci. Nanotechnol, 15 (2015), pp. 7950–7954 [PubMed: 26726445]

[127]. Wang L, Kang T-F, Lu L-P, Zhang J-G, Xue R, Cheng S-Y Microcystin-(leucine-arginine) immunosensor based on iron(II, III) magnetic nanoparticles Anal. Lett, 47 (2014), pp. 2939–2949

[128]. Wu J, Yang Z, Chen N, Zhu W, Hong J, Huang C, Zhou X Vanillin-molecularly targeted extraction of stir bar based on magnetic field induced self-assembly of multifunctional Fe_3O_4@Polyaniline nanoparticles for detection of vanilla-flavor enhancers in infant milk powders J. Colloid Interface Sci, 442 (2015), pp. 22–29 [PubMed: 25514645]

[129]. Chen Y, Xianyu Y, Wang Y, Zhang X, Cha R, Sun J, Jiang X One-step detection of pathogens and viruses: combining magnetic relaxation switching and magnetic separation ACS Nano, 9 (2015), pp. 3184–3191 [PubMed: 25743636]

[130]. Hou Y, Zhou J, Gao Z, Sun X, Liu C, Shangguan D, Yang W, Gao M Protease-activated ratiometric fluorescent probe for pH mapping of malignant tumors ACS Nano, 9 (2015), pp. 3199–3205 [PubMed: 25670342]

[131]. Min Q, Li S, Chen X, Abdel-Halim ES, Jiang L-P, Zhu J-J Magnetite/ceria-codecorated titanoniobate nanosheet: a 2D catalytic nanoprobe for efficient enrichment and programmed dephosphorylation of phosphopeptides ACS Appl. Mater. Interfaces, 7 (2015), pp. 9563–9572 [PubMed: 25806593]

[132]. Zhong S, Zhou C, Zhang X, Zhou H, Li H, Zhu X, Wang Y A novel molecularly imprinted material based on magnetic halloysite nanotubes for rapid enrichment of 2,4-dichlorophenoxyacetic acid in water J. Hazard. Mater, 276 (2014), pp. 58–65 [PubMed: 24862469]

[133]. Song X-J, Qin Z-Q, Wang X-B, Yang F, Fang Q-L, She C-G β-Cyclodextrin modified with magnetic nanoparticles noncovalently for β-naphthol removal from wastewater Synth. React. Inorg. Met.-Org. Nano-Met. Chem, 46 (2016), pp. 143–146

[134]. Chiu Y-C, Chen P-A, Chang P-Y, Hsu C-Y, Tao C-W, Huang C-C, Chiang HK Enhanced Raman sensitivity and magnetic separation for urolithiasis detection using phosphonic acid-terminated Fe3O4 nanoclusters J. Mater. Chem. B, 3 (2015), pp. 4282–4290 [PubMed: 32262305]

[135]. Mezger A, Fock J, Antunes P, Østerberg FW, Boisen A, Nilsson M, Hansen MF, Ahlford A, Donolato M Scalable DNA-based magnetic nanoparticle agglutination assay for bacterial detection in patient samples ACS Nano, 9 (2015), pp. 7374–7382 [PubMed: 26166357]

[136]. Bu T, Zako T, Zeltner M, Sörgjerd KM, Schumacher CM, Hofer CJ, Stark WJ, Maeda M Adsorption and separation of amyloid beta aggregates using ferromagnetic nanoparticles coated with charged polymer brushes J. Mater. Chem. B, 3 (2015), pp. 3351–3357 [PubMed: 32262329]

[137]. Pourghazi K, Amoli-Diva M, Beiraghi A Speciation of ultra-trace amounts of inorganic arsenic in water and rice samples by electrothermal atomic absorption spectrometry after solid-phase extraction with modified Fe_3O_4 nanoparticles Int. J. Environ. Anal. Chem, 95 (2015), pp. 324–338

[138]. Zhang S, Li H, Wang Z, Liu J, Zhang H, Wang B, Yang Z A strongly coupled Au/Fe_3O_4/GO hybrid material with enhanced nanozyme activity for highly sensitive colorimetric detection, and rapid and efficient removal of Hg^{2+} in aqueous solutions Nanoscale, 7 (2015), pp. 8495–8502 [PubMed: 25896803]

[139]. Ju S, Yu J, Ma Y, Yang Y, Liu M Rapid determination of cadmium and lead in maca (Lepidium meyenii) by magnetic solid-phase extraction and flame atomic absorption spectrometry Anal. Lett, 48 (2015), pp. 2566–2580

[140]. Wang L, Hang X, Chen Y, Wang Y, Feng X Determination of cadmium by magnetic multiwalled carbon nanotube flow injection preconcentration and graphite furnace atomic absorption spectrometry Anal. Lett, 49 (2016), pp. 818–830

[141]. Bayat M, Shemirani F, Hossein B, Mostafa D, Farahani M Ionic liquid-modified Fe_3O_4 nanoparticle combined with central composite design for rapid preconcentration and determination of palladium ions Desalin. Water Treat, 56 (2015), pp. 814–825

[142]. Naghizadeh M, Taher MA, Behzadi M, Moghaddam FH Simultaneous preconcentration of bismuth and lead ions on modified magnetic core–shell nanoparticles and their determination by ETAAS Chem. Eng. J, 281 (2015), pp. 444–452

[143]. Karimi M, Aboufazeli F, Lotfi Zadeh Zhad HR, Sadeghi O, Najafi E Use of dipyridile amine functionalized magnetic nanoparticles for preconcentration and determination of lead ions in food samples J. AOAC Int, 97 (2014), pp. 1446–1451 [PubMed: 25902998]

[144]. Mwilu SK, Siska E, Nasir Baig RB, Varma RS, Heithmar E, Rogers KR Separation and measurement of silver nanoparticles and silver ions using magnetic particles Sci. Total Environ, 472 (2014), pp. 316–323 [PubMed: 24295749]

[145]. He Y, Li M, Jiang W, Yang W, Lin L, Xu L, Fu F Phosphatidylserine-functionalized Fe_3O_4@SiO_2 nanoparticles combined with enzyme-encapsulated liposomes for the visual detection of Cu^{2+} J. Mater. Chem. B, 4 (2016), pp. 752–759 [PubMed: 32262956]

[146]. Qu J, Dong Y, Wang Y, Lou T, Du X, Qu J Novel nanofilm sensor based on poly-(alizarin red)/Fe_3O_4 magnetic nanoparticles-multiwalled carbon nanotubes composite material for determination of nitrite J. Nanosci. Nanotechnol, 16 (2016), pp. 2731–2736 [PubMed: 27455699]

[147]. Bharath G, Madhu R, Chen S-M, Veeramani V, Mangalaraj D, Ponpandian N Solvent-free mechanochemical synthesis of graphene oxide and Fe_3O_4-reduced graphene oxide nanocomposites for sensitive detection of nitrite J. Mater. Chem. A, 3 (2015), pp. 15529–15539

[148]. Zhi L, Wang Z, Liu J, Liu W, Zhang H, Chen F, Wang B White emission magnetic nanoparticles as chemosensors for sensitive colorimetric and ratiometric detection, and degradation of ClO^- and SCN^- in aqueous solutions based on a logic gate approach Nanoscale, 7 (2015), pp. 11712–11719 [PubMed: 26102484]

[149]. Mohapatra S, Sahu S, Nayak S, Ghosh SK Design of Fe_3O_4@SiO_2@carbon quantum dot based nanostructure for fluorescence sensing, magnetic separation, and live cell imaging of fluoride ion Langmuir, 31 (2015), pp. 8111–8120 [PubMed: 26114840]

[150]. Zhang G, Lu S, Qian J, Zhong K, Yao J, Cai D, Cheng Z, Wu Z Magnetic relaxation switch detecting boric acid or borate ester through one-pot synthesized poly(vinyl alcohol) functionalized nanomagnetic iron oxide ACS Appl. Mater. Interfaces, 7 (2015), pp. 16837–16841 [PubMed: 26171794]

[151]. Ye M, Wei Z, Hu F, Wang J, Ge G, Hu Z, Shao M, Lee S-T, Liu J Fast assembling microarrays of superparamagnetic Fe_3O_4@Au nanoparticle clusters as reproducible substrates for surface-enhanced Raman scattering Nanoscale, 7 (2015), pp. 13427–13437 [PubMed: 26079311]

[152]. Wang C, Xu J, Wang J, Rong Z, Li P, Xiao R, Wang S Polyethylenimine-interlayered silver-shell magnetic-core microspheres as multifunctional SERS substrates J. Mater. Chem. C, 3 (2015), pp. 8684–8693

[153]. Zhu S, Fan C, Wang J, He J, Liang E, Chao M Realization of high sensitive SERS substrates with one-pot fabrication of Ag–Fe_3O_4 nanocomposites J. Colloid Interface Sci, 438 (2015), pp. 116–121 [PubMed: 25454433]

[154]. Du J, Cui J, Jing C Rapid in situ identification of arsenic species using a portable Fe_3O_4@Ag SERS sensor Chem. Commun, 50 (2014), pp. 347–349

[155]. Yang Q, Lan F, Liu Z, Ma S, Li W, Wu Y, Gu Z Uniform superparamagnetic Fe_3O_4/CMCS composite nanospheres for lysozyme adsorption J. Nanosci. Nanotechnol, 16 (2016), pp. 2233–2238 [PubMed: 27455623]

[156]. Ni Q, Chen B, Dong S, Tian L, Bai Q Preparation of core–shell structure Fe_3O_4@SiO_2 superparamagnetic microspheres immoblized with iminodiacetic acid as immobilized metal ion affinity adsorbents for His-tag protein purification Biomed. Chromatogr, 30 (2016), pp. 566–573 [PubMed: 26268650]

[157]. Gan Q, Zhu J, Yuan Y, Liu C pH-responsive Fe_3O_4 nanopartilces-capped mesoporous silica supports for protein delivery J. Nanosci. Nanotechnol, 16 (2016), pp. 1533–4880

[158]. Xu Y, Wang S, Han H, Chen K, Qin L, Xu J, Wang J, Li L, Guo X Enhancement of enzymatic activity by magnetic spherical polyelectrolyte brushes: a potential recycling strategy for enzymes Langmuir, 30 (2014), pp. 11156–11164 [PubMed: 25181307]

[159]. Cheng G, Zheng S-Y Construction of a high-performance magnetic enzyme nanosystem for rapid tryptic digestion Sci. Rep, 4 (2014), p. 6947 [PubMed: 25374397]

[160]. Long J, Li X, Wu Z, Xu E, Xu X, Jin Z, Jiao A Immobilization of pullulanase onto activated magnetic chitosan/Fe_3O_4 nanoparticles prepared by in situ mineralization and effect of surface functional groups on the stability Colloids Surf. A: Physicochem. Eng. Aspects, 472 (2015), pp. 69–77

[161]. Tao Q-L, Li Y, Shi Y, Liu R-J, Zhang Y-W, Guo J Application of molecular imprinted magnetic Fe_3O_4@SiO_2 nanoparticles for selective immobilization of cellulose J. Nanosci. Nanotechnol, 16 (2016), pp. 6055–6060 [PubMed: 27427671]

[162]. Hudson R, Feng Y, Varma RS, Moores A Bare magnetic nanoparticles: sustainable synthesis and applications in catalytic organic transformations Green Chem., 16 (2014), pp. 4493–4505

[163]. Thangaraj B, Muniyandi B, Ranganathan S, Xin H Functionalized magnetic nanoparticles for catalytic application—a review Rev. Adv. Sci. Eng, 4 (2015), pp. 106–119

[164]. Wu W, Jiang C, Vellaisamy ALR Recent progress in magnetic iron oxide–semiconductor composite nanomaterials as promising photocatalysts Nanoscale, 7 (2015), pp. 38–58 [PubMed: 25406760]

[165]. Karimi B, Mansouri F, Mirzaei HM Recent applications of magnetically recoverable nanocatalysts in CC and CX coupling reactions ChemCatChem, 7 (2015), pp. 1736–1789

[166]. Hildebrand H, Mackenzie K, Kopinke FD Pd/Fe_3O_4 nano-catalysts for selective dehalogenation in wastewater treatment processes-influence of water constituents Appl. Catal. B: Environ, 91 (2009), pp. 389–396

[167]. Mi F, Chen X, Ma Y, Yin S, Yuan F, Zhang H Facile synthesis of hierarchical core–shell Fe_3O_4@MgAl–LDH@Au as magnetically recyclable catalysts for catalytic oxidation of alcohols Chem. Commun, 47 (2011), pp. 12804–12806

[168]. Shah MT, Balouch A, Rajar K, Sirajuddin IAB, Umar AA Selective heterogeneous catalytic hydrogenation of ketone (C=O) to alcohol (OH) by magnetite nanoparticles following Langmuir–Hinshelwood kinetic approach ACS Appl. Mater. Interfaces, 7 (2015), pp. 6480–6489 [PubMed: 25785883]

[169]. Shelke SN, Bankar SR, Mhaske GR, Kadam SS, Murade DK, Bhorkade SB, Rathi AK, Bundaleski N, Teodoro OMND, Zboril R, Varma RS, Gawande MB Iron oxide-supported copper oxide nanoparticles (Nanocat-Fe-CuO): magnetically recyclable catalysts for the synthesis of pyrazole derivatives, 4-methoxyaniline, and Ullmann-type condensation reactions ACS Sustain. Chem. Eng, 2 (2014), pp. 1699–1706

[170]. Wang H, Wei Z, Matsui H, Zhou S Fe_3O_4/carbon quantum dots hybrid nanoflowers for highly active and recyclable visible-light driven photocatalyst J. Mater. Chem. A, 2 (2014), pp. 15740–15745

[171]. Modisha P, Antunes E, Nyokong T Photophysical properties of zinc tetracarboxy phthalocyanines conjugated to magnetic nanoparticles J. Nanosci. Nanotechnol, 15 (2015), pp. 3688–3696 [PubMed: 26504993]

[172]. Moghaddam MM, Pieber B, Glasnov T, Kappe CO Immobilized iron oxide nanoparticles as stable and reusable catalysts for hydrazine-mediated nitro reductions in continuous flow ChemSusChem, 7 (2014), pp. 3122–3131 [PubMed: 25209099]

[173]. Easterday R, Leonard C, Sanchez-Felix O, Losovyj Y, Pink M, Stein BD, Morgan DG, Lyubimova NA, Nikoshvili L.Zh., Sulman EM, Mahmoud WE, Al- Ghamdi AA, Bronstein LM Fabrication of magnetically recoverable catalysts based on mixtures of Pd and iron oxide nanoparticles for hydrogenation of alkyne alcohols ACS Appl. Mater. Interfaces, 6 (2014), pp. 21652–21660 [PubMed: 25383749]

[174]. Zhang W, Liu B, Zhang B, Bian G, Qi Y, Yang X, Li C Synthesis of monodisperse magnetic sandwiched gold nanoparticle as an easily recyclable catalyst with a protective polymer shell Colloids Surf. A: Physicochem. Eng. Aspects, 466 (2015), pp. 210–218

[175]. Yang S, Cao C, Sun Y, Huang P, Wei F, Song W Nanoscale magnetic stirring bars for heterogeneous catalysis in microscopic systems Angew. Chem, 127 (2015), pp. 2699–2702

[176]. Hajipour A, Azizi G Fabrication of covalently functionalized mesoporous silica core–shell magnetite nanoparticles with palladium(II) acetylacetonate: application as a magnetically separable nanocatalyst for Suzuki cross-coupling reaction of acyl halides with boronic acids Appl. Organometal. Chem, 29 (2015), pp. 247–253

[177]. Khakiani BA, Pourshamsian K, Veisi H A highly stable and efficient magnetically recoverable and reusable Pd nanocatalyst in aqueous media heterogeneously catalysed Suzuki C–C cross-coupling reactions Appl. Organometal. Chem, 29 (2015), pp. 259–265

[178]. Elazab HA, Siamaki AR, Moussa S, Gupton BF, El- Shall MS Highly efficient and magnetically recyclable graphene-supported Pd/Fe_3O_4 nanoparticle catalysts for Suzuki and Heck cross-coupling reactions Appl. Catal. A: Gen, 491 (2015), pp. 58–69

[179]. Yao T, Zuo Q, Wang H, Wu J, Xin B, Cui F, Cui T A simple way to prepare Pd/Fe_3O_4/polypyrrole hollow capsules and their applications in catalysis J. Colloid Interface Sci, 450 (2015), pp. 366–373 [PubMed: 25845884]

[180]. Maleki B, Chalaki SBN, Ashrafi SS, Seresht ER, Moeinpour F, Khojastehnezhad A, Tayebee R Caesium carbonate supported on hydroxyapatite-encapsulated $Ni_{0.5}Zn_{0.5}Fe_2O_4$ nanocrystallites as a novel magnetically basic catalyst for the one-pot synthesis of pyrazolo[1,2-b]phthalazine-5,10-diones Appl. Organometal. Chem, 29 (2015), pp. 290–295

[181]. Bai J, Zhao R, Diao G Fabrication of a novel Fe_3O_4/BiOCl nanocomposite as magnetic visible light photocatalytic materials Curr. Nanosci, 11 (2015), pp. 186–190

[182]. Mousavi M, Habibi-Yangjeh A Magnetically separable ternary g-C_3N_4/Fe_3O_4/BiOI nanocomposites: novel visible-light-driven photocatalysts based on graphitic carbon nitride J. Colloid Interface Sci, 465 (2016), pp. 83–92 [PubMed: 26669494]

[183]. Ghorbani-Choghamarani A, Darvishnejad Z, Norouzi M Cu(II)–Schiff base complex-functionalized magnetic Fe_3O_4 nanoparticles: a heterogeneous catalyst for various oxidation reactions Appl. Organometallic Chem, 29 (2015), pp. 170–175

[184]. Liu Y, Liu Z, Cui Y An efficient nanoparticle-supported and magnetically recoverable copper(I) catalyst for synthesis of furans from ene-yne-ketone Chin. J. Chem, 33 (2015), pp. 175–180

[185]. Wang L, Ma Y, Qing S, Gao Z, Eli W, Wang T Magnetically separable Fe_3O_4 supported Co–Rh bimetallic catalysts for dicyclopentadiene hydroformylation to value-added fine chemicals Energy Environ. Focus, 4 (2015), pp. 334–339

[186]. Fan G-Y, Huang W-J Solvent-free hydrogenation of nitrobenzene catalyzed by magnetically recoverable Pt deposited on multiwalled carbon nanotubes Synth. React. Inorg. Met.-Org. Nano-Met. Chem, 45 (2015), pp. 1819–1825

[187]. Baird N, Losovyj Y, Yuzik-Klimova EY, Kuchkina NV, Shifrina ZB, Pink M, Stein BD, Morgan DG, Wang T, Rubin MA, Sidorov AI, Sulman EM, Bronstein LM Zinc-containing magnetic

oxides stabilized by a polymer: one phase or two? ACS Appl. Mater. Interfaces, 8 (2016), pp. 891–899 [PubMed: 26673012]

[188]. Cao M, Wang P, Ao Y, Wang C, Hou J, Qian J Visible light activated photocatalytic degradation of tetracycline by a magnetically separable composite photocatalyst: graphene oxide/magnetite/cerium-doped titania J. Colloid Interface Sci, 467 (2016), pp. 129–139 [PubMed: 26799623]

[189]. Herrera A, Reyes A, Colina-Márquez J Evaluation of the photocatalytic activity of iron oxide nanoparticles functionalized with titanium dioxide J. Phys.: Conf. Ser, 687 (2016), pp. 12034–12037

[190]. Tan C, Gao N, Deng Y, Deng J, Zhou S, Li J, Xin X Radical induced degradation of acetaminophen with Fe_3O_4 magnetic nanoparticles as heterogeneous activator of peroxymonosulfate J. Hazard. Mater, 15 (2014), pp. 452–460

[191]. Ruan X, Gu X, Lu S, Qiu Z, Sui Q Trichloroethylene degradation by persulphate with magnetite as a heterogeneous activator in aqueous solution Environ. Technol, 36 (2015), pp. 1389–1397 [PubMed: 25496173]

[192]. Jiang S, Zhu J, Ding Y, Bai S, Guan Y, Wang J Degradation effect and mechanism of dinitrotoluene wastewater by magnetic nano-Fe_3O_4/H_2O_2 Fenton-like Ozone: Sci. Eng, 38 (2016), pp. 225–232

[193]. Lei Y, Chen C-S, Tu Y-J, Huang Y-H, Zhang H Heterogeneous degradation of organic pollutants by persulfate activated by CuO-Fe_3O_4: mechanism, stability, and effects of pH and bicarbonate ions Environ. Sci. Technol, 49 (2015), pp. 6838–6845 [PubMed: 25955238]

[194]. Feng M, Qu R, Zhang X, Sun P, Sui Y, Wang L, Wang Z Degradation of flumequine in aqueous solution by persulfate activated with common methods and polyhydroquinone-coated magnetite/multi-walled carbon nanotubes catalysts Water Res., 85 (2015), pp. 1–10 [PubMed: 26281959]

[195]. Wang Y, Sun H, Ang HM, Tade MO, Wang S Synthesis of magnetic core/shell carbon nanosphere supported manganese catalysts for oxidation of organics in water by peroxymonosulfate J. Colloid. Interface Sci, 433 (2014), pp. 68–75 [PubMed: 25112914]

[196]. Shan G, Fu Y, Chu X, Chang C, Zhu L Highly active magnetic bismuth tungstate/magnetite composite under visible light irradiation in the presence of hydrogen peroxide J. Colloid Interface Sci, 444 (2015), pp. 123–131 [PubMed: 25594803]

[197]. Zhong Y, Liang X, He Z, Tan W, He H, Zhu R, Zhong Y, Zhu J, Yuan P, Jiang Z The UV/Fenton degradation of tetrabromobisphenol a catalyzed by nanocrystalline chromium substituted magnetite J. Nanosci. Nanotechnol, 14 (2014), pp. 7307–7314 [PubMed: 25924407]

[198]. Ardo SG, Nélieu S, Ona-Nguema G, Delarue G, Brest J, Pironin E, Morin G Oxidative degradation of nalidixic acid by nano-magnetite via Fe^{2+}/O_2-mediated reactions Environ. Sci. Technol, 49 (2015), pp. 4506–4514 [PubMed: 25756496]

[199]. Hammouda SB, Adhoum N, Monser L Synthesis of magnetic alginate beads based on Fe_3O_4 nanoparticles for the removal of 3-methylindole from aqueous solution using Fenton process J. Hazard. Mater, 294 (2015), pp. 128–136 [PubMed: 25867585]

[200]. Huang S, Xu Y, Xie M, Xu H, He M, Xia J, Huang L, Li H Synthesis of magnetic $CoFe_2O_4$/g-C_3N_4 composite and its enhancement of photocatalytic ability under visible-light Colloids Surf. A: Physicochem. Eng. Aspects, 478 (2015), pp. 71–80

[201]. Yao Y, Lu F, Zhu Y, Wei F, Liu X, Lian C, Wang S Magnetic core–shell $CuFe_2O_4@C_3N_4$ hybrids for visible light photocatalysis of Orange II J. Hazard. Mater, 297 (2015), pp. 224–233 [PubMed: 25974659]

[202]. Huang R, Fang Z, Fang X, Tsang EP Ultrasonic Fenton-like catalytic degradation of bisphenol A by ferroferric oxide (Fe_3O_4) nanoparticles prepared from steel pickling waste liquor J. Colloid Interface Sci, 436 (2014), pp. 258–266 [PubMed: 25280370]

[203]. Xu Y, Ai J, Zhang H The mechanism of degradation of bisphenol A using the magnetically separable $CuFe_2O_4$/peroxymonosulfate heterogeneous oxidation process J. Hazard. Mater, 309 (2016), pp. 87–96 [PubMed: 26875144]

[204]. Hosseini-Monfared H, Parchegani F, Alavi S Carboxylic acid effects on the size and catalytic activity of magnetite nanoparticles J. Colloid Interface Sci, 437 (2015), pp. 205–210 [PubMed: 25313485]

[205]. Wang Z-Z, Zhai S-R, Zhai B, An Q-D One-step green synthesis of multifunctional Fe_3O_4/Cu nanocomposites toward efficient reduction of organic dyes Eur. J. Inorg. Chem, 10 (2015), pp. 1692–1699

[206]. Hou Y, Ma J, Wang T, Fu Q Phosphotungstic acid supported on magnetic core–shell nanoparticles with high photocatalytic activity Mater. Sci. Semicond. Process, 39 (2015), pp. 229–234

[207]. Zhang P, Mo Z-L, Zhang C, Han L-J, Zheng L Preparation and photocatalytic properties of magnetic responsive TiO_2/graphene nanocomposites J. Mater. Eng, 43 (2015), pp. 72–77

[208]. Nasrollahzadeh M, Bagherzadeh M, Karimi H Preparation, characterization and catalytic activity of $CoFe_2O_4$ nanoparticles as a magnetically recoverable catalyst for selective oxidation of benzyl alcohol to benzaldehyde and reduction of organic dyes J. Colloid Interface Sci, 465 (2016), pp. 271–278 [PubMed: 26674244]

[209]. Du Y, Ma W, Liu P, Zou B, Ma J Magnetic $CoFe_2O_4$ nanoparticles supported on titanate nanotubes ($CoFe_2O_4$/TNTs) as a novel heterogeneous catalyst for peroxymonosulfate activation and degradation of organic pollutants J. Hazard. Mater, 308 (2016), pp. 58–66 [PubMed: 26808243]

[210]. Tóth IY, Szekeres M, Turcu R, Sáringer S, Illés E, Nesztor D, Tombácz E Mechanism of in situ surface polymerization of gallic acid in an environmental-inspired preparation of carboxylated core–shell magnetite nanoparticles Langmuir, 30 (2014), pp. 15451–15461 [PubMed: 25517214]

[211]. Ye CZ, Ariya PA Co-adsorption of gaseous benzene, toluene, ethylbenzene, m-xylene (BTEX) and SO_2 on recyclable Fe_3O_4 nanoparticles at 0–101% relative humidities J. Environ. Sci, 31 (2015), pp. 164–174

[212]. Li G, Li L, Wu B, Li J, Yuan Y, Shi J Controlled one-step synthesis of Pt decorated octahedral Fe_3O_4 and its excellent catalytic performance for CO oxidation Nanoscale, 7 (2015), pp. 17855–17860 [PubMed: 26459966]

[213]. Elazab HA, Moussa S, Gupton BF, El-Shall MS Microwave-assisted synthesis of Pd nanoparticles supported on Fe_3O_4 Co_3O_4, and $Ni(OH)_2$ nanoplates and catalysis application for CO oxidation J. Nanopart. Res, 16 (2014), p. 2477

[214]. Lopez A, Larrea A, Sebastian V, Calatayud MP, Irusta S, Santamaria J Ultrasmall platinum nanoparticles on Fe_3O_4: a low-temperature catalyst for the preferential oxidation reaction ChemCatChem, 8 (2016), pp. 1479–1484

[215]. Arcibar-Orozco JA, Wallace R, Mitchell JK, Bandosz TJ Role of surface chemistry and morphology in the reactive adsorption of H_2S on iron (hydr)oxide/graphite oxide composites Langmuir, 31 (2015), pp. 2730–2742 [PubMed: 25675243]

[216]. Shi D, Li Y, Ji S Synthesis of magnetically recyclable TiO_2@SiO_2@Fe_3O_4 photocatalysts and their performance of photochemical reduction of CO_2 Energy Environ. Focus, 4 (2015), pp. 87–94

[217]. Sharma VK, McDonald TJ, Kim H, Garg VK Magnetic graphene-carbon nanotube iron nanocomposites as adsorbents and antibacterial agents for water purification Adv. Colloid Interface Sci, 225 (2015), pp. 229–240 [PubMed: 26498500]

[218]. Dong H, Huang J, Koepsel RR, Ye P, Russell AJ, Matyjaszewski K Recyclable antibacterial magnetic nanoparticles grafted with quaternized poly (2-dimethylamino) ethyl methacrylate brushes Biomacromolecules, 12 (2011), pp. 1305–1311 [PubMed: 21384911]

[219]. Deng C-H, Gong J-L, Zeng G-M, Niu C-G, Niu Q-Y, Zhang W, Liu H-Y Inactivation performance and mechanism of Escherichia coli in aqueous system exposed to iron oxide loaded graphene nanocomposites J. Hazard. Mater, 276 (2014), pp. 66–76 [PubMed: 24862470]

[220]. Pina AS, Batalha ÍL, Fernandes CSM, Aoki MA, Roque ACA Exploring the potential of magnetic antimicrobial agents for water disinfection Water Res., 66 (2014), pp. 160–168 [PubMed: 25201339]

[221]. Zablotskaya A, Segal I, Popelis Y, Mishnev A, Maiorov M, Zablotsky D, Blums E, Nikolajeva V, Eze D Iron oxide superparamagnetic nanocarriers bearing amphiphilic N-heterocyclic choline analogues as potential antimicrobial agents Appl. Organometal. Chem, 29 (2015), pp. 376–383

[222]. Zhang X, Wang W, Zhang Y, Yan J, Jia C, Chang L facile and green synthesis of silver nanoparticles immobilized magnetite@polydopamine nanocomposite with enhanced antibacterial activity Energy Environ. Focus, 3 (2014), pp. 309–315

[223]. Xu J-W, Gao Z-D, Han K, Liu Y, Song Y-Y Synthesis of magnetically separable Ag_3PO_4/TiO_2/Fe_3O_4 heterostructure with enhanced photocatalytic performance under visible light for photoinactivation of bacteria ACS Appl. Mater. Interfaces, 6 (2014), pp. 15122–15131 [PubMed: 25140916]

[224]. Yu Q, Fu A, Li H, Liu H, Lv R, Liu J, Guo P, Zhao XS Synthesis and characterization of magnetically separable Ag nanoparticles decorated mesoporous Fe_3O_4@carbon with antibacterial and catalytic properties Colloids Surf. A: Physicochem. Eng. Aspects, 457 (2014), pp. 288–296

[225]. Zhang HZ, Zhang C, Zeng GM, Gong JL, Ou XM, Huan SY Easily separated silver nanoparticle-decorated magnetic graphene oxide: synthesis and high antibacterial activity J. Colloid Interface Sci, 471 (2016), pp. 94–102 [PubMed: 26994349]

[226]. Ma S, Zhan S, Jia Y, Zhou Q Highly efficient antibacterial and Pb(II) removal effects of Ag-$CoFe_2O_4$-GO nanocomposite ACS Appl. Mater. Interfaces, 7 (2015), pp. 10576–10586 [PubMed: 25905556]

[227]. Giannousi K, Menelaou M, Arvanitidis J, Angelakeris M, Pantazaki A, Dendrinou-Samara C Hetero-nanocomposites of magnetic and antifungal nanoparticles as a platform for magnetomechanical stress induction in Saccharomyces cerevisiae J. Mater. Chem. B, 3 (2015), pp. 5341–5351 [PubMed: 32262610]

[228]. Giri MN, Agarwala V Synthesis and characterization of novel magnetic chitosan bead and their antibacterial applications J. Bionanosci, 9 (2015), pp. 276–280

[229]. Sun P, Hui C, Wang S, Khan RA, Zhang Q, Zhao Y-H Enhancement of algicidal properties of immobilized Bacillus methylotrophicus ZJU by coating with magnetic Fe_3O_4 nanoparticles and wheat bran J. Hazard. Mater, 301 (2016), pp. 65–73 [PubMed: 26342577]

[230]. Homayoonfal M, Mehrnia MR, Shariaty-Niassar M, Akbari A, Sarrafzadeh MH, Ismail AF Fabrication of magnetic nanocomposite membrane for separation of organic contaminant from water Desalin. Water Treat, 54 (2015), pp. 3603–3609

[231]. Hwang J-H, Han D-W Optimization and modeling of reduction of wastewater sludge water content and turbidity removal using magnetic iron oxide nanoparticles (MION) J. Environ. Sci. Health Part A, 50 (2015), pp. 1307–1315

[232]. Hernandez JST, Muriel AA, Tabares JA, Alcázar GAP, Bolaños A Preparation of Fe_3O_4 nanoparticles and removal of methylene blue through adsorption J. Phys.: Conf. Ser, 614 (2015), pp. 12007–12010

[233]. Mahmoodi NM, Bagherpour F, Nariyan E Amine functionalized magnetic carbon nanotube: synthesis and binary system dye removal Desalin. Water Treat, 56 (2015), pp. 107–120

[234]. Chen RP, Zhang YL, Wang XY, Zhu CY, Ma AJ, Jiang WM Removal of methylene blue from aqueous solution using humic-acid coated magnetic nanoparticles Desalin. Water Treat, 55 (2015), pp. 539–548

[235]. Tan X, Lu L, Wang L, Zhang J Facile synthesis of bimodal mesoporous Fe_3O_4@SiO_2 composite for efficient removal of methylene blue Eur. J. Inorg. Chem, 18 (2015), pp. 2928–2933

[236]. Kim DW, Bach LG, Hong S-S, Park CL, Kwon T A facile route towards the synthesis of Fe_3O_4/graphene oxide nanocomposites for environmental applications Mol. Cryst. Liquid Cryst, 599 (2014), pp. 43–50

[237]. Zhang X, Zeng T, Wang S, Niu H, Wang X, Cai Y One-pot synthesis of C18-functionalized core–shell magnetic mesoporous silica composite as efficient sorbent for organic dye J. Colloid Interface Sci, 448 (2015), pp. 189–196 [PubMed: 25734221]

[238]. Dolatkhah A, Wilson LD Magnetite/polymer brush nanocomposites with switchable uptake behavior toward methylene blue ACS Appl. Mater. Interfaces, 8 (2016), pp. 5595–5607 [PubMed: 26751742]

[239]. Akın D, Yakar A, Gündüz U Synthesis of magnetic Fe_3O_4-chitosan nanoparticles by ionic gelation and their dye removal ability Water Environ. Res, 87 (2015), pp. 425–436 [PubMed: 26460462]

[240]. Rajabi HR, Arjmand H, Hoseini SJ, Nasrabadi H Surface modified magnetic nanoparticles as efficient and green sorbents: synthesis, characterization, and application for the removal of anionic dye J. Mag. Mag. Mater, 394 (2015), pp. 7–13

[241]. Li L, Yuan LJ, Hong W, Fan L, Mao LB, Liu L Hybrid Fe_3O_4/MOFs for the adsorption of methylene blue and methyl violet from aqueous solution Desalin. Water Treat, 55 (2015), pp. 1973–1980

[242]. Dong L, Zhipeng Z, Yigang D A Simple method to prepare magnetic modified corncobs and its application for Congo red adsorption J. Dispers. Sci. Technol, 37 (2016), pp. 73–79

[243]. Zhao Y, Chen H, Li J, Chen C Hierarchical MWCNTs/Fe_3O_4/PANI magnetic composite as adsorbent for methyl orange removal J. Colloid Interface Sci, 450 (2015), pp. 189–195 [PubMed: 25819003]

[244]. Lin KY, Yang H Magnetically controllable Pickering emulsion prepared by a reduced graphene oxide-iron oxide composite J. Colloid Interface Sci, 438 (2015), pp. 296–305 [PubMed: 25454454]

[245]. Zhao J, Luque R, Qi W, Lai J, Gao W, Gilani MRHS, Xu G Facile surfactant-free synthesis and characterization of Fe_3O_4@3-aminophenol–formaldehyde core–shell magnetic microspheres J. Mater. Chem. A, 3 (2015), pp. 519–524

[246]. Xiang Y, Wang H, He Y, Song G Efficient degradation of methylene blue by magnetically separable Fe_3O_4/chitosan/TiO_2 nanocomposites Desalin. Water Treat, 55 (2015), pp. 1018–1025

[247]. Tian H, Chen J, He J, Liu F Pd-loaded magnetic mesoporous nanocomposites: a magnetically recoverable catalyst with effective enrichment and high activity for DDT and DDE removal under mild conditions J. Colloid Interface Sci, 457 (2015), pp. 195–202 [PubMed: 26188725]

[248]. Zhao Z-Y, Xiong Z-H Removal of four nitrofurans drugs from aqueous solution by magnetic multi-wall carbon nanotubes Fullerenes Nanotubes Carbon Nanostruct, 23 (201) (2016), pp. 640–648

[249]. Tang S, Chia GH, Lee HK Magnetic core–shell iron(II,III) oxide@layered double oxide microspheres for removal of 2,5-dihydroxybenzoic acid from aqueous solutions J. Colloid. Interface Sci, 437 (2015), pp. 316–323 [PubMed: 25441367]

[250]. Li K, Zeng Z, Xiong J, Yan L, Guo H, Liu S, Dai Y, Chen T Fabrication of mesoporous Fe_3O_4@SiO_2@CTAB–SiO_2 magnetic, microspheres with a core/shell structure and their efficient adsorption performance for the removal of trace PFOS from water Colloids Surf. A: Physicochem. Eng. Aspects, 465 (2015), pp. 113–123

[251]. Liu Q, Zheng Y, Zhong L, Cheng X Removal of tetracycline from aqueous solution by a Fe_3O_4 incorporated PAN electrospun nanofiber mat J. Environ. Sci, 28 (2015), pp. 29–36

[252]. Liu Q, Zhong LB, Zhao QB, Frear C, Zheng YM Synthesis of Fe_3O_4/polyacrylonitrile composite electrospun nanofiber mat for effective adsorption of tetracycline ACS Appl. Mater. Interfaces, 27 (2015), pp. 14573–14583

[253]. Guo L, Liang Y, Chen X, Xu W, Wu K, Wei H, Xiong Y Effective removal of tetracycline from aqueous solution by organic acid-coated magnetic nanoparticles J. Nanosci. Nanotechnol, 16 (2016), pp. 2218–2226 [PubMed: 27455621]

[254]. Shi L, Ma F, Han Y, Zhang X, Yu H Removal of sulfonamide antibiotics by oriented immobilized laccase on Fe_3O_4 nanoparticles with natural mediators J. Hazard. Mater, 30 (2014), pp. 203–2011

[255]. Jiang M, Yang W, Zhang Z, Yang Z, Wang Y Adsorption of three pharmaceuticals on two magnetic ion-exchange resins J. Environ. Sci, 31 (2015), pp. 226–234

[256]. Yoon SU, Mahanty B, Kim CG Preparation of superparamagnetic iron oxide nanoparticles and evaluation of their adsorption capacity toward carbamazepine and diatrizoate Desalin. Water Treat, 57 (2016), pp. 7789–7800

[257]. Wang M, Liu P, Wang Y, Zhou D, Ma C, Zhang D, Zhan J Core–shell superparamagnetic Fe_3O_4@β-CD composites for host–guest adsorption of polychlorinated biphenyls (PCBs) J. Colloid Interface Sci, 47 (2015), pp. 1–7

[258]. Park H-S, Koduru JR, Choo K-H, Lee B Activated carbons impregnated with iron oxide nanoparticles for enhanced removal of bisphenol A and natural organic matter J. Hazard. Mater, 286 (2015), pp. 315–324 [PubMed: 25594935]

[259]. Wang J, Tian H, Ji Y Adsorption behavior and mechanism of humic acid on aminated magnetic nanoadsorbent Sep. Sci. Technol, 50 (2015), pp. 1285–1293

[260]. Sheng Y, Guan H, Zhang Y, Zhang X, Zhou Q, Lin Z Double-functionalised magnetic nanoparticles for efficient extraction of bisphenol A from river water Environ. Chem, 13 (2015), pp. 43–49

[261]. Obeid L, Kolli NE, Talbot D, Welschbillig M, Bée A Influence of a cationic surfactant on adsorption of p-nitrophenol by a magsorbent based on magnetic alginate beads J. Colloid Interface Sci, 457 (2015), pp. 218–224 [PubMed: 26188728]

[262]. Liu F, Wu Z, Wang D, Yu J, Jiang X, Chen X Magnetic porous silica–graphene oxide hybrid composite as a potential adsorbent for aqueous removal of *p*-nitrophenol Colloids Surf. A: Physicochem. Eng. Aspects, 490 (2016), pp. 207–214

[263]. Jin Z, Wang X, Sun Y, Ai Y, Wang X Adsorption of 4-*n*-nonylphenol and bisphenol-A on magnetic reduced graphene oxides: a combined experimental and theoretical studies Environ. Sci. Technol, 49 (2015), pp. 9168–9175 [PubMed: 26161689]

[264]. Shen H-Y, Chen Z-X, Li Z-H, Hu M-Q, Dong X-Y Controlled synthesis of 2,4,6-trichlorophenol-imprinted amino-functionalized nano-Fe_3O_4-polymer magnetic composite for highly selective adsorption Colloids Surf. A: Physicochem. Eng. Aspects, 481 (2015), pp. 439–450

[265]. Hao Y, Wang Z, Gou J, Wang Z Kinetics and thermodynamics of diquat removal from water using magnetic graphene oxide nanocomposite Can. J. Chem. Eng, 93 (2015), pp. 1713–1720

[266]. Shi P, Ma R, Zhou Q, Li A, Wu B, Miao Y, Chen X, Zhang X Chemical and bioanalytical assessments on drinking water treatments by quaternized magnetic microspheres J. Hazard. Mater, 285 (2015), pp. 53–60 [PubMed: 25481701]

[267]. Ge S, Agbakpe M, Zhang W, Kuang L Heteroaggregation between PEI-coated magnetic nanoparticles and algae: effect of particle size on algal harvesting efficiency ACS Appl. Mater. Interfaces, 7 (2015), pp. 6102–6108 [PubMed: 25738208]

[268]. Ge S, Agbakpe M, Zhang W, Kuang L, Wu Z, Wang X Recovering magnetic Fe_3O_4-ZnO nanocomposites from algal biomass based on hydrophobicity shift under UV irradiation ACS Appl. Mater. Interfaces, 7 (2015), pp. 11677–11682 [PubMed: 25965291]

[269]. Yang S, Chen L, Mu L, Ma P-C Magnetic graphene foam for efficient adsorption of oil and organic solvents J. Colloid Interface Sci, 430 (2014), pp. 337–344 [PubMed: 24974246]

[270]. Liu C, Yang J, Tang Y, Yin L, Tang H, Li C Versatile fabrication of the magnetic polymer-based graphene foam and applications for oil–water separation Colloid Surf. A, 468 (2015), pp. 10–16

[271]. Yu F, Ma J, Wang J, Zhang M, Zheng J Magnetic iron oxide nanoparticles functionalized multi-walled carbon nanotubes for toluene, ethylbenzene and xylene removal from aqueous solution Chemosphere, 146 (2016), pp. 162–172 [PubMed: 26714299]

[272]. Flores JA, Pavía-Sanders A, Chen Y, Pochan DJ, Wooley KL Recyclable hybrid inorganic/organic magnetically active networks for the sequestration of crude oil from aqueous environments Chem. Mater, 27 (2015), pp. 3775–3782

[273]. Saber O, Mohamed NH, Al Jaafari AA Synthesis of magnetic nanoparticles and nanosheets for oil spill removal Nanosci. Nanotechnol.—Asia, 5 (2015), pp. 32–43

[274]. Mirshahghassemi S, Lead JR Oil recovery from water under environmentally relevant conditions using magnetic nanoparticles Environ. Sci. Technol, 49 (2015), pp. 11729–11736 [PubMed: 26358198]

[275]. Zhang L, Li L, Dang Z-M Bio-inspired durable, superhydrophobic magnetic particles for oil/water separation J. Colloid Interface Sci, 463 (2016), pp. 266–271 [PubMed: 26550784]

[276]. Pan Y, Wang J, Sun C, Liu X, Zhang H Fabrication of highly hydrophobic organic–inorganic hybrid magnetic polysulfone microcapsules: a lab-scale feasibility study for removal of oil and organic dyes from environmental aqueous samples J. Hazard. Mater, 309 (2016), pp. 65–76 [PubMed: 26874312]

[277]. Liu J, Zhao Z, Jiang G Coating Fe_3O_4 magnetic nanoparticles with humic acid for high efficient removal of heavy metals in water Environ. Sci. Technol, 42 (2008), pp. 6949–6954 [PubMed: 18853814]

[278]. Su C, Puls RW Arsenate and arsenite sorption on magnetite: relations to groundwater arsenic remediation using zerovalent iron and natural attenuation Water Air Soil Pollut., 193 (2008), pp. 65–78

[279]. Yavuz CT, Mayo JT, Yu WW, Prakash A, Falkner JC, Yean S, Cong L, Shipley HJ, Kan A, Tomson M, Natelson D, Colvin VL Low-field magnetic separation of monodisperse Fe_3O_4 nanocrystals Science, 314 (2006), pp. 964–967 [PubMed: 17095696]

[280]. Yean S, Cong L, Yavuz CT, Mayo JT, Yu WW, Kan AT, Colvin VL, Tomson MB Effects of magnetite particle size on adsorption and desorption of arsenite and arsenate J. Mater. Res, 20 (2005), pp. 3255–3264

[281]. Chowdhury SR, Yanful EK Arsenic and chromium removal by mixed magnetite-maghemite nanoparticles and the effect of phosphate on removal J. Environ. Manage, 91 (2010), pp. 2238–2247 [PubMed: 20598797]

[282]. Jin Y, Liu F, Tong M, Hou Y Removal of arsenate by cetyltrimethylammonium bromide modified magnetic nanoparticles J. Hazard. Mater, 227–228 (2012), pp. 461–468

[283]. Wu X-L, Wang L, Chen C-L, Xu A-W, Wang X-K Water-dispersible magnetite-graphene-LDH composits for efficient arsenate removal J. Mater. Chem, 21 (2011), pp. 17353–17359

[284]. Yoon Y, Park WK, Hwang T-M, Yoon DH, Yang WS, Kang J-W Comparative evaluation of magnetite–graphene oxide and magnetite-reduced graphene oxide composite for As(III) and As(V) removal J. Hazard. Mater, 304 (2016), pp. 96–204

[285]. An B, Liang QQ, Zhao DY Removal of arsenic(V) from spent ion exchange brine using a new class of starch-bridged magnetite nanoparticles Water Res., 45 (2011), pp. 1961–1972 [PubMed: 21288549]

[286]. Liang QQ, Zhao DY, Qian TW, Freeland K, Feng YC Effects of stabilizers and water chemistry on arsenate sorption by polysaccharide-stabilized magnetite nanoparticles Ind. Eng. Chem. Res, 51 (2011), pp. 2407–2418

[287]. Shipley HJ, Yean S, Kan AT, Tomson MB Adsorption of arsenic to magnetite nanoparticles: effect of particle concentration pH, ionic strength, and temperature Environ. Toxicol. Chem, 28 (2009), pp. 509–515 [PubMed: 18939890]

[288]. Yantasee W, Warner CL, Sangvanich T, Addleman RS, Carter TG, Wiacek RJ, Fryxell GE, Timchalk C, Warner MG Removal of heavy metals from aqueous systems with thiol functionalized superparamagnetic nanoparticles Environ. Sci. Technol, 41 (2007), pp. 5114–5119 [PubMed: 17711232]

[289]. Kango S, Kumar R Magnetite nanoparticles coated sand for arsenic removal from drinking water Environ. Earth Sci, 75 (2016), pp. 381–392

[290]. Liu CH, Chuang YH, Chen TY, Tian Y, Li H, Wang MK, Zhang W Mechanism of arsenic adsorption on magnetite nanoparticles from water: thermodynamic and spectroscopic studies Environ. Sci. Technol, 49 (2015), pp. 7726–7734 [PubMed: 26055623]

[291]. Farrell JW, Fortner J, Work S, Avendano C, Gonzalez-Pech NI, Araiza RZ, Li Q, Alvarez PJJ, Colvin V, Kan A, Tomson M Arsenic removal by nanoscale magnetite in Guanajuato Mexico Environ. Eng. Sci, 31 (2014), pp. 393–402

[292]. Beduk F Superparamagnetic nanomaterial Fe_3O_4–TiO_2 for the removal of As(V) and As(III) from aqueous solutions Environ. Technol, 37 (2016), pp. 1790–1801 [PubMed: 26831455]

[293]. Podder MS, Majumder CB Studies on the removal of As(III) and As(V) through their adsorption onto granular activated carbon/$MnFe_2O_4$ composite: isotherm studies and error analysis Compos. Interfaces, 23 (2016), pp. 327–372

[294]. Chen R, Zhi C, Yang H, Bando Y, Zhang Z, Sugiur N, Golberg D Arsenic (V) adsorption on Fe_3O_4 nanoparticle-coated boron nitride nanotubes J. Colloid Interface Sci, 359 (2011), pp. 261–268 [PubMed: 21507418]

[295]. Morillo D, Uheida A, Pérez G, Muhammed M, Valiente M Arsenate removal with 3-mercaptopropanoic acid-coated superparamagnetic iron oxide nanoparticles J. Colloid Interface Sci, 438 (2015), pp. 227–234 [PubMed: 25454446]

[296]. Chen B, Zhu Z, Ma J, Yang M, Hong J, Hu X, Qiu Y, Chen J One-pot, solid-phase synthesis of magnetic multiwalled carbon nanotube/iron oxide composites and their application in arsenic removal J. Colloid Interface Sci, 434 (2014), pp. 9–17 [PubMed: 25151091]

[297]. Abdollahi M, Zeinali S, Nasirimoghaddam S, Sabbaghi S Effective removal of As(III) from drinking water samples by chitosan-coated magnetic nanoparticles Desalin. Water Treat, 56 (2015), pp. 2092–2104

[298]. Luo X, Wang C, Luo S, Dong R, Tu X, Zeng G Adsorption of As(III) and As(V) from water using magnetite Fe_3O_4-reduced graphite oxide–MnO_2 nanocomposites Chem. Eng. J, 187 (2012), pp. 45–52

[299]. Cui H-J, Cai J-K, Zhao H, Yuan B, Ai C-L, Fu M-L Fabrication of magnetic porous Fe–Mn binary oxide nanowires with superior capability for removal of As(III) from water J. Hazard. Mater, 279 (2014), pp. 26–31 [PubMed: 25036997]

[300]. Zhu J, Baig SA, Sheng T, Lou Z, Wang Z, Xu X Fe_3O_4 and MnO_2 assembled on honeycomb briquette cinders (HBC) for arsenic removal from aqueous solutions J. Hazard. Mater, 286 (2015), pp. 220–228 [PubMed: 25585269]

[301]. Kumar S, Nair RR, Pillai PB, Gupta SN, Iyengar MAR, Sood AK Ggraphene oxide–$MnFe_2O_4$ magnetic nanohybrids for efficient removal of lead and arsenic from water ACS Appl. Mater. Interfaces, 6 (2014), pp. 17426–17436 [PubMed: 25222124]

[302]. Babu CM, Palanisamy B, Sundaravel B, Shanthi K, Murugesan V Dihalogen crosslinked Fe_3O_4-reduced graphene oxide nanocomposites for arsenic and mercury adsorption Sci. Adv. Mater, 7 (2015), pp. 794–805

[303]. Salazar-Camacho C, Villalobos M, de la Luz Rivas-Sánchez M, Arenas-Alatorre J, Alcaraz-Cienfuegos J, Gutiérrez-Ruiz ME Characterization and surface reactivity of natural and synthetic magnetites Chem. Geol, 347 (2013), pp. 233–245

[304]. Chiou C-S, Lin Y-F, Chen H-W, Chang C-C, Chang S-H Adsorption of phosphate in aqueous solution by magnetite modified with diethylenetriamine J. Nanosci. Nanotechnol, 15 (2015), pp. 2850–2857 [PubMed: 26353504]

[305]. Wang W, Zhang H, Zhang L, Wan H, Zheng S, Xu Z Adsorptive removal of phosphate by magnetic Fe_3O_4@C@ZrO_2 Colloids Surf. A: Physicochem. Eng. Aspects, 469 (2015), pp. 100–106

[306]. Lai L, Xie Q, Chi L, Gu W, Wu D Adsorption of phosphate from water by easily separable Fe_3O_4@SiO_2 core/shell magnetic nanoparticles functionalized with hydrous lanthanum oxide J. Colloid Interface Sci, 465 (2016), pp. 76–82 [PubMed: 26641568]

[307]. Yan LG, yang K, Shan RR, Yan T, Wei J, Yu SJ, Yu HQ, Du B Kinetic, isotherm and thermodynamic investigations of phosphate adsorption onto core–shell Fe_3O_4@LDHs composites with easy magnetic separation assistance J. Colloid Interface Sci, 448 (2015), pp. 508–516 [PubMed: 25778739]

[308]. Xia S, Xu X, Xu C, Wang H, Zhang X, Liu G Preparation characterization, and phosphate removal and recovery of magnetic $MnFe_2O_4$ nano-particles as adsorbents Environ. Technol, 37 (2016), pp. 795–804 [PubMed: 26292922]

[309]. Ma W, Sha X, Gao L, Cheng Z, Meng F, Cai J, Tan D, Wang R Effect of iron oxide nanocluster on enhanced removal of molybdate from surface water and pilot scale test Colloids Surf. A: Physicochem. Eng. Aspects, 478 (2015), pp. 45–53

[310]. Tu Y-J, Chan T-S, Tu H-W, Wang S.-Li., You C-F, Chang C-K Rapid and efficient removal/recovery of molybdenum onto $ZnFe_2O_4$ nanoparticles Chemosphere, 148 (2016), pp. 452–458 [PubMed: 26835649]

[311]. Wan Z, Chen W, Liu C, Liu Y, Dong C Preparation and characterization of γ-AlOOH@CS magnetic nanoparticle as a novel adsorbent for removing fluoride from drinking water J. Colloid Interface Sci, 443 (2015), pp. 115–124 [PubMed: 25540828]

[312]. Rehman MA, Yusoff I, Alias Y Fluoride adsorption by doped and un-doped magnetic ferrites $CuCe_xFe_{2-x}O_4$: preparation, characterization, optimization and modeling for effectual remediation technologies J. Hazard. Mater, 299 (2015), pp. 316–324 [PubMed: 26143194]

[313]. Wei X, Bhojappa S, Lin L-S, Viadero RC Jr. Performance of nano-magnetite for removal of selenium from aqueous solutions Environ. Eng. Sci, 29 (2012), pp. 526–532

[314]. Wang H, Liu Y-G, Zeng G-M, Hu X-J, Hu X, Li T-T, Li H-Y, Wang Y-Q, Jiang L-H Grafting of β-cyclodextrin to magnetic graphene oxide viaethylenediamine and application for Cr(VI) removal Carbohydr. Polym, 113 (2014), pp. 166–173 [PubMed: 25256471]

[315]. Jiang W, Cai Q, Xu W, Yang M, Cai Y, Dionysiou DD, O'shea KE Cr(VI) adsorption and reduction by humic acid coated on magnetite Environ. Sci. Technol, 48 (2014), pp. 8078–8085 [PubMed: 24901955]

[316]. Qiu B, Gu H, Yan X, Guo J, Wang Y, Sun D, Wang Q, Khan M, Zhang X, Weeks BL, Young DP, Guo Z, Wei S Cellulose derived magnetic mesoporous carbon nanocomposites with enhanced hexavalent chromium removal J. Mater. Chem. A, 2 (2014), pp. 17454–17462

[317]. Yao W, Rao P, Lo IMC, Zhang W, Zheng W Preparation of cross-linked magnetic chitosan with quaternary ammonium and its application for Cr(VI) and P(V) removal J. Environ. Sci, 26 (2014), pp. 2379–2386

[318]. Kumari M, Pittman CU, Mohan D Heavy metals [chromium(VI) and lead(II)] removal from water using mesoporous magnetite (Fe_3O_4) nanospheres J. Colloid Interface Sci, 442 (2015), pp. 120–132 [PubMed: 25531287]

[319]. Rajput S, Pittman CU, Mohan D Magnetic magnetite (Fe_3O_4) nanoparticle synthesis and applications for lead (Pb^{2+}) and chromium (Cr^{6+}) removal from water J. Colloid Interface Sci, 468 (2016), pp. 334–346 [PubMed: 26859095]

[320]. Swindle AL, Cozzarelli IM, Madden ASE Using chromate to investigate the impact of natural organics on the surface reactivity of nanoparticulate magnetite Environ. Sci. Technol, 49 (2015), pp. 2156–2162 [PubMed: 25607467]

[321]. Egodawatte S, Datt A, Burns EA, Larsen SC Chemical insight into the adsorption of chromium(III) on iron oxide/mesoporous silica nanocomposites Langmuir, 31 (2015), pp. 7553–7562 [PubMed: 26134074]

[322]. Silva-Silva MJ, Mijangos-Ricardez OF, Vázquez-Hipólito V, Martinez-Vargas S, López-Luna J Single and mixed adsorption of Cd(II) and Cr(VI) onto citrate-coated magnetite nanoparticles Desalin. Water Treat, 57 (2016), pp. 4008–4017

[323]. Tian X, Wang W, Tian N, Zhou C, Yang C, Komarneni S Cr(VI) reduction and immobilization by novel carbonaceous modified magnetic Fe_3O_4/halloysite nanohybrid J. Hazard. Mater, 309 (2016), pp. 151–156 [PubMed: 26894287]

[324]. Vélez E, Campillo GE, Morales G, Hincapié C, Osorio J, Arnache O, Uribe JI, Jaramillo F Mercury removal in wastewater by iron oxide nanoparticles J. Phys.: Conf. Ser, 687 (2016), pp. 12050–12053

[325]. Shan C, Ma Z, Tong M, Ni J Removal of Hg(II) by poly(1-vinylimidazole)-grafted Fe_3O_4@SiO_2 magnetic nanoparticles Water Res., 69 (2015), pp. 252–260 [PubMed: 25497175]

[326]. Pan S, Shen H, Xu Q, Luo J, Hu M Surface mercapto engineered magnetic Fe_3O_4 nanoadsorbent for the removal of mercury from aqueous solutions J. Colloid Interface Sci, 365 (2012), pp. 204–212 [PubMed: 21974922]

[327]. Zeng G, Pang Y, Zeng Z, Tang L, Zhang Y, Liu Y, Zhang J, Lei X, Li Z, Xiong Y, Xie G Removal and recovery of Zn^{2+} and Pb^{2+} by imine-functionalized magnetic nanoparticles with tunable selectivity Langmuir, 28 (2012), pp. 468–473 [PubMed: 22126706]

[328]. Chung J, Chun J, Woo J, Lee SH, Lee YJ, Hong SW Sorption of Pb(II) and Cu(II) onto multi-amine grafted mesoporous silica embedded with nano-magnetite: effects of steric factors J. Hazard. Mater, 239–240 (2012), pp. 183–191

[329]. Mahmoud ME, Rashad AR Enhanced separation and extraction of cadmium and lead by a novel magnetite-immobilized-gelatin nano-sorbent Sep. Sci. Technol, 51 (2016), pp. 767–777

[330]. Mohmood I, Lopes CB, Lopes I, Tavares DS, Soares AMVM, Duarte AC, Trindade T, Ahmad I, Pereira E Remediation of mercury contaminated saltwater with functionalized silica coated magnetite nanoparticles Sci. Total Environ, 557–558 (2016), pp. 712–721

[331]. Anirudhan TS, Shainy F Effective removal of mercury(II) ions from chlor-alkali industrial wastewater using 2-mercaptobenzamide modified itaconic acid-grafted-magnetite nanocellulose J. Colloid Interface Sci, 456 (2015), pp. 22–31 [PubMed: 26086434]

[332]. Cui L, Wang Y, Gao L, Hu L, Wei Q, Du B Removal of Hg(II) from aqueous solution by resin loaded magnetic β-cyclodextrin bead and graphene oxide sheet: synthesis, adsorption mechanism and separation J. Colloid Interface Sci, 456 (2015), pp. 42–49 [PubMed: 26092115]

[333]. Ma Y, La P, Lei W, Lu C, Du X Adsorption of Hg(II) from aqueous solution using amino-functionalized graphite nanosheets decorated with Fe_3O_4 nanoparticles Desalin. Water Treat, 57 (2016), pp. 5004–5012

[334]. Shih Y-C, Ke C-Y, Yu C-J, Lu C-Y, Tseng W-L Combined tween 20-stabilized gold nanoparticles and reduced graphite oxide–Fe_3O_4 nanoparticle composites for rapid and efficient removal of mercury species from a complex matrix ACS Appl. Mater. Interfaces, 6 (2014), pp. 17437–17445 [PubMed: 25238563]

[335]. Li K, Wang Y, Huang M, Yan H, Yang H, Xiao S, Li A Preparation of chitosan-graft-polyacrylamide magnetic composite microspheres for enhanced selective removal of mercury ions from water J. Colloid Interface Sci, 455 (2015), pp. 261–270 [PubMed: 26073848]

[336]. Wang Y, Shi L, Gao L, Wei Q, Cui L, Hu L, Yan L, Du B The removal of lead ions from aqueous solution by using magnetic hydroxypropyl chitosan/oxidized multiwalled carbon nanotubes composites J. Colloid Interface Sci, 451 (2015), pp. 7–14 [PubMed: 25863447]

[337]. Jiang L, Liu P Design of magnetic attapulgite/fly ash/poly(acrylic acid) ternary nanocomposite hydrogels and performance evaluation as selective adsorbent for Pb^{2+} ion ACS Sustain. Chem. Eng, 2 (2014), pp. 1785–1794

[338]. Chen D, Shen W, Wu S, Chen C, Luo X, Guo L Ion exchange induced removal of Pb(II) by MOF-derived magnetic inorganic sorbents Nanoscale, 8 (2016), pp. 7172–7179 [PubMed: 26967550]

[339]. Chen Z, Geng Z, Zhang Z, Ren L, Tao T, Yang R, Guo Z Synthesis of magnetic Fe_3O_4@C nanoparticles modified with SO_3H and COOH groups for fast removal of Pb^{2+} Hg^{2+}, and Cd^{2+} ions Eur. J. Inorg. Chem, 2014 (2014), pp. 3172–3177

[340]. Shi H, Yang J, Zhu L, Yang Y, Yuan H, Yang Y, Liu X Removal of Hg^{2+} Pb^{2+}, and Cu^{2+} by chain-like Fe_3O_4@SiO_2@chitosan magnetic nanoparticles J. Nanosci. Nanotechnol, 16 (2016), pp. 1871–1882 [PubMed: 27433691]

[341]. Mahmouda ME, Abdelwahaba MS, Abdoua AEH Enhanced removal of lead and cadmium from water by Fe_3O_4-cross linked-O-phenylenediamine nano-composite Sep. Sci. Technol, 51 (2016), pp. 237–247

[342]. Wang J, Zhang W, Yue X, Yang Q, Liu F, Wang Y, Zhang D, Li Z, Wang J One-pot synthesis of multifunctional magnetic ferrite–MoS2–carbon dot nanohybrid adsorbent for efficient Pb(II) removal J. Mater. Chem. A, 4 (2016), pp. 3893–3900

[343]. Pan S, Li J, Wan G, Liu C, Fan W, Wang L Nanosized yolk–shell Fe_3O_4@Zr $(OH)_x$ spheres for efficient removal of Pb(II) from aqueous solution J. Hazard. Mater, 309 (2016), pp. 1–9 [PubMed: 26872327]

[344]. Shan C, Ma Z, Tong M Efficient removal of free and nitrilotriacetic acid complexed Cd(II) from water by poly(1-vinylimidazole)-grafted Fe_3O_4@SiO_2 magnetic nanoparticles J. Hazard. Mater, 299 (2015), pp. 479–485 [PubMed: 26247623]

[345]. Babaei AA, Bahrami M, Firouzi AF, Esfahani AR, Alidokht L Adsorption of cadmium onto modified nanosized magnetite: kinetic modeling, isotherm studies, and process optimization Desalin. Water Treat, 56 (2015), pp. 3380–3392

[346]. Bao S, Tang L, Li K, Ning P, Peng J, Guo H, Zhu T, Liu Y Highly selective removal of Zn(II) ion from hot-dip galvanizing pickling waste with amino-functionalized Fe_3O_4@SiO_2 magnetic nano-adsorbent J. Colloid Interface Sci, 462 (2016), pp. 235–242 [PubMed: 26458121]

[347]. Bakr AA, Moustafa YM, Khalil MMH, Yehia MM, Motawea EA Magnetic nanocomposite beads: synthesis and uptake of Cu(II) ions from aqueous solutions Can. J. Chem, 93 (2015), pp. 289–296

[348]. Wanna Y, Chindaduang A, Tumcharern G, Phromyothin D, Porntheerapat S, Nukeaw J, Hofmann H, Pratontep S Efficiency of SPIONs functionalized with polyethylene glycol bis(amine) for heavy metal removal J. Magn. Magn. Mater, 414 (2016), pp. 32–37

[349]. Prucek R, Tuček J, Kolařík J, Hušková I, Filip J, Varma RS, Sharma VK, Zbořil R Ferrate(VI)-prompted removal of metals in aqueous media: mechanistic delineation of enhanced efficiency via metal entrenchment in magnetic oxides Environ. Sci. Technol, 49 (2015), pp. 2319–2327 [PubMed: 25607569]

[350]. Zhao F, Tang WZ, Zhao D, Meng Y, Yin D, Sillanpaa M Adsorption kinetics, isotherms and mechanisms of Cd(II) Pb(II), Co(II) and Ni(II) by a modified magnetic polyacrylamide microcomposite adsorbent J. Water Process Eng, 4 (2014), pp. 47–57

[351]. Cui L, Wang Y, Gao L, Hu L, Yan L, Wei Q, Du B EDTA functionalized magnetic graphene oxide for removal of Pb(II), Hg(II) and Cu(II) in water treatment: adsorption mechanism and separation property Chem. Eng. J, 281 (2015), pp. 1–10

[352]. Hu X-J, Liu Y-G, Zeng G-M, Wang H, You S-H, Hu X, Tan X-F, Chen A-W, Guo F-Y Effects of inorganic electrolyte anions on enrichment of Cu(II) ions with aminated Fe_3O_4/graphene oxide: Cu(II) speciation prediction and surface charge measurement Chemosphere, 127 (2015), pp. 35–41 [PubMed: 25655695]

[353]. Tan L, Wang J, Liu Q, Sun Y, Zhang H, Wang Y, Jing X, Liu J, Song D Facile preparation of oxine functionalized magnetic Fe_3O_4 particles for enhanced uranium(VI) adsorption Colloids Surf. A: Physicochem. Eng. Aspects, 466 (2015), pp. 85–91

[354]. Tan L, Zhang X, Liu Q, Jing X, Liu J, Song D, Hu S, Liu L, Wang J Synthesis of Fe_3O_4@TiO_2 core–shell magnetic composites for highly efficient sorption of uranium(VI) Colloids Surf. A: Physicochem. Eng. Aspects, 469 (2015), pp. 279–286

[355]. Chen L, Zhao D, Chen S, Wang X, Chen C One-step fabrication of amino functionalized magnetic graphene oxide composite for uranium(VI) removal J. Colloid Interface Sci, 472 (2016), pp. 99–107 [PubMed: 27016915]

[356]. Ding C, Cheng W, Sun Y, Wang X Novel fungus-Fe_3O_4 bio-nanocomposites as high performance adsorbents for the removal of radionuclides J. Hazard. Mater, 295 (2015), pp. 127–137 [PubMed: 25897694]

[357]. Ozcan F, Bayrakcı M, Ertul Synthesis S and preparation of novel magnetite nanoparticles containing calix[4]arenes with different chelating group towards uranium anions J. Macromol. Sci. Part A, 52 (2015), pp. 599–608

[358]. Marshall TA, Morris K, Law GTW, Mosselmans JFW, Bots P, Roberts H, Shaw S Uranium fate during crystallization of magnetite from ferrihydrite in conditions relevant to the disposal of radioactive waste Mineral. Mag, 79 (2015), pp. 1265–1274

[359]. Yang H-M, Hong SB, Choi YS, Lee K-W, Seo B-K, Moon J-K Copper ferrocyanide-functionalized magnetic adsorbents using polyethyleneimine coated Fe_3O_4 nanoparticles for the removal of radioactive cesium J. Nanosci. Nanotechnol, 16 (2016), pp. 3067–3070 [PubMed: 27455762]

[360]. Wylie EM, Olive DT, Powell BA Effects of titanium doping in titanomagnetite on neptunium sorption and speciation Environ. Sci. Technol, 50 (2016), pp. 1853–1858 [PubMed: 26756748]

[361]. Smith FN, Um W, Taylor CD, Kim D-S, Schweiger MJ, Kruger AA Computational investigation of technetium(IV) incorporation into inverse spinels: magnetite (Fe_3O_4) and Trevorite ($NiFe_2O_4$) Environ. Sci. Technol, 50 (2016), pp. 5216–5224 [PubMed: 27049925]

[362]. Patra S, Roy E, Madhuri R, Sharma PK Fast and selective preconcentration of europium from wastewater and coal soil by graphene oxide/silane@Fe_3O_4 dendritic nanostructure Environ. Sci. Technol, 49 (2015), pp. 6117–6126 [PubMed: 25895010]

[363]. Basualto C, Gaete J, Molina L, Valenzuela F, Yañez C, Marco JF Lanthanide sorbent based on magnetite nanoparticles functionalized with organophosphorus extractants Sci. Technol. Adv. Mater, 16 (2015), pp. 35010–35018

[364]. Zhang F, Song Y, Song S, Zhang R, Hou W Synthesis of magnetite-graphene oxide-layered double hydroxide composites and applications for the removal of Pb(II) and 2,4-dichlorophenoxyacetic acid from aqueous solutions ACS Appl. Mater. Interfaces, 7 (2015), pp. 7251–7263 [PubMed: 25791354]

[365]. Han Z, Sani B, Mrozik W, Obst M, Beckingham B, Karapanagioti HK, Werner D Magnetite impregnation effects on the sorbent properties of activated carbons and biochars Water Res., 70 (2015), pp. 394–403 [PubMed: 25555224]

[366]. Bai X, Feng R, Hua Z, Zhou L, Shi H Adsorption of 17β-estradiol (E2) and Pb(II) on Fe_3O_4/graphene oxide (Fe_3O_4/GO) nanocomposites Environ. Eng. Sci, 32 (2015), pp. 370–378

[367]. Ge X, Gu CD, Wang XL, Tu JP Spinel type CoFe oxide porous nanosheets as magnetic adsorbents with fast removal ability and facile separation J. Colloid Interface Sci, 454 (2015), pp. 134–143 [PubMed: 26005799]

[368]. Cui L, Guo X, Wei Q, Wang Y, Gao L, Yan L, Yan T, Du B Removal of mercury and methylene blue from aqueous solution by xanthate functionalized magnetic graphene oxide: sorption kinetic and uptake mechanism J. Colloid Interface Sci, 439 (2015), pp. 112–120 [PubMed: 25463182]

[369]. Liu J, Wang C, Xiong Z Adsorption behavior of magnetic multiwalled carbon nanotubes for the simultaneous adsorption of furazolidone and Cu(II) from aqueous solutions Environ. Eng. Sci, 32 (2015), pp. 960–969

[370]. Zhang X, Qian J, Pan B Fabrication of novel magnetic nanoparticles of multifunctionality for water decontamination Environ. Sci. Technol, 50 (2016), pp. 881–889 [PubMed: 26695341]

[371]. Li J, Fan Q, Wu Y, Wang X, Chen C, Tang Z, Wang X Magnetic polydopamine decorated with Mg–Al LDH nanoflakes as a novel bio-based adsorbent for simultaneous removal of potentially toxic metals and anionic dyes J. Mater. Chem. A, 4 (2016), pp. 1737–1746

[372]. Sun Y, Liu X, Kainuma M, Wang W, Takaoka M, Takeda N Dechlorination of polychlorinated biphenyls by iron and its oxides Chemosphere, 137 (2015), pp. 78–86 [PubMed: 26011415]

[373]. Wang Y, Si X, Si Y Dechlorination of 3,3′,4,4′-tetrachlorobiphenyl in aqueous solution by hybrid Fe^0/Fe_3O_4 nanoparticle system J. Exp. Nanosci, 10 (2015), pp. 1166–1179

[374]. Tian H, Liu F, He J Multifunctional Fe_3O_4@nSiO_2@mSiO_2-Fe core–shell microspheres for highly efficient removal of 1,1,1-trichloro-2,2-bis(4-chlorophenyl) ethane (DDT) from aqueous media J. Colloid Interface Sci, 431 (2014), pp. 90–96 [PubMed: 24992299]

[375]. Gan M, Huang Y, Zhang Y, Pan J, Shi W, Yan Y Fabrication of Ag/halloysite nanotubes/Fe_3O_4 nanocatalyst and their catalytic performance in 4-nitrophenol reduction Desalin. Water Treat, 56 (2015), pp. 425–434

[376]. Xu J, Liu X, Lowry GV, Cao Z, Zhao H, Zhou JL, Xu X Dechlorination mechanism of 2,4-dichlorophenol by magnetic MWCNTS supported Pd/Fe nanohybrids: rapid adsorption, gradual dechlorination, and desorption of phenol ACS Appl. Mater. Interfaces, 8 (2016), pp. 7333–7342 [PubMed: 26938876]

[377]. Shan D, Deng S, Zhao T, Wang B, Wang Y, Huang J, Yu G, Winglee J, Wiesner MR Preparation of ultrafine magnetic biochar and activated carbon for pharmaceutical adsorption and subsequent degradation by ball milling J. Hazard. Mater, 305 (2016), pp. 156–163 [PubMed: 26685062]

[378]. Villacís-García M, Villalobos M, Gutiérrez- Ruiz M Ruiz Optimizing the use of natural and synthetic magnetites with very small amounts of coarse Fe(0) particles for reduction of aqueous Cr(VI) J. Hazard. Mater, 281 (2015), pp. 77–86 [PubMed: 25065818]

[379]. Watts MP, Coker VS, Parry SA, Pattrick RAD, Thomas RAP, Kalin R, Lloyd JR Biogenic nano-magnetite and nano-zero valent iron treatment of alkaline Cr(VI) leachate and chromite ore processing residue Appl. Geochem, 54 (2015), pp. 27–42 [PubMed: 26109747]

[380]. Wang T, Zhang L, Li C, Yang W, Song T, Tang C, Meng Y, Dai S, Wang H, Chai L, Luo J Synthesis of core–shell magnetic Fe_3O_4@poly(m-phenylenediamine) particles for chromium reduction and adsorption Environ Sci. Technol, 49 (2015), pp. 5654–5662 [PubMed: 25867789]

[381]. Cho D-W, Song H, Schwartz FW, Kim B, Jeon B-H The role of magnetite nanoparticles in the reduction of nitrate in groundwater by zero-valent iron Chemosphere, 125 (2015), pp. 41–49 [PubMed: 25665757]

[382]. Suanon F, Sun Q, Mama D, Li J, Dimon B, Yua C-P Effect of nanoscale zero-valent iron and magnetite (Fe_3O_4) on the fate of metals during anaerobic digestion of sludge Water Res, 88 (2016), pp. 897–903 [PubMed: 26613183]

[383]. Joseph S, Anawar HM, Storer P, Blackwell P, Chia C, Lin Y, Munroe P, Donne S, Horvat J, Wang J, Solaiman ZM Effects of enriched biochars containing magnetic iron nanoparticles on mycorrhizal colonisation plant growth, nutrient uptake and soil quality improvement Pedosphere, 25 (2015), pp. 749–760

[384]. Usman M, Faure P, Ruby C, Hanna K Remediation of PAH-contaminated soils by magnetite catalyzed Fenton-like oxidation Appl. Catal. B: Environ, 117–118 (2012), pp. 10–17

[385]. Liang QQ, Zhao DY Immobilization of arsenate in a sandy loam soil using starch-stabilized magnetite nanoparticles J. Hazard. Mater, 271 (2014), pp. 16–23 [PubMed: 24584068]

[386]. Sun J, Chillrud SN, Mailloux BJ, Stute M, Singh R, Dong H, Lepre CJ, Bostick BC Enhanced and stabilized arsenic retention in microcosms through the microbial oxidation of ferrous iron by nitrate Chemosphere, 144 (2016), pp. 1106–1115 [PubMed: 26454120]

[387]. Funes A, de Vicente J, Cruz-Pizarro L, Álvarez-Manzaneda I, de Vicente I Magnetic microparticles as a new tool for lake restoration: a microcosm experiment for evaluating the impact on phosphorus fluxes and sedimentary phosphorus pools Water Res., 89 (2016), pp. 366–374 [PubMed: 26724732]

[388]. Li C, Yi X, Dang Z, Yu H, Zeng T, Wei C, Feng C Fate of Fe and Cd upon microbial reduction of Cd-loaded polyferric flocs by Shewanella oneidensis MR-1 Chemosphere, 144 (2016), pp. 2065–2072 [PubMed: 26583288]

[389]. Lee W, Batchelor B Abiotic reductive dechlorination of chlorinated ethylenes by iron-bearing soil minerals. 1. Pyrite and magnetite Environ. Sci. Technol, 36 (2002), pp. 5147–5154 [PubMed: 12523432]

[390]. McCormick ML, Adriaens P Carbon tetrachloride transformation on the surface of nanoscale biogenic magnetite particles Environ. Sci. Technol, 38 (2004), pp. 1045–1053 [PubMed: 14998017]

[391]. Hanoch RJ, Shao H, Butler EC Transformation of carbon tetrachloride by bisulfide treated goethite, hematite, magnetite, and kaolinite Chemosphere, 63 (2006), pp. 323–334 [PubMed: 16154172]

[392]. Danielsen K, Hayes KF pH dependence of carbon tetrachloride reductive dechlorination by magnetite Environ. Sci. Technol, 38 (2004), pp. 4745–4752 [PubMed: 15487782]

[393]. Zwank L, Elsner M, Aeberhard A, Schwarzenbach RP, Haderlein SB Carbon isotope fractionation in the reductive dehalogenation of carbon tetrachloride at iron (hydr)oxide and iron sulfide minerals Environ. Sci. Technol, 39 (2005), pp. 5634–5641 [PubMed: 16124297]

[394]. Vikesland PJ, Heathcock AM, Rebodos RL, Makus KE Particle size and aggregation effects on magnetite reactivity toward carbon tetrachloride Environ. Sci. Technol, 41 (2007), pp. 5277–5283 [PubMed: 17822091]

[395]. Ferrey ML, Wilkin RT, Ford RG, Wilson JT Non-biological removal of cis-dichloroethylene and 1,1-dichloroethylene in aquifer sediment containing magnetite Environ. Sci. Technol, 38 (2004), pp. 1746–1752 [PubMed: 15074684]

[396]. Ayala-Luis KB, Cooper NG, Koch CB, Hansen HC Efficient dechlorination of carbon tetrachloride by hydrophobic green rust intercalated with dodecanoate anions Environ. Sci. Technol, 46 (2012), pp. 3390–3397 [PubMed: 22360442]

[397]. Jeong HY, Anantharaman K, Hyun SP, Son M, Hayes KF pH impact on reductive dechlorination of cis-dichloroethylene by Fe precipitates: an X-ray absorption spectroscopy study Water Res., 47 (2013), pp. 6639–6649 [PubMed: 24074816]

[398]. He YT, Wilson JT, Su C, Wilkin RT Review of abiotic degradation of chlorinated solvents by reactive iron minerals in aquifers Groundwater Monit. Remediat, 35 (2015), pp. 57–75

[399]. Giri SK, Das NN Visible light induced photocatalytic decolourisation of rhodamine B by magnetite nanoparticles synthesised using recovered iron from waste iron ore tailing Desalin. Water Treat, 57 (2016), pp. 900–907

[400]. Nasrollahzadeh M, Sajadi SM Preparation of Pd/Fe_3O_4 nanoparticles by use of Euphorbia stracheyi Boiss root extract: a magnetically recoverable catalyst for one-pot reductive amination of aldehydes at room temperature J. Colloid Interface Sci, 464 (2016), pp. 147–152 [PubMed: 26615511]

[401]. Virkutyte J, Varma RS Eco-friendly magnetic iron oxide pillared montmorillonite for advanced catalytic degradation of dichlorophenol ACS Sustain. Chem. Eng, 2 (2014), pp. 1545–1550

[402]. Shirkhodaie M, Beyki MH, Shemirani F Biogenic synthesis of magnetic perlite@iron oxide composite: application as a green support for dye removal Desalin. Water Treat, 25 (2016), pp. 11859–11871

[403]. Su C, Puls RW, Krug TA, Watling MT, O'Hara SK, Quinn JW, Ruiz NE A two and half-year-performance evaluation of a field test on treatment of source zone tetrachloroethene and its chlorinated daughter products using emulsified zero valent iron nanoparticles Water Res., 46 (2012), pp. 5071–5084 [PubMed: 22868086]

[404]. Su C, Puls RW, Krug TA, Watling MT, O'Hara SK, Quinn JW, Ruiz NE Travel distance and transformation of injected emulsified zero valent iron nanoparticles in the subsurface during two and half years Water Res., 47 (2013), pp. 4095–4106 [PubMed: 23562563]

[405]. Liu T, Li X, Waite TD Depassivation of aged Fe^0 by divalent cations: correlation between contaminant degradation and surface complexation constants Environ. Sci. Technol, 48 (2014), pp. 14564–14571 [PubMed: 25383907]

[406]. Lin C-H, Shih Y-H, MacFarlane J Amphiphilic compounds enhance the dechlorination of pentachlorophenol with Ni/Fe bimetallic nanoparticles Chem. Eng. J, 262 (2015), p. 59

[407]. Ou Y-H, Wei C-Y, Shih Y-H Short-chain organic acids increase the reactivity of zerovalent iron nanoparticles to polychlorinated aromatic pollutants in water Chem. Eng. J, 284 (2016), pp. 372–379

[408]. An B, Zhao DY Immobilization of As(III) in soil and groundwater using a new class of polysaccharide stabilized Fe-Mn oxide nanoparticles J. Hazard. Mater, 211 (2012), pp. 332–341 [PubMed: 22119304]

[409]. Etique M, Jorand FPA, Ruby C Magnetite as a precursor for green rust through the hydrogenotrophic activity of the ironreducing bacteria Shewanella putrefaciens Geobiology, 14 (2016), pp. 237–254 [PubMed: 26715461]

Highlights

- Environmental impact of engineered MNPs.
- MNPs and their hybrids explored for use in energy, analytical chemistry, and catalysis.
- Surface modification to MNPs allow biocompatible applications.
- Adsorptive and separative removal of a wide range of contaminants from aquatic environments.
- Active remediation and natural attenuation of contaminants in soil and groundwater using MNPs.

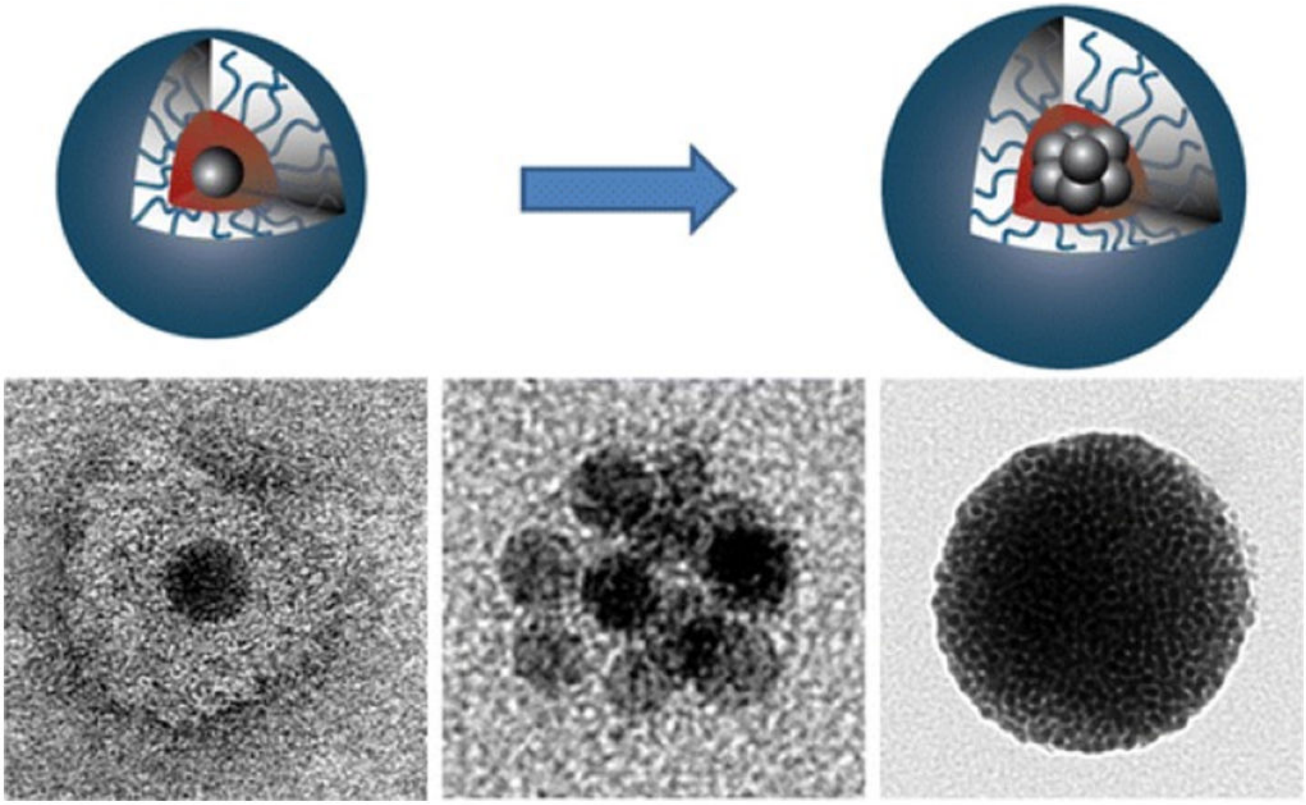

Figure 1.

Polymer-assisted self-assembly of superparamagnetic iron oxide nanoparticles into well-defined clusters that controls the collective magnetic properties. Reprinted from Ref. [51]. Copyright 2014 American Chemical Society.

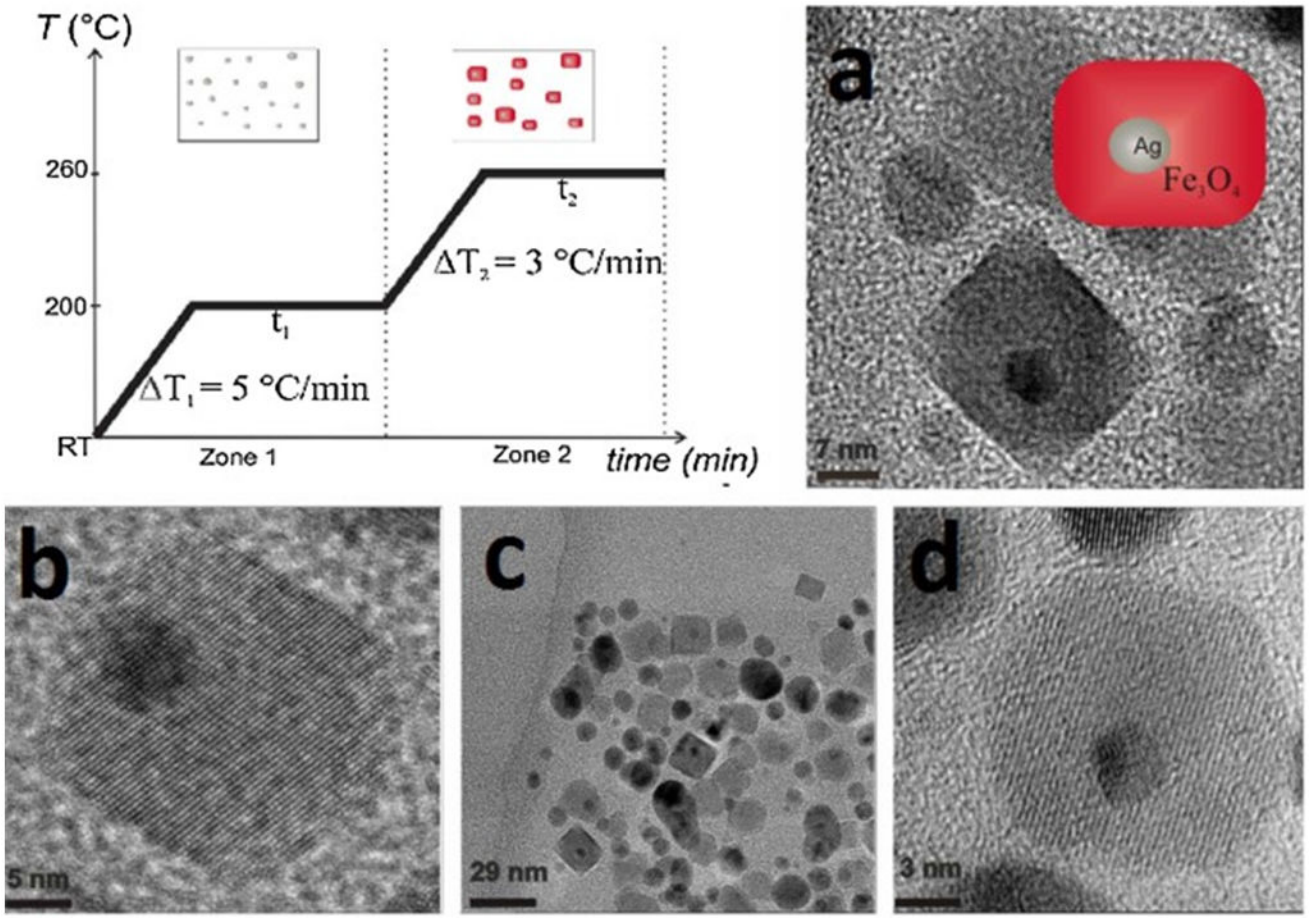

Figure 2.

Temperature profile of the temperature-paused single-step thermal decomposition synthesis. Boxes sketch the expected predominant structures for each time zone. Typically, both waiting times are 120 min. Images: TEM images of brick-like nanoparticles (BLNs) obtained following the temperature-paused single-step protocol. Ag corresponds to the dark contrast, while lighter particles correspond to magnetite. Plain magnetite nanoparticles which are formed are also shown in (c). (a, b and d) are different amplifications of BLNs in order to understand the structure. Reprinted from Ref. [62]. Copyright 2015 American Scientific Publishers.

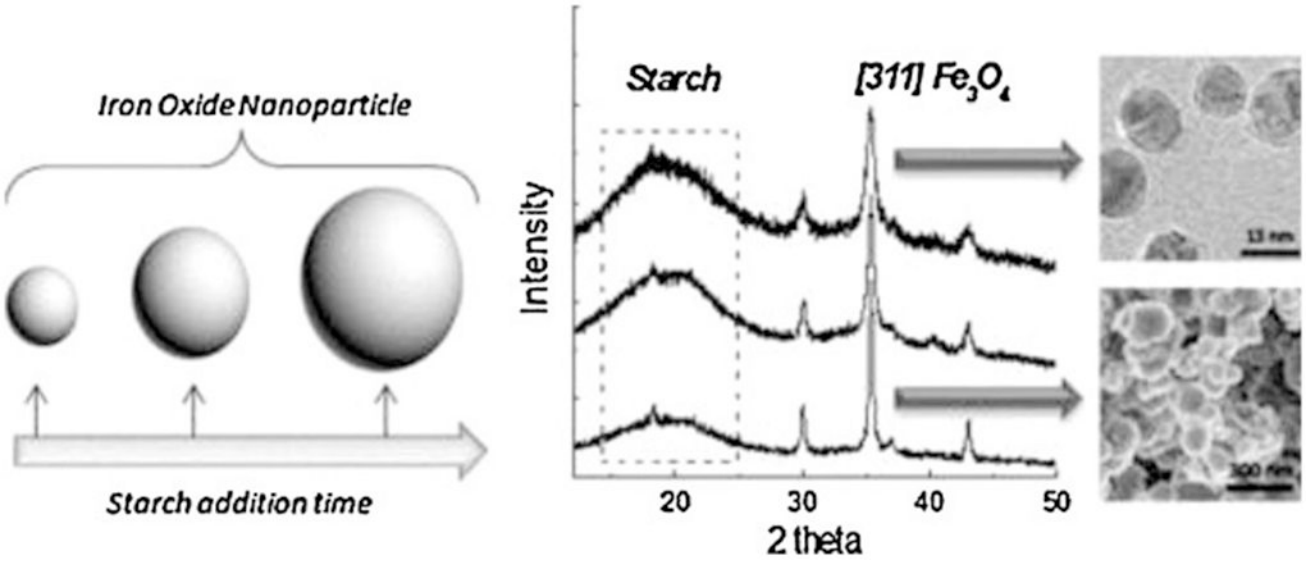

Figure 3.

Starch coated Fe_3O_4 nanoparticles are synthesized by the precipitation oxidation method. Starch is employed as an effective control agent to tune the nanoparticle size and starch coated nanoparticles are water dispersible and forms a ferrofluid. Reprinted from Ref. [64]. Copyright 2015 Taylor & Francis.

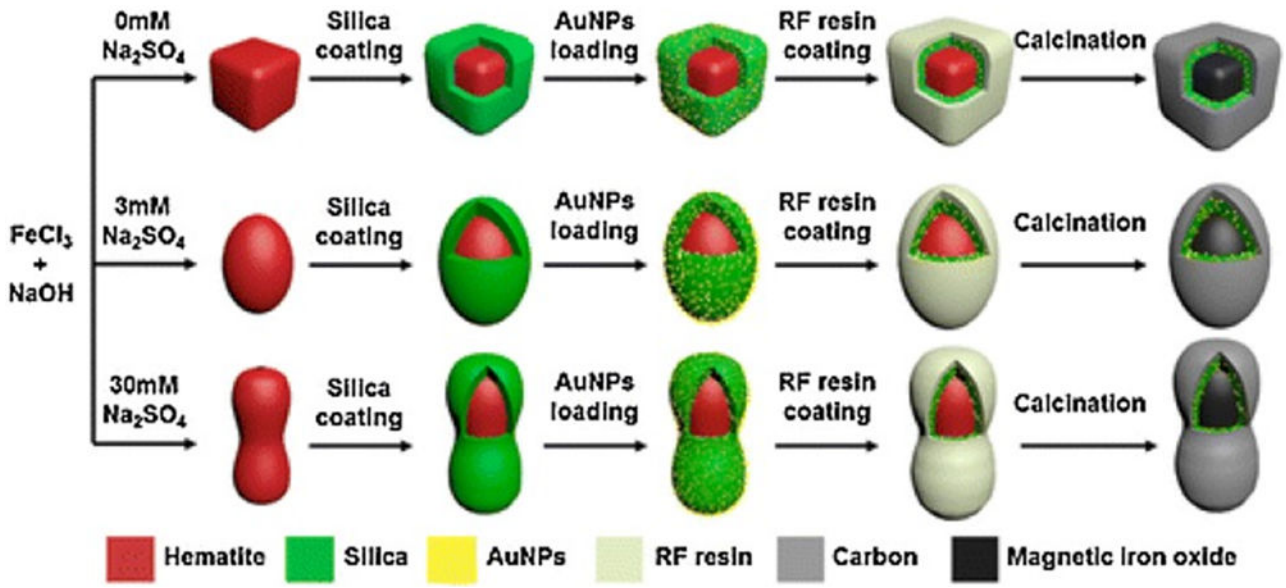

Figure 4.

Magnetic iron oxide@SiO_2–Au@C particles with shapes of pseduocube, ellipsoid, and peanut, are synthesized using hematite as templates and precursors of magnetic iron oxide. The Au NPs of ~6 nm are uniformly distributed between the silica and carbon layers, preventing the aggregation and reduced the loss of the metal nanocrystals during recycling. Reprinted from Ref. [69]. Copyright 2015 American Chemical Society.

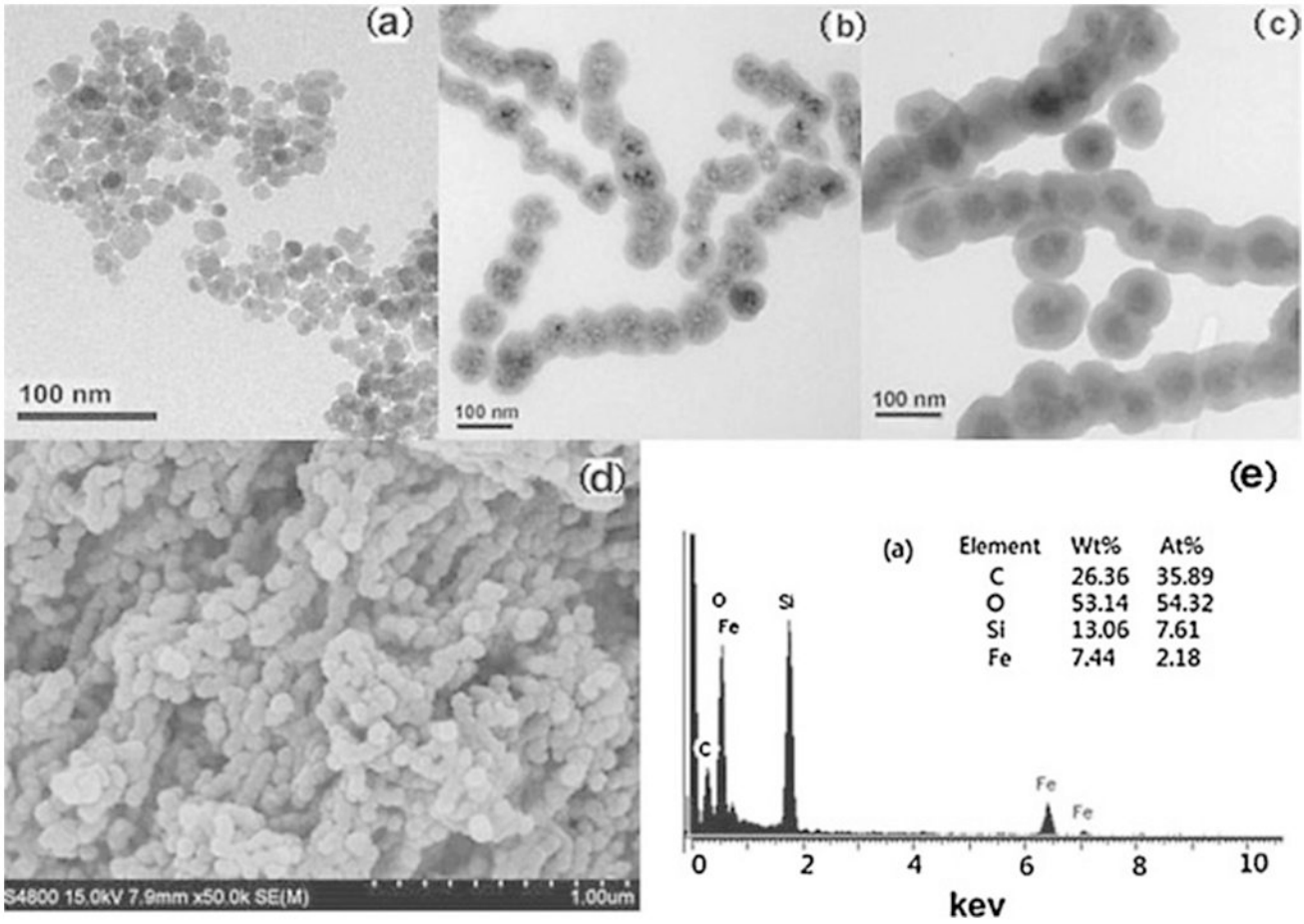

Figure 5.

The TEM of (a), Fe_3O_4 (22 nm), (b), Fe_3O_4@SiO_2 (core 60 nm, shell 10 nm) and (c), Fe_3O_4@SiO_2@chitosan (total 105 nm, thickness of chitosan 12 nm) and (d), the SEM of Fe_3O_4@SiO_2@chitosan, and (e), the EDS of sample-chitosan. The composite NPs having spherical core–shell and chain-like structure with a good dispersion are effective adsorbents for aquosus Hg^{2+}, Pb^{2+}, and Cu^{2+}. Reprinted from Ref. [79]. Copyright 2016 American Scientific Publishers.

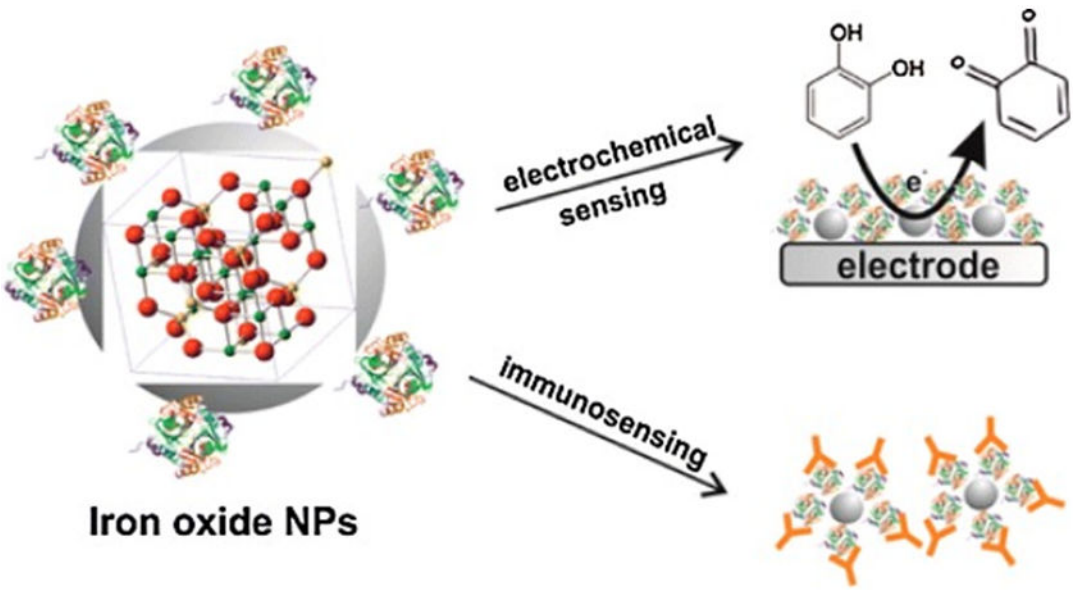

Figure 6.

Iron oxide NPs such as nanomagnetite as a platform for electrochemical and chemical biosensors. Reprinted from Ref. [121]. Copyright 2014 American Chemical Society.

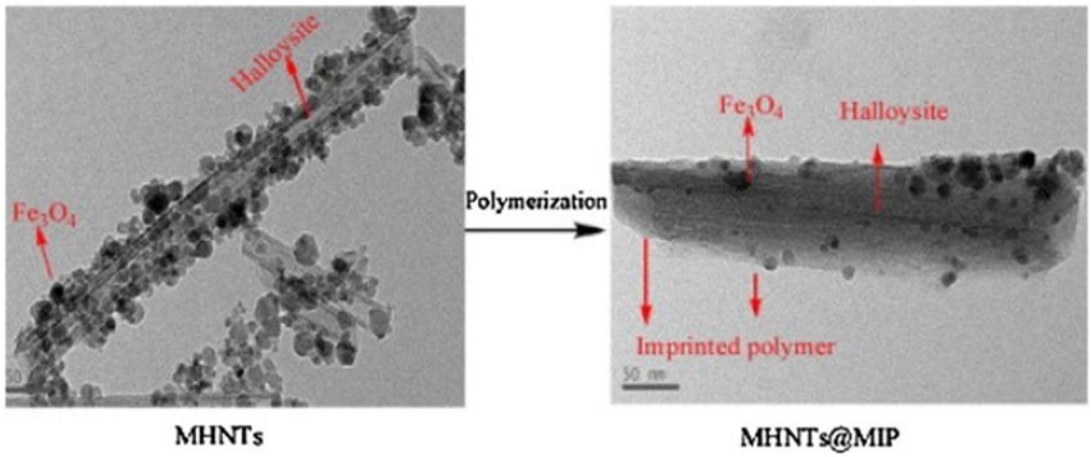

Figure 7.

A new type of magnetic halloysite nanotubes molecularly imprinted polymer (MHNTs@MIP) based on halloysite nanotubes (HNTs) with embedded magnetic nanoparticles is prepared through surface imprinting technology, using 2,4-dichlorophenoxyacetic acid (2,4-D) as a template, 4-vinylpyridine as the monomer, divinylbenzene as cross-linking agents, and 2,2-azodiisobutyronitrile as initiator. MHNTs@MIP is applied as an adsorbent for sample pretreatment extraction followed by high-performance liquid chromatography detection of 2,4-D residue in water. Reprinted from Ref. [132]. Copyright 2014 Elsevier Ltd.

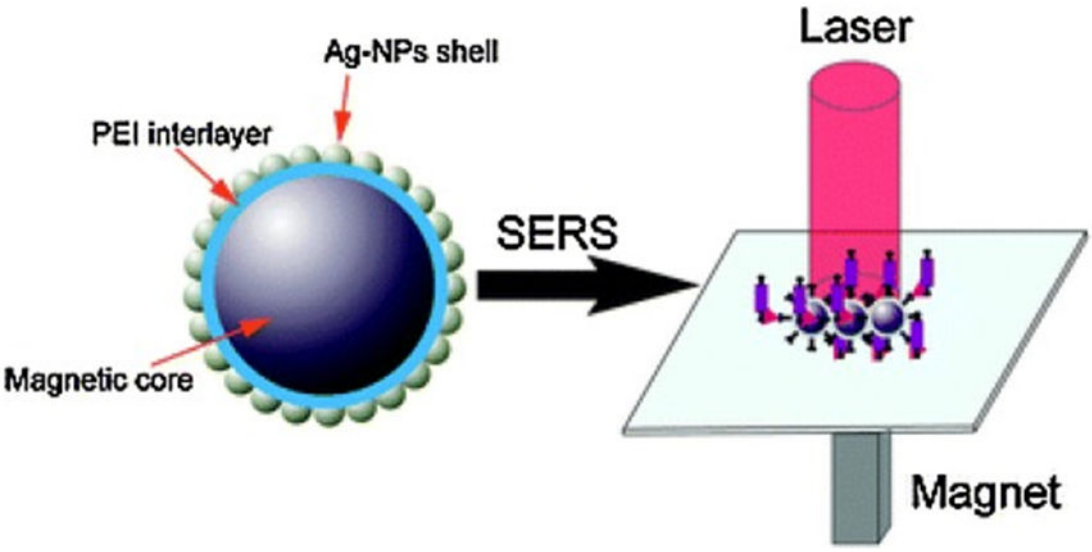

Figure 8.

Novel Ag-coated magnetic core–shell microspheres (Fe_3O_4@PEI@Ag) with polyethyleneimine (PEI) as an interlayer is used to measure adsorbed PATP (p-aminothiophenol) molecules and human IgG with a detection limit as low as 10^{-11} M and 10^{-14} g mL^{-1}, respectively. Reprinted from Ref. [152]. Copyright 2015 Royal Society of Chemistry.

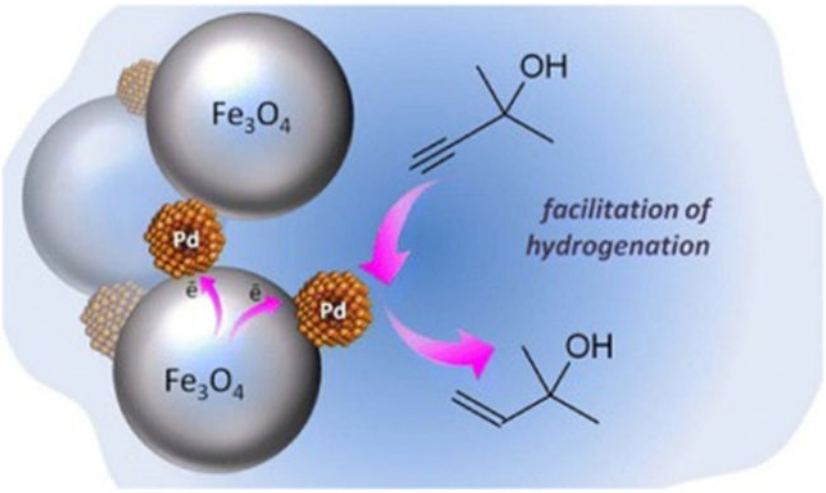

Figure 9.

Fabrication of magnetically recoverable catalysts based on mixtures of Pd and magnetite nanoparticles for hydrogenation of alkyne alcohols. Reprinted from Ref. [173]. Copyright 2014 American Chemical Society.

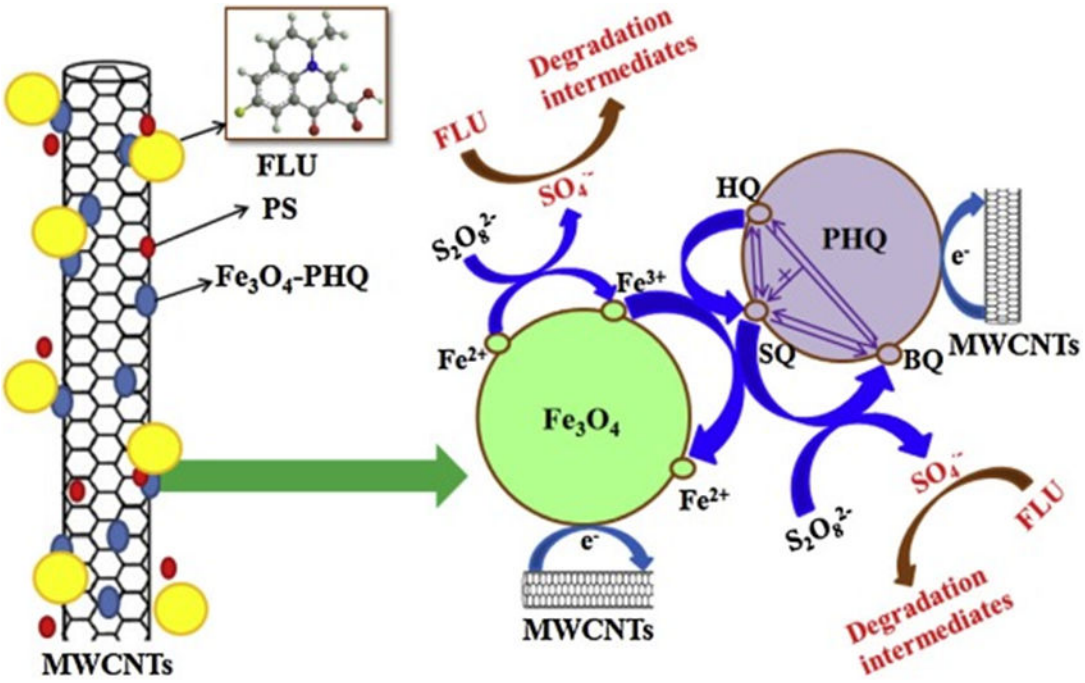

Figure 10.

A novel heterogeneous catalyst, namely, polyhydroquinone-coated magnetite/multi-walled carbon nanotubes (Fe_3O_4/MWCNTs/PHQ) can be used as the efficient heterogeneous catalysts for persulfate oxidation of antibiotic flumequine (FLU). Reprinted from Ref. [194]. Copyright 2015 Elsevier Ltd.

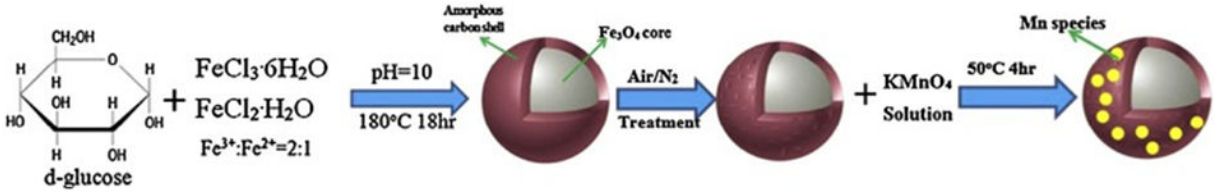

Figure 11.

Synthesis procedure of magnetic Fe_3O_4@C supported manganese catalysts for oxidation of organics in water by peroxymonosulfate. Reprinted from Ref. [195]. Copyright 2015 Elsevier Ltd.

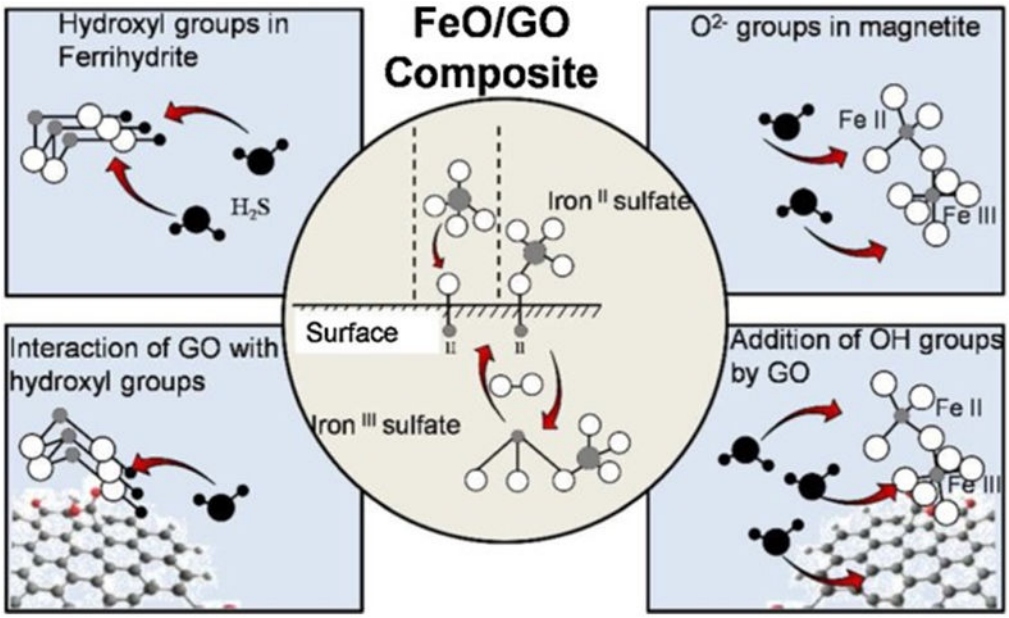

Figure 12.

Composites of magnetite and two-line ferrihydrite with graphite oxide (GO) are synthesized and tested as hydrogen sulfide adsorbents. The addition of GO increased the surface area of the composites due to the formation of new micropores. Reprinted from Ref. [215]. Copyright 2015 American Chemical Society.

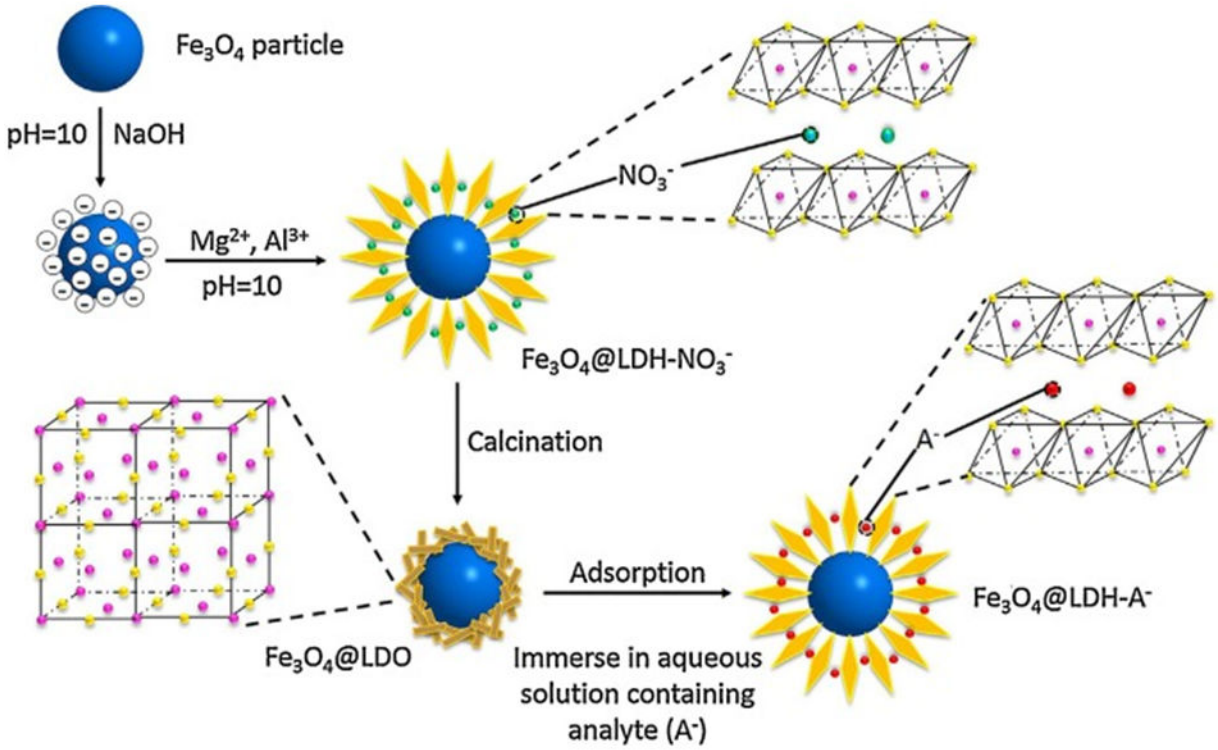

Figure 13.

Schematic depicting the synthesis of Fe_3O_4@LDO microspheres, and regeneration of the LDH structure with intercalated analyte anion during the removal experiments. Reprinted from Ref. [249]. Copyright 2015 Elsevier Ltd.

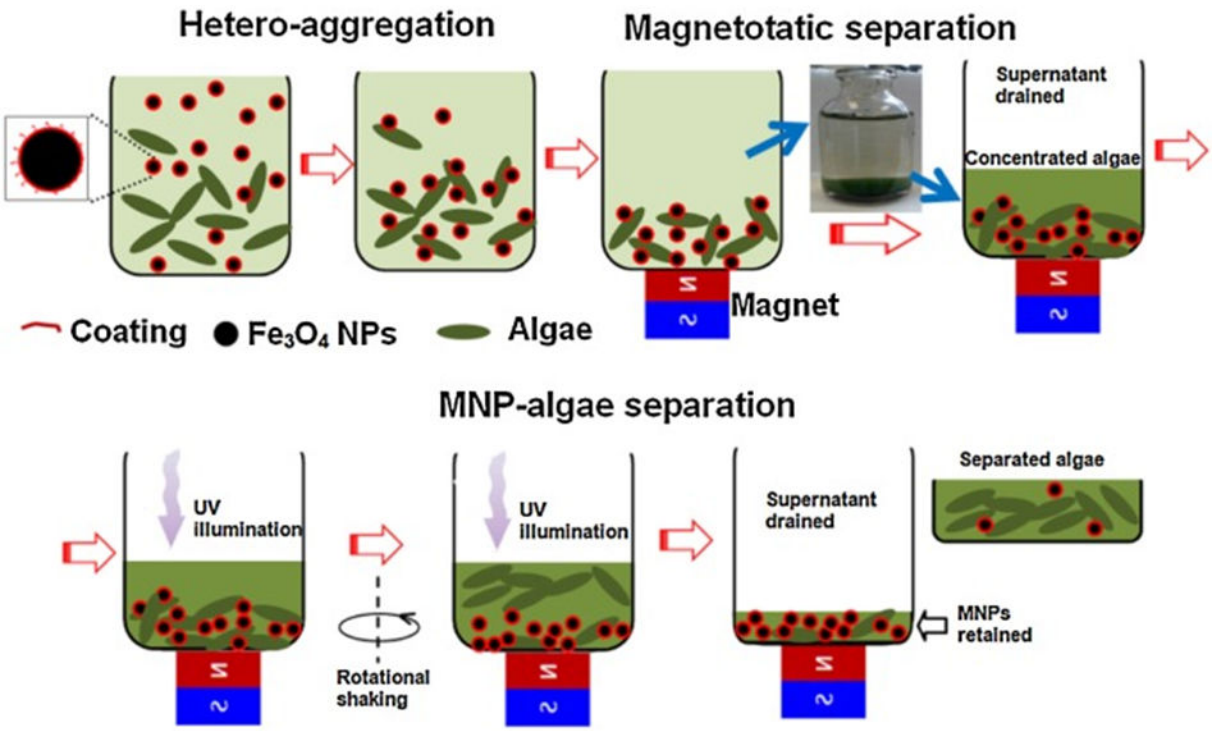

Figure 14.

A steric acid-coated Fe_3O_4–ZnO nanocomposite shifts hydrophobicity under UV365 irradiation that leads to magnetic nanocomposites detachment from the concentrated algal biomass. Such unique hydrophobicity shift may also find many other potential applications that require recovery, recycle, and reuse of valuable nanomaterials to increase sustainability and economically viability. Reprinted from Ref. [268]. Copyright 2015 American Chemical Society.

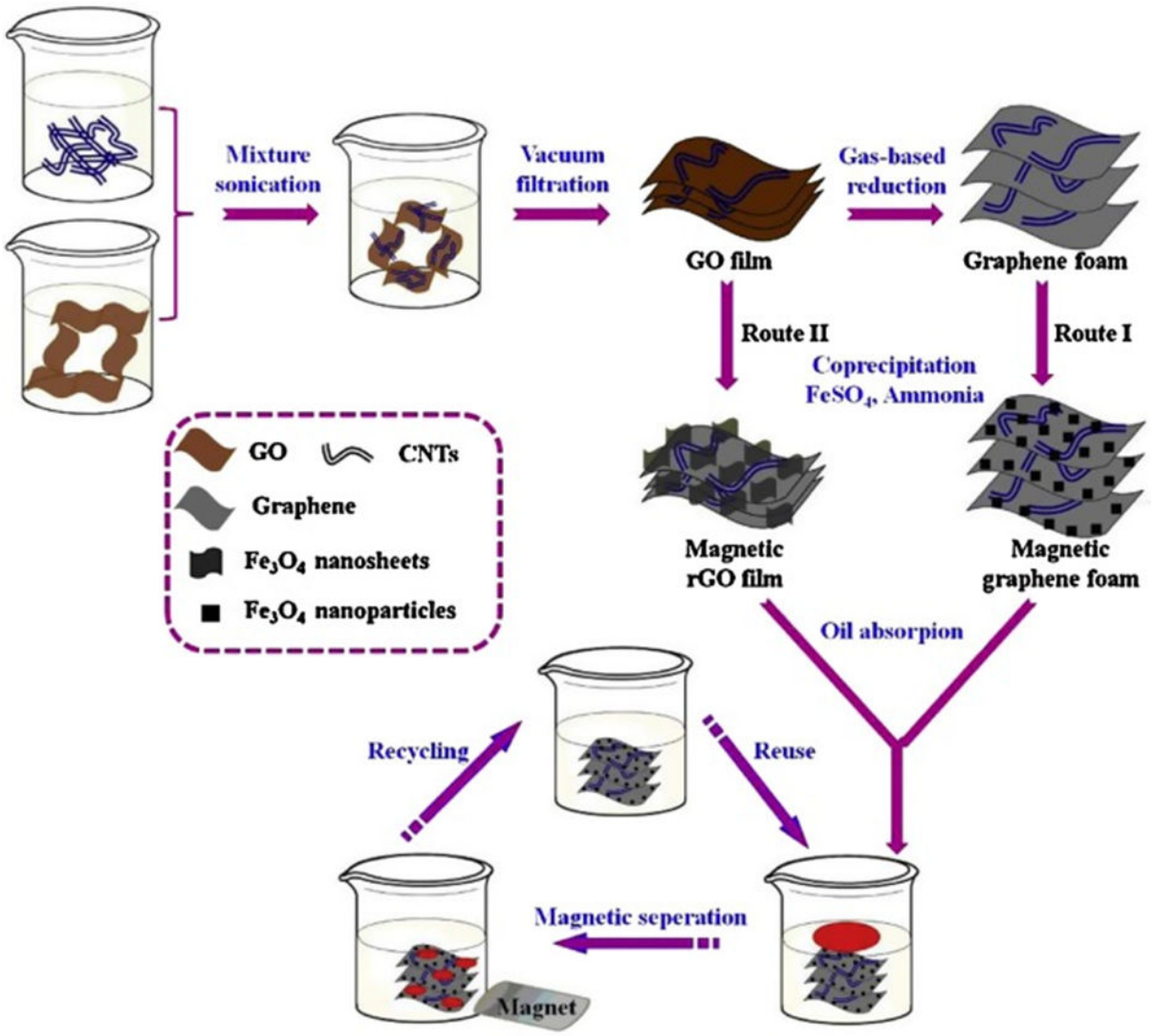

Figure 15.

Schematics showing the strategies to prepare graphene foams and their application for the removal of oils from water. Reprinted from Ref. [269]. Copyright 2014 Elsevier Ltd.

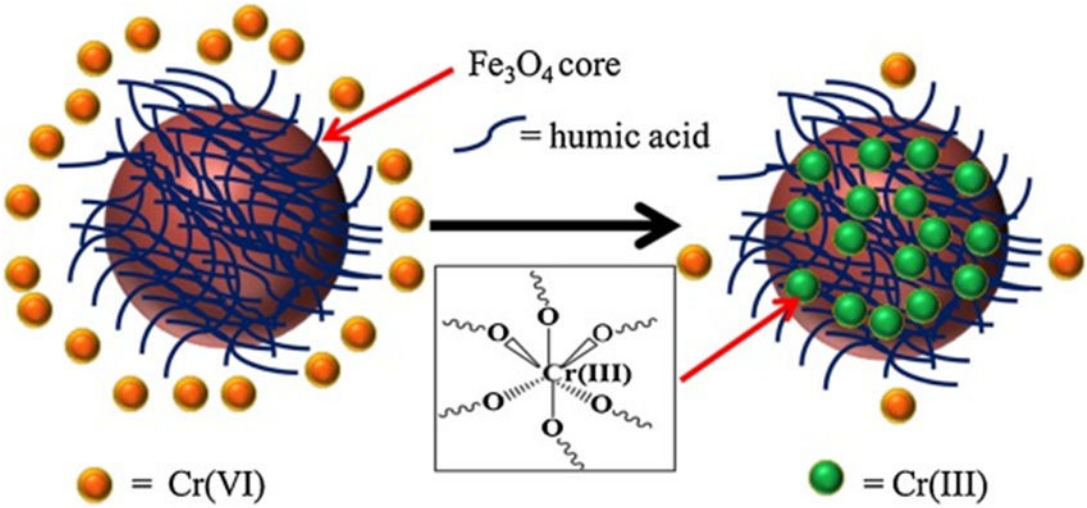

Figure 16.
Schematics showing reduction of Cr(VI) by magnetite-coated humic acid. Reprinted from Ref. [315]. Copyright 2014 American Chemical Society.

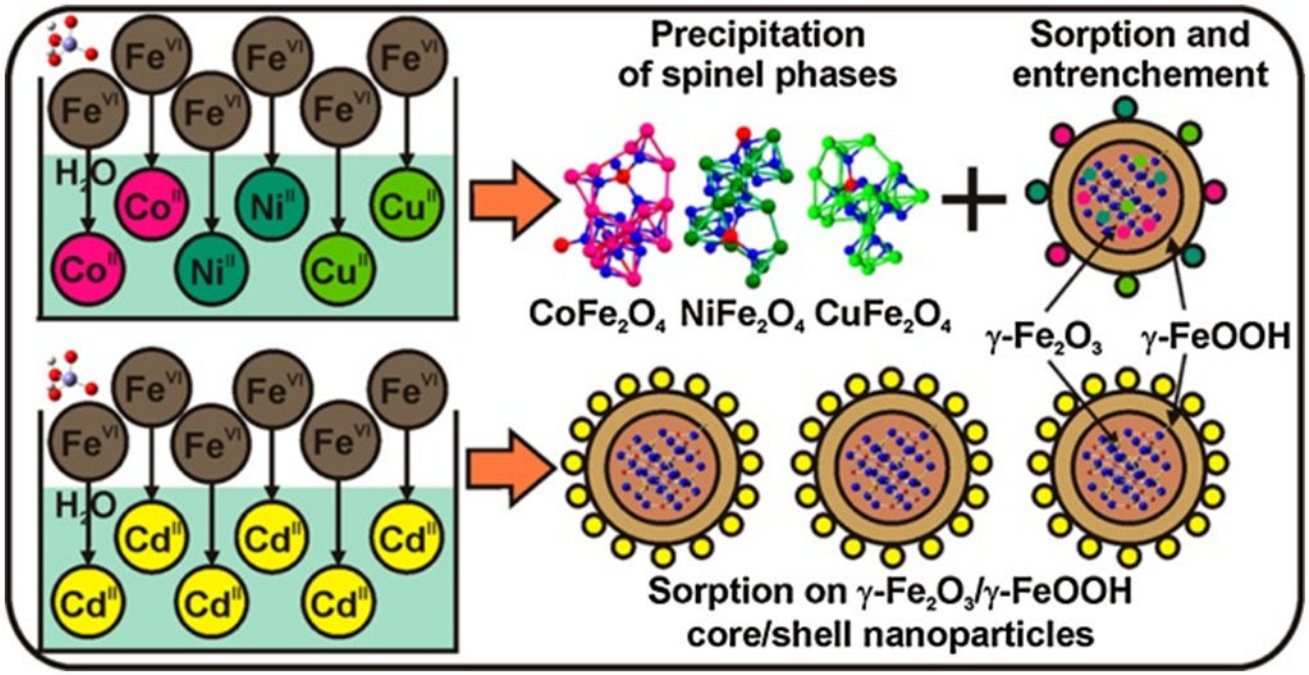

Figure 17.
Ferrate(VI)-prompted removal of metals in aqueous media with enhanced efficiency via metal entrenchment in magnetic oxides. Reprinted from Ref. [349]. Copyright 2015 American Chemical Society.

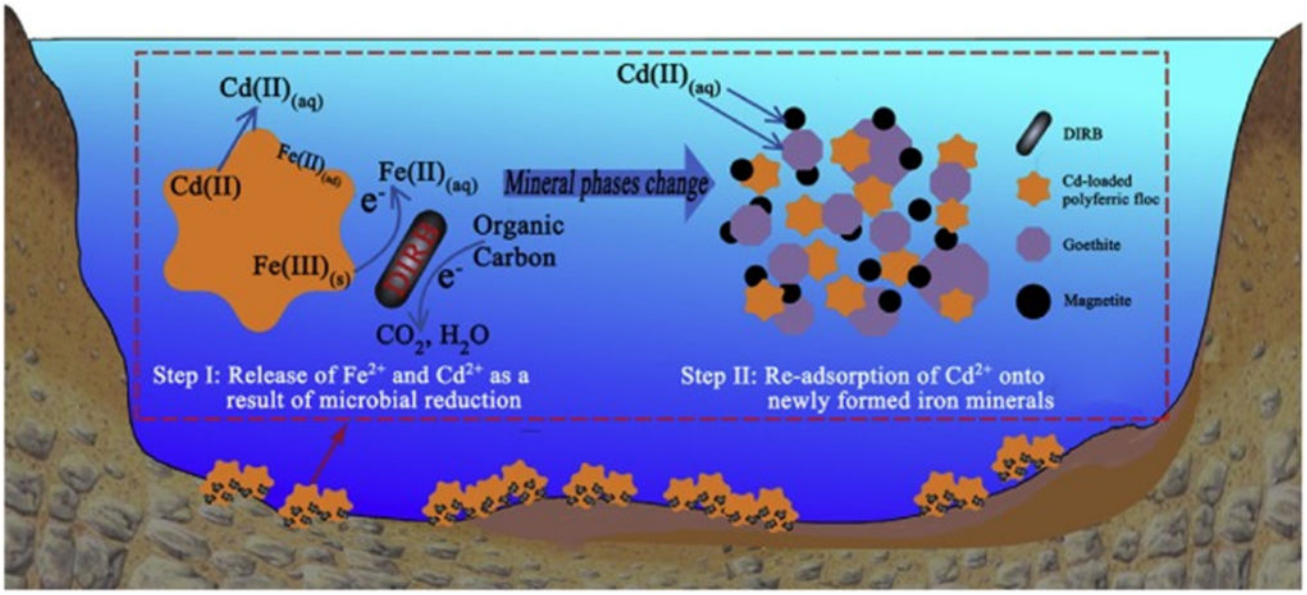

Figure 18.

Proposed schematic illustrating the fate of Fe and Cd as a consequence of microbial reduction of Cd-loaded polyferric flocs by Shewanella oneidensis MR-1. Reprinted from Ref. [388]. Copyright 2016 Elsevier Ltd.

Table 1.

Common methods and examples for synthesis of MNPs and their hybrids.

Method	Reagents and conditions	Stabilizer	Product	Ref.
Co-precipitation	$FeSO_4{\cdot}7H_2O$, $FeCl_3$, NH_4OH	PVA	Fe_3O_4, 4–10 nm	[15]
	$FeCl_2$, $FeCl_3$, NH_4OH, 25–80 °C,		Fe_3O_4, 20 nm	[16]
	$FeSO_4{\cdot}7H_2O$, $FeCl_3{\cdot}6H_2O$, NaOH	Citrate or not	Fe_3O_4, 8 nm with citrate, 14–28 nm without citrate	[18]
	$FeSO_4{\cdot}7H_2O$, $FeCl_3{\cdot}6H_2O$, NH_4OH, 80 °C	Phosphate	Fe_3O_4, 9–40 nm	[20]
	$Fe(acac)_3$, $Co(acac)_2$, Oleic acid, benzyl ether, 290 °C		$Co_xFe_{3-x}O_4$, 35–110 nm	[21]
	$FeCl_3$, $AlCl_3{\cdot}6H_2O$, $CoCl_2{\cdot}6H_2O$, 70 °C		$CoFe_{2-x}Al_xO_4$, 20–63 nm	[22]
Thermodecomposition	$FeCl_3{\cdot}6H_2O$, 2-pyrrolidone, 245 °C, reflux 1–24 h		Fe_3O_4, 4–60 nm	[30]
	$Fe(acac)_3$, 2-pyrrolidone, 200–240 °C	α,ω-dicarboxyl-terminated poly(ethylene glycol)	Fe_3O_4, 6–15 nm with average 11 nm	[31]
	$Fe(acac)_3$, oleylamine and benzyl ether,		Fe_3O_4, 8 ± 0.4 nm	[36]
Combustion waves	Fe_2O_3 NPs, nitrocellulose, 740 °C		Fe_3O_4, 5–20 nm	[37]
Hydrothermal synthesis	metal linoleate (solid), an ethanol–linoleic acid liquid phase, and a water–ethanol solution		Fe_3O_4, 9 nm $CoFe_2O_4$, 12 nm	[38]
	$FeCl_3$, ethylene glycol, NaOAc, 200 °C		Fe_3O_4–graphite, 100 nm	[42]
	Composition controlled synthesis	Various surfactants	MFe_2O_4, M = Mg, Fe, Co, Ni, Cu, Zn, 3 nm	[44]
Emulsion synthesis	Fe_3O_4, histidine		Fe_3O_4–histidine composite, 500 nm	[46]
Microbial synthesis	β-FeOOH, $Zn_xFe_{1-x}OOH$, *Clostridium* sp.		Fe_3O_4, 5–10 nm using β-FeOOH, $Zn_xFe_{3-x}O_4$, 3–8 nm using $Zn_xFe_{1-x}OOH$	[47]
	β-FeOOH, *S. putrefaciens* CN32, 9,10-anthraquinone-2,6-disulfonate		Fe_3O_4, framboidal, 20–50 nm	[48]
Green synthesis	Natural biorenewable resources	Plant extracts	Fe_3O_4, hybrids	[87]

Table 2.

Select examples of environmental applications of MNPs and their hybrids.

Media and Treatment	Contaminants	MNPs and hybrids	Mode of action	Ref.
Air cleanup	BTEX	Fe_3O_4	Adsorption	[211]
	CO	$Pt@Fe_3O_4$	Oxidation	[212], [216]
	CO	$Pd@Fe_3O_4$	Oxidation	[213]
	H_2S	Fe_3O_4@GO	Adsorption	[215]
	CO_2	$TiO_2@SiO_2@Fe_3O_4$ and Cu/ $TiO_2@SiO_2@Fe_3O_4$	Reduction to produce methanol	[216]
Antimicrobial for water disinfection	*E. coli, S. aureus*	Fe_3O_4@GO–CNTs	Inactivation	[217]
	E. coli	$PQA@Fe_3O_4$	100% biocidal	[218]
	E. coli, S. aureus	Fe_3O_4@PDA@Ag	Inactivation	[222]
	E. coli	Ag_3PO_4–TiO_2–Fe_3O_4	Photocatalytic inactivation	[223]
	M. aeruginosa	*B. methylotrophicus*, ZJU immobilized on Fe_3O_4	Algicida	[229]
Water treatment: Adsorptive organics removal	Dyes,	Fe_3O_4	Separative Adsorption	[232]
	Cationic dyes	AFMCNT		[233]
	Congo Red, MB	Fe_3O_4@GO		[236]
	BB	Fe_3O_4/chitosan		[239]
	MB, MV	Fe_3O_4/MOF		[241]
	Nitrofurans	Fe_3O_4/MWCNTs		[248]
	PFOS	$Fe_3O_4@SiO_2$@CTAB–SiO_2)		[250]
	Antibiotics (TC)	Fe_3O_4/polyacrylonitrial mat		[251]
	Pharmaceuticals	MAA coated Fe_3O_4		[256]
	PCBs	Fe_3O_4@β-CD		[257]
	BPA	DFMNPs		[260]
	p-nitrophenol	$Fe_3O_4@mSiO_2$/GO		[262]
	2,4,6–TCP	$n Fe_3O_4@NH_2$MIP		[264]
	Herbicide (diquat)	Fe_3O_4@GO		[265]
Water treatment: Oxidative organics removal	APAP	Fe_3O_4, PMS	Catalytic oxidation	[190]
	TCE	Fe_3O_4, persulfate		[191]
	Dinitrotoluene	Fe_3O_4, H_2O_2		[192]
	Phenol	CuO–Fe_3O_4, persulfate		[193]
	Antibiotic flumequine	Fe_3O_4/MWCNTs/PHQ, persulfate		[194]
	Phenol	Fe_3O_4@C, PMS		[195]
	RhB	Fe_3O_4–Bi_2WO_6, H_2O_2		[196]

Media and Treatment	Contaminants	MNPs and hybrids	Mode of action	Ref.
	TBBPA	$Fe_{2.04}Cr_{0.96}O_4$, UV/H_2O_2		[197]
	Antibacterial nalidixic acid	Fe_3O_4, H_2O_2		[198]
	3 methyl-indole	Fe_3O_4–alginate, H_2O_2		[199]
	MB	$CoFe_2O_4$/g-C_3N_4, UV/VIS		[200]
	Orange II	$CuFe_2O_4$/C_3N_4, H_2O_2		[201]
	BPA	Fe_3O_4, H_2O_2		[202]
	BPA	$CuFe_2O_4$, PMS		[203]
	Cyclic olefins	Fe_3O_4–diethylene glycol, H_2O_2		[204]
	RhB, MB	Fe_3O_4–Cu, $NaBH_4$		[205]
	RhB	Fe_3O_4@SiO_2@HPW, UV		[206]
	MB	Fe_3O_4–TiO_2–GO, solar light		[207]
	Benzyl alcohol	$CoFe_2O_4$, H_2O_2		[208]
	RhB	$CoFe_2O_4$/TNTs, PMS		[209]
Water treatment: Algae removal	*S. dimorphus*	PEI-coated Fe_3O_4	Separative Adsorption	[267]
	Algae	Steric acid–Fe_3O_4–ZnO		[268]
Water treatment: Oil spill cleanup	Crude oil, petroleum products	Fe_3O_4 conjugated with carbonaceous NMs	Separative Adsorption	[270], [271], [272], [273], [274], [275], [276]
Water treatment: Anionic inorganics removal	As(V), As(III)	Fe_3O_4, 12 nm	Separative Adsorption	[279]
	As(V)	Fe_3O_4–coated sand		[289]
	As(V)	Fe_3O_4, 98 nm		[291]
	As(V)	Fe_3O_4–starch		[285]
	As(V), As(III)	Fe_3O_4–TiO_2		[292]
	As(III)	Fe_3O_4–chitosan		[287]
	As(V), As(III)	Fe_3O_4–MnO_2-GO		[298]
	Phosphate	NH_2–Al/SiO_2/Fe_3O_4		[304]
	Phosphate	MFC@ZrO_2		[305]
	Phosphate	Fe_3O_4@SiO_2–lanthanum oxide		[306]
	Phosphate	Fe_3O_4@LDH		[307]
	Phosphate	$MnFe_2O_4$, 5 nm		[308]
	Molybdate	Fe_3O_4 and ferric ions		[309]
	Molybdate	$ZnFe_2O_4$		[310]
	Fluoride	$CuCe_xFe_{2-x}O_4$ (x = 0.0–0.5)		[312]
	Selenate	Fe_3O_4, 10–20 nm		[313]
	Cr(VI)	CD-E-MGO		[314]
	Cr(VI)	Fe_3O_4@HNTs@C	Reduction	[322]

Media and Treatment	Contaminants	MNPs and hybrids	Mode of action	Ref.
Water treatment: Cationic heavy metal ions removal	Hg^{2+}	Fe_3O_4, 100 nm	Separative Adsorpton	[324]
	Hg^{2+}	Fe_3O_4@SiO_2		[325]
	Hg^{2+}	MCD–GO–R		[332]
	Hg^{2+}	Tween20–AuNP–Fe_3O_4		[334]
	Hg^{2+}, Pb^{2+}, Cu^{2+}	CS-PAM-MCM		[335]
	Hg^{2+}, Pb^{2+}, Cd^{2+}	Fe_3O_4@C		[339]
	Hg^{2+}, Pb^{2+}, Cu^{2+}	Fe_3O_4@SiO_2@chitosan		[340]
	Pb^{2+}	MnFMC, CoFMC		[342]
	Pb^{2+}	Fe_3O_4@$Zr(OH)_x$		[343]
	Cd^{2+}	Fe_3O_4@SiO_2–poly(1-vinylimidazole)		[344]
	Cd^{2+}	Fe_3O_4–sodium dodecyl sulfate		[345]
	Zn^{2+}	Amino–Fe_3O_4@SiO_2		[346]
	Cu^{2+}	Fe_3O_4–sodium alginate		[347]
	Cu^{2+}, Mn^{2+}, Zn^{2+}	Fe_3O_4–PMMA		[348]
	Cu^{2+}, Ni^{2+}, Co^{2+}	K_2FeO_4		[349]
	Cd^{2+}, Pb^{2+}, Co^{2+}, Ni^{2+}	M–PAM–HA		[350]
	Pb^{2+}, Hg^{2+}, Cu^{2+}	EDTA–MGO		[351]
Water treatment: Radionuclides removal	U(VI)	Fe_3O_4–TiO_2	Separative Adsorption	[354]
	U(VI)	Amino–Fe_3O_4@GO		[355]
	Sr(II), Th(II), U(VI)	Fungus–Fe_3O_4		[356]
	U(VI)	APTMS–MNP		[357]
	Cs^{+}	Fe_3O_4–copper ferrocyanide		[359]
	NpO_2^{+}	Ti substituted Fe_3O_4	Reduction	[360]
Water treatment: Rare earth elements	Eu	Silane@Fe_3O_4	Separative	[362]
	La, Ce, Pr, Nd	Fe_3O_4–oleic acid	Adsorption	[363]
Water treatment: Simultaneous organics and inorganics removal	2,4-D, Pb^{2+}	Fe_3O_4–GO–LDH	Separative Adsorption	[364]
	Phenanthrene, Cu^{2+}, Zn^{2+}, Pb^{2+}	Fe_3O_4–AC–biochar		[365]
	17β-estradiol, Pb^{2+}	Fe_3O_4–GO		[366]
	Congo red, Cr(VI)	$Co_{2.698}Fe_{0.302}O_4$		[367]
	MB, Hg^{2+}	Fe_3O_4–GO		[368]
	Furazolidone, Cu^{2+}	Fe_3O_4–MWCNT		[369]
	Pathogens, heavy metals, anions	Fe_3O_4–QAC		[370]

Media and Treatment	Contaminants	MNPs and hybrids	Mode of action	Ref.
	Congo red, methyl orange, Cu^{2+}	Fe_3O_4–PDA-LDH		[371]
Water treatment: Chemical reductive removal	PCBs	Fe_3O_4 under N_2	Reduction	[372]
	PCB77	Fe_3O_4 + NZVI		[373]
	DDT	Pd–Fe_3O_4@*n*SiO_2@*m*SiO_2		[247]
	4-NP	Ag–HNTS–Fe_3O_4 in $NaBH_4$		[375]
	2,4-dichlorophenol	MWCNTs–Fe_3O_4–Pd/Fe		[376]
	CBZ, TC	Fe_3O_4–AC, Fe_3O_4–biochar, ball milling		[377]
	Cr(VI)	Fe_3O_4, synthetic and natural		[378]
	Cr(VI)	Fe_3O_4, synthetic and biogenic		[379]
	Cr(VI)	Fe_3O_4@PmPDs		[380]
	Nitrate	Fe_3O_4–ZVI		[381]
Sewage sludge stabilization	Cd^{2+}, Co^{2+}, Cu^{2+}, Zn^{2+}, Ni^{2+}, Cr	Fe_3O_4–NZVI	Immobilization	[382]
Soil improvement		Fe_3O_4–biochar	Improvement of soil quality	[383]
Soil remediation	PAHs	Fe_3O_4–AC, Fe_3O_4–biochar	Adsorption	[384]
	As(V)	Fe_3O_4–starch		[385]
	As	*In situ* biogenic Fe_3O_4 formation		[386]
Sediment remediation	Phosphate	Microsized ZVI with Fe_3O_4 as corrosion products	Immobilization	[387]
	Cd^{2+}	Biogenic Fe_3O_4	Adsorption	[388]
Groundwater remediation	Chlorinated solvents	Synthetic and natural Fe_3O_4	Reductive dechlorination	[389], [390], [391], [392], [393], [394], [395], [396], [397], [398]

Table 3.

Adsorption capacity of select MNPs and their hybrids for select metalloids (As) and metal ions (i: initial; e: equilibrium; RT: room temperature; rpm: revolutions per minute of shaking; q_e: equilibrium adsorption; q_m: maximum adsorption capacity calculated using Langmuir isotherm; $q_{m(L)}$: maximum adsorption capacity calculated using Freundlich isotherm).

Adsorbents	Reaction conditions	Adsorption capacity ($mg\ g^{-1}$)	Ref.
Fe_3O_4, 11.72 nm, 20 nm, 300 nm, 0.011–2.5 g L^{-1}	pH 4.8–8.0, $[As]_i$ 0–34 mg L^{-1}, RT, 4 rpm, 24 h	q_m As(V): 0.75–172 q_m As(III): 1.6–135	[280]
Fe_3O_4–γ-Fe_2O_3, 0.4 g L^{-1}	pH 2, $[As(V)]_i$ and $[As(III)]_i$ 1.5 mg L^{-1}, $[Cr(VI)]_i$ 1.0 mg L^{-1}, RT, 28 rpm, 24 h	Without phosphate q_e As(V): 3.7 q_e As(III): 3.7 q_e Cr(VI): 2.4 With Phosphate at 3–5 mg L^{-1}, adsorption decreased by 40–50%	[281]
Fe_3O_4–CTAB, Fe_3O_4, 0.1 g L^{-1}	pH 6.0, $[As(V)]_i$ 0.1–7 mg L^{-1}, 25 °C, 200 rpm, 2 h	q_m: 23 for Fe_3O_4–CTAB, q_m: 7.6 for Fe_3O_4 only	[282]
Fe_3O_4–graphene-LDH, LDH, 0.5 g L^{-1}	pH 6.0, $[As(V)]_i$ 0–160 mg L^{-1}, RT, shaking, 24 h	q_m: 73 for Fe_3O_4–graphene-LDH q_m: 38 for LDH	[283]
Fe_3O_4–GO, Fe_3O_4–rGO 0.1 g L^{-1}	pH 7, $[As_i]$ 0–600 mg L^{-1}, 25 °C, shaking but no rpm reported, 24 h	Fe_3O_4–GO q_m As(V): 18.8 q_m As(III): 42.9 Fe_3O_4–rGO q_m As(V): 8.42 q_m As(III): 29.8	[284]
Fe_3O_4–starch, 1.0 g L^{-1} as Fe	pH 5.0, pH 6.9, $[As(V)]_i$ 38–617 mg L^{-1}, RT, 200 rpm, 48 h	q_e: 248 at pH 5.0 q_e: 198 at pH 6.9	[285]
AC–$MnFe_2O_4$	Optimum pH 4.0 for As(V), pH 7.0 for As(III), 30 °C, 70 min	q_m As(V): 1314 q_m As(III): 1253	[293]
Mesoporous Fe_3O_4, 2.0 g L^{-1}	pH 4.0 for Cr(VI), pH 5.0 for Pb^{2+}, $[M]_i$ 0–100 mg L^{-1}, 25 °C, 35 °C, 45 °C,	q_m Pb^{2+}: 13.4, 14.1, 18.5 q_m Cr(VI): 6.64, 7.31, 8.90	[318]
Fe_3O_4/Mg–Al–CO_3–LDH, Mg–Al–CO_3–LDH, 4.0 g L^{-1}	No pH adjusting, $[Cd^{2+}]_e$ 0–200 mg L^{-1}, 30–50 °C, 1–5 h,	q_m Cd^{2+}: 45.6–54.7 for Fe_3O_4/Mg–Al–CO_3–LDH, q_m Cd^{2+}: 61.4–70.2 for Mg–Al–CO_3–LDH	[82]
Fe_3O_4–humic acid, 0.01 g L^{-1}	pH 6.0, $[M]_i$ 0.01–5 mg L^{-1}, 20 °C, stirring, 0.5 h	q_m Cu^{2+}: 46.3 q_m Cd^{2+}: 50.4 q_m Pb^{2+}: 92.4 q_m Hg^{2+}: 97.7	[277]
DSMA–Fe_3O_4, 0.002 g L^{-1}	pH 8.1, $[Hg^{2+}]_e$ 0–2 mg L^{-1}	q_m Hg^{2+}: 227	[288]
SH–Fe_3O_4–NMPs, 0.5 g L^{-1}	pH 3.0, $[Hg^{2+}]_i$ 20–500 mg L^{-1}	$q_{m(L)}$ Hg^{2+}: 523	[326]
Fe_3O_4–polyethylenimine, 1.0 g L^{-1}	pH 6, $[M]_i$ 0–5 mmol L^{-1}, 23–25 °C, 150 rpm, 12 h	q_m Zn^{2+}: 68 q_m Pb^{2+}: 168	[327]
N–MSU–F–S/Fe_3O_4, NN–MSU–F–S/Fe_3O_4, NNN–MSU–F–S/Fe_3O_4	pH 5.75, pH 5.7, $[M]_i$ 10–200 mg L^{-1}, RT, 10 rpm, 24 h	q_m Pb^{2+}: 222, 219, 191 q_m Cu^{2+}: 57.9, 50.6, 53.3	[328]
Fe_3O_4–Si–N = Gelatin	pH 4.0 for Cd^{2+}, pH 7.0 for Pb^{2+}, RT, shaking but no rpm reported, 0.5 h	q_e Cd^{2+}: 49.5 q_e Pb^{2+}: 82.9	[329]
MHC/OMCNTs	pH 5.0, $[Pb^{2+}]_i$ 10–200 mg L^{-1} 2h	q_m Pb^{2+}: 116	[336]
ZnO/$ZnFe_2O_4$/C		q_m Pb^{2+}: 345	[338]
$MnFe_2O_4$–MoS_2–CD, $CoFe_2O_4$–MoS_2–CD,	pH 1–6, 25 °C	q_m Pb^{2+}: 588 q_m Pb^{2+}: 661	[342]
Fe_3O_4@SiO_2@chitosan	pH 5.4–8.5, $[M]_i$ 10 mg L^{-1}, 25 °C, 4 h	q_e Hg^{2+}: 8.5–8.9 q_e Pb^{2+}: 6.0–6.9 q_e Cu^{2+}: 3.4–7.0	[79]